9950-1308

Washington
WASHINGTON·UNIVERSITY·IN·ST·LOUIS

SCHOOL OF
ENGINEERING
AND
APPLIED SCIENCE

CZOCHRALSKI CRYSTAL GROWTH MODELING STUDIES

FINAL TECHNICAL REPORT FOR THE PERIOD 1/1/85 - 6/30/86

September 22, 1986

by

M. P. Dudukovič, P. A. Ramachandran, R. K. Srivastava and D. Dorsey
Chemical Reaction Engineering Laboratory
Washington University
St. Louis, Missouri 63130

WASHINGTON UNIVERSITY / ST. LOUIS / MISSOURI 63130

JPL

November 4, 1988

NASA Scientific and Technical
    Information Facility
P.O. Box 8757
Baltimore-Washington International Airport
Maryland 21240

Attn: Acquisitions Branch

Gentlemen:

Enclosed for your system input and for listing in STAR are two copies of the
following subcontractor reports:

Contract No.	Corporate Source	Report No.	File No.
*957463	Claremont Graduate School		9950-1292
*954929	Clemson University		9950-1246
957158	Washington University		9950-1308
*956999	Westinghouse R&D Center		9950-1196
*957170	UCLA School of Engineering and Applied Science		9950-1254
*957358	TRW Space & Tech. Group	TRW No. 46810-6004-UT-OD	9950-1317
957247	University of Wisconsin Washborn Observatory		9950-1321
956981	University of So. Calif.		9950-1306
957284	University of Texas		9950-1326
956494	Construction Technology Laboratories, Inc.		9950-1328
957114	University of California		9950-1206

*1 Copy Only

Very truly yours,

Linda Worrel
Document Review Group
Documentation Section

LW:dk
Enclosures
cc: P. French
        Acquisitions Branch

CZOCHRALSKI CRYSTAL GROWTH MODELING STUDIES

FINAL TECHNICAL REPORT FOR THE PERIOD 1/1/85 - 6/30/86

September 22, 1986

by

M. P. Duduković P. A. Ramachandran, R. K. Srivastava and D. Dorsey

Chemical Reaction Engineering Laboratory

Washington University

St. Louis, Missouri 63130

TABLE OF CONTENTS

ABSTRACT

Over 80% of the current production of single crystal silicon, which is the preferred material for solar cells, is manufactured by the Czochralski (CZ) crystal growth technique. The manufacture of high quality crystals requires full quantification of the thermal environment in the CZ puller and the development of quantitative relationships among the many process, design and operating variables. Since this cannot be accomplished solely by experimental work a modeling study was undertaken. This modeling effort provides the proper framework for the evaluation of the effects of various variables on crystal quality. The accomplishments of the present study are as follows:

i) A complete finite-element heat-transfer model for the CZ-puller is established under the assumption that heat transfer is conduction dominated in the melt. All other heat transfer mechanisms including radiation are treated with rigor, and the crystal-melt interface shape is calculated from the heat balance as part of the solution. This model should provide the complete solution to the CZ growth problem if supplied with heat transfer coefficients from the melt side which in turn requires the solution of the melt hydrodynamics.

ii) Radiation view factors for short crystals were established. This is necessary information for the initial growth stage of the process.

iii) The model developed in i) was used to yield simpler models to be used on-line in control of crystal diameter and interface shape.

iv) A rigorous finite-element model was developed for calculation of residual thermal stresses in the crystal.

v) A preliminary model of the melt hydrodynamics was established and basic hydrodynamic phenomenon were investigated.

SUMMARY

This study focuses on the development of a mathematical model for the simulation of the Czochralski (CZ) process used for the manufacture of silicon crystals. The model predicts the temperature field in the crystal and the melt along with the crystal-melt interface shape and the pull rate assuming either conduction dominated heat transfer in the melt or known heat transfer coefficients. The shape of the crystal-melt interface affects the quality of the crystal by influencing the radial dopant concentration profile. The pull rate is important in keeping the diameter of the crystal constant and in achieving the acceptable level of productivity. The temperature field in the crystal is needed to calculate the thermal stresses in the crystal, which in turn are used to estimate the extent of dislocations in the wafers along the crystal. The proposed CZ simulator provides useful information in determining the process conditions for: (1) The growth of a uniform diameter crystal; (2) optimization of the pull rate; (3) maintenance of uniform dopant concentration; (4) the production of dislocation free crystals. The model is also useful for interpretation of the experimental data and for pursuing improvements in the various aspects of the growth process. The statement of work included the following specific objectives (tasks):

1) Perform a critical literature survey relating to mathematical modeling of the crystal growth process.

2) Develop an algorithm/model suitable for predicting the temperature distribution in the crystal, and for calculating the melt-crystal interface.

3) Perform parametric studies using the computer algorithm/model developed in (2).

4) Develop the detailed modeling of the hydrodynamics in the melt.

5) Assess the capability of the model using available experimental data.

The accomplishment of the above tasks is described in this report. The detailed literature survey on thermal modeling and melt hydrodynamics was reviewed and summarized in the 1st quarterly report. It was concluded that most of the past studies in the literature are based on simplifying assumptions and focus on some specific aspect of the process. Thus, a complete model of the system was lacking. The present modeling approach looks at the complete system consisting of the crystal, melt and the enclosure. The effects of the melt-gas meniscus shape and detailed radiation calculations, accounting for both direct and reflected radiation, have been incorporated in the model. A sequential modular computational approach is used for the simulation. This work was described in the 1st quarterly report.

The detailed model of the CZ process has been used for extensive parametric studies. The effects of important variables on growth rate and interface shape are examined and explained. the results of the detailed model are used to develop a simple model which describes the relationships among the important variables such as crystal radius (R), pull rate (v), crucible temperature (T_c), melt volume (V_m) and interface shape.

The simple model can be used to simulate the entire growth cycle of the CZ process. The model can also be used to develop and implement various operating strategies to monitor the growth process. This was discussed in detail in the 2nd and 4th quarterly reports.

A novel technique which uses a gas jet to control the growth process is developed and demonstrated based on the above simulations. The adjustments of the gas flow rate through the jet can be used to control the crystal diameter. The crystal diameter is more stable when the crystal is grown in a convection dominated environment, and diameter control by gas jet cooling is more effective than control through adjustments of crucible temperature or pulling rate. In the presence of jet cooling, it may be possible to simultaneously control

both the diameter and the interface shape. The details of this work were presented in the 3rd quarterly report.

A steady-state model of the hydrodynamics in the melt was also developed to study the relative effects of conduction and convection heat transfer. The Navier-Stokes equations with the Boussinesq approximation are solved with a finite element solution technique. The model and the computer code are useful in studying and characterizing the relative importance of the various phenomena (such as natural convection, crystal rotation, thermocapillary flow, etc.) that dictate the melt flow field. However, convergence is not achieved at the Reynolds and Grashoff numbers characteristic of the commercial operating region of interest. This implies that the flow field may be of oscillatory nature and a transient model may be needed. This would indicate that quality crystals cannot be grown without the stabilizing effect of a magnetic field. Hydrodynamic modeling is discussed in section VII of the report.

Thermally induced stresses are one of the major causes of dislocations (by slip and twinning) in the crystal. Preliminary stress calculations were performed to study the dislocation density distribution on the wafer surface. It was concluded that the best quality of the wafer is obtained in the region between the center and the outer periphery. This distribution has also been observed in past experimental investigations. The key to reducing the stress levels in the crystal is to have growth at low Biot numbers.

The work performed at the Chemical Reaction Engineering Laboratory (CREL) under this contract resulted in the following publications.

1. Ramachandran, P. A. and M. P. Duduković, "Simulation of Temperature Distribution in Crystals Grown by Czochralski Method", J. Crystal Growth 71 (1985): 399-408.

2. Srivastava, R. K., P. A. Ramachandran and M. P. Duduković, "Interface Shape in Czochralski Grown Crystals: Effect of Conduction and Radiation", J. Crystal Growth 73 (1985): 487-504.

3. Srivastava, R. K., P. A. Ramachandran and M. P. Duduković, "Radiation View Factors in Czochralski Crystal Growth Apparatus for Short Crystals", J. Crystal Growth 74 (1986): 281-291.

4. Srivastava, R. K., P. A. Ramachandran and M. P. Duduković, "Czochralski Growth of Crystals: Simple Models for Growth Rate and Interface Shape J. Electrochem. Soc.: Solid-State and Technology 133 (1985): 1009-1015.

5. Srivastava, R. K., P. A. Ramachandran and M. P. Duduković, "Simulation of Jet Cooling Effects on Czochralski Crystal Growth", J. Crystal Growth (1986). Accepted for publication.

6. Dorsey, D., P. A. Ramachandran and M. P. Duduković, "Numerical Simulation of the Hydrodynamics and Heat Transfer in Czochralski-Melts: Preliminary Results", AIChE One Day Symp., St. Louis, April 17, 1985.

I. INTRODUCTION

The Czochralski (CZ) process (also known as the Teal-Little Technique) is the backbone of today's semiconductor industry and one of the main sources of solar grade silicon. The growth process at first sight looks simple. The raw material is melted in a quartz crucible and kept in the molten state by inductive or resistive heating. A seed crystal, of suitable orientation, is suspended over the crucible in a chuck. For growth, the seed is inserted into the melt until its end is molten. It is then slowly withdrawn resulting in a single crystal which grows by progressive freezing at the liquid-solid interface. The entire assembly is enclosed within a quartz envelope which is water cooled and flushed with an inert gas such as argon. The schematic of the furnace is shown in Figure 1. To assure constancy of the diameter, the heater power (crucible temperature) is manipulated using a PID controller. The crucible position is also gradually lifted to compensate for the drop in the melt level. The idea is to maintain the same position of the solid-liquid interface relative to the heater orientation throughout the entire growth cycle. Both the crucible and the crystal are rotated to suppress free convection cells. By suitable programming of spin and pull rates, a resistivity range as high as 25-50 ohm-cm and crystal diameters up to as large as 150 mm over 80% of the ingot length are obtained.

The production of superior quality Si crystals demands that the following requirements be fulfilled.

1) Uniform diameter of the ingot.

2) Optimization of the pull rate.

3) High (axially and radially uniform) resistivity.

4) Production of uniform dislocation free crystals.

The diameter of the growing crystal is mainly determined by the interaction of the set pull rate and the heat transfer environment in the crystal,

- 1 -
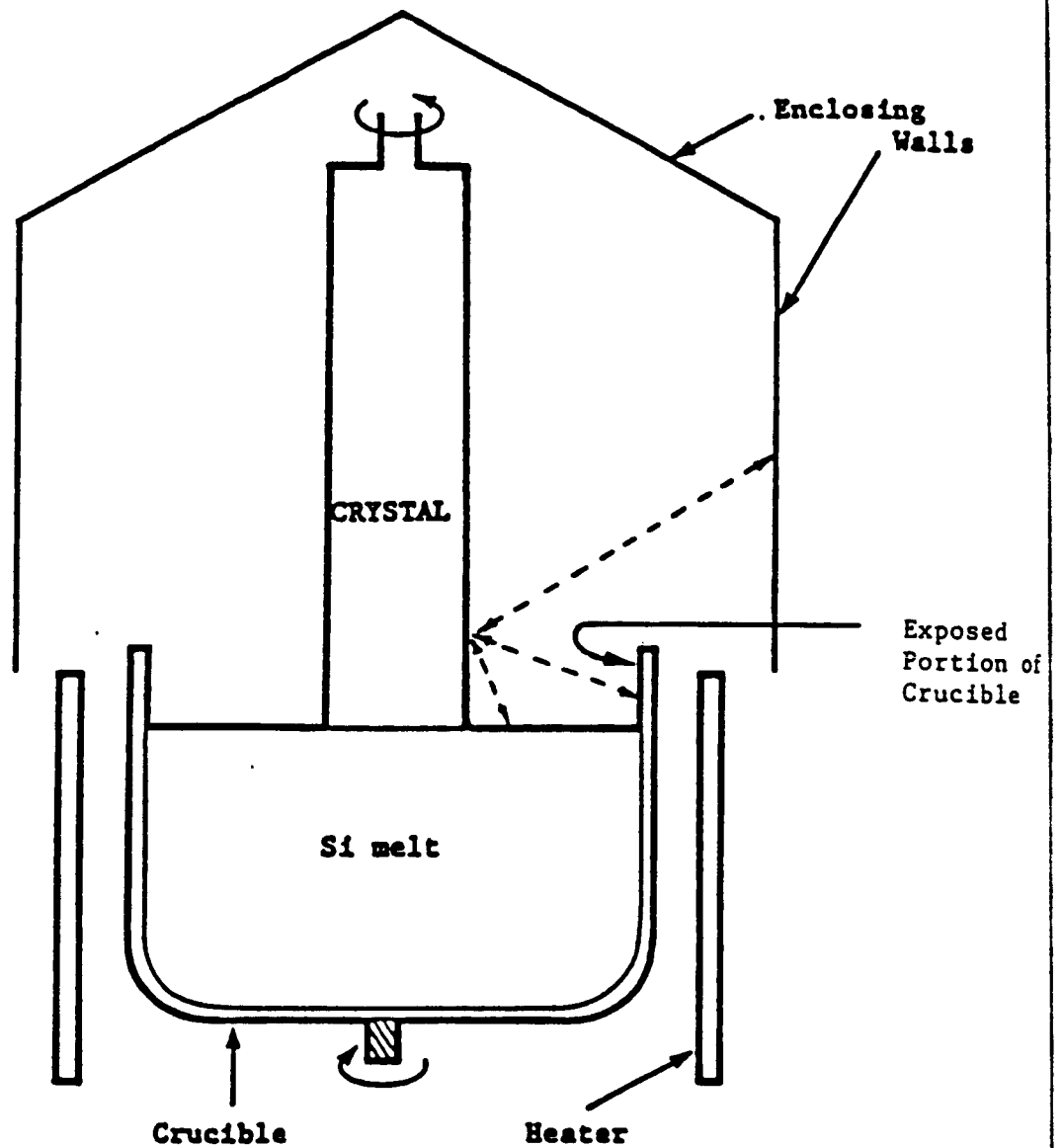
Figure 1. Schematic of a Czochralski Single Crystal Puller
--- indicates radiation interaction between
various surfaces.

melt and the furnace (ambient and the walls). The resistivity profiles
can be related to imbedded dopant and impurity concentrations. The dopant
profiles in the crystal are very closely related to the nature of the crystal-
melt interface and the mass transport in the melt. The extent of dislocations
generated in the crystal are determined by the level of thermally induced
residual stresses in the crystal, which in turn are directly related to
the temperature field in the crystal. Additionally, the heat and mass
transport in the melt are affected by the melt hydrodynamics due to the
interactions of forced and natural convection.

It is established that the quality of the growing crystal is related
in a quantitative way to the hydrodynamics, mass and heat transfer in the
melt and to heat transfer in and from the crystal. These phenomena are
affected by several variables which can be classified as follows:

i)   Geometric variables which are fixed for a given puller, e. g.,
     crucible and enclosure shape, heater position, etc. (These could
     also be categorized as puller design variables).

ii) Process variables which are governed by the selected operating
     schedule, e.g., melt depth, height of exposed crucible wall,
     crystal diameter, etc.

iii) Manipulative variables which could be used for control, e.g., heater
     power, pull rate, crystal and crucible rotation speed, crucible
     lift rate, gas flow rate, etc.

The problem of calculating the temperature profile in the crystal is
coupled with the problem of determining profiles in the melt, and hence,
a complete analysis of the combined system (crystal + melt) is necessary for
proper modeling of the process. The temperature profile in the melt is in it-
self coupled with the flow field or hydrodynamics of the system due to the
interaction of forced and natural convection and thermocapillary flow.

- 3 -

Further complexity arises due to the fact that the melt-crystal interface cannot be fixed a priori and must be determined by energy balance considerations. Thus, the problem is of the 'floating' boundary condition type and the interface shape has to be determined as part of the solution. Hence, it is not surprising that literature studies focus only on some selected aspects of the system and a complete and rigorous model is lacking.

In addition to the prediction of temperature profiles in the system, it is necessary to predict the concentration distribution of impurities, such as oxygen and carbon, and dopants such as boron. It is also necessary to examine the operating conditions which can lead to a desired distribution of these 'solutes'. Here again the problem is complex due to the fact that the solute distribution is affected by the convective flow field in the melt which is, in turn, dependent on the temperature profiles.

The systematic modular approach to this complex problem developed at the Chemical Reaction Engineering Laboratory (CREL) is shown schematically in Figure 2. The specific objectives of this project were as follows:

1. Perform a critical literature survey relating to mathematical modeling of the CZ growth process.

2. Develop an algorithm/model for the CZ process suitable for predicting the temperature field in the crystal including the pull rate and the interface shape. Conduction is assumed to be the dominant mode of heat transport in the melt.

3. Perform parametric studies using the computer algorithm/model developed in (2).

4. Develop simple models which describe the relationships between the pertinent variables in the multiparameter space. These models can then run on line to implement the desired operating policy.

OVERALL SCHEMATIC OF CZ MODELING

Selected Operating Schedule and Process Variables

Geometric Variables

Manipulated Input Variables:
- Crucible temp., T_c
- Pull-rate, V_p
- Heat transfer in gas, h_a

  etc.

CZ Model
- Hydrodynamics of the Melt
- Heat and Mass Transfer in Melt
- Heat Transfer in and from Crystal

Output Variables to be Controlled:
- Crystal diameter
- Interface shape
- Dopant distribution

Model for Thermally Induced Stresses, r_a

Output Variables to be controlled:
- dislocations
- twinning

Figure 2. Overall Schematic of CZ Modeling.

- 5 -

5. Develop a novel technique of improving the controllability of the crystal diameter and achieving a simultaneous control of crystal diameter and interface shape. The concept relies on regulating the convection cooling component of the crystal by using inert gas jets. This technique will be particularly useful for growing low cost, high quality, large diameter crystals for solar cell applications.

6. Develop the detailed modeling of the hydrodynamics of the melt.

7. Develop a thermal stress model.

This final report summarizes the work done during the period of investigation (1/1/85 - 6/1/86) and shows how the various tasks listed above have been accomplished.

It should be noted that the program duration was reduced to a year and a half instead of the originally planned time. All of the above quoted tasks could not have been accomplished if additional support was not obtained from the Electric Power Research Institute (EPRI) under contract No. RP-8001-1.

II. CURRENT STATE-OF-THE-ART IN MODELING

The modeling of Czochralski growth has been studied by many investigators based on various simplifying assumptions. The problem is complex due to the interaction of the hydrodynamics and heat transfer in the melt, the unknown position of the melt-crystal interface (which must be determined as part of the solution), meniscus shape of the melt at the melt-crystal-gas line of contact, and the effect of both direct and reflected radiation interactions among the various 'surfaces' in the enclosure.

A. THERMAL MODELING

Simplified versions of the combined problems of the temperature distribution in the melt and the crystal have been studied extensively in Japan by Kobayashi and Arizumi (1970, 1972) and Kobayashi (1981) and recently by Derby and Brown (1986) in the United States. Kobayashi and Arizumi (1972) assumed conduction to be the dominant mechanism for heat transport in both the crystal and the melt. In a separate study (Kobayashi and Arizumi, 1970; Kobayashi, 1981) the flow pattern in the melt was also included in the model. A finite difference method was used for the solution of the model. This computational scheme is suitable only for nearly planar interfaces due to the difficulties in handling nonplanar regions. Furthermore, a simplified radiation model was used in their work.

In a recent paper Derby and Brown (1986) modeled the combined-problem assuming that the heat transfer in the melt occurs by conduction only. The radiation interaction between the various surfaces was not included in the model. These assumptions restrict the validity of the model. Their model, however, included the shape of the melt meniscus which was obtained by solution of the Laplace-Young equation. The crystal radius corresponding to a given pulling rate was determined as part of the solution. The solution

- 7 -

procedure was based on a finite element method coupled with a global Newton Raphson scheme for all the unknowns (temperature, interface shape, meniscus shape, crystal radius). Although such a scheme is useful for rapid convergence, the method has limitations in that it cannot be readily adapted to more complex models for the melt and may ultimately require a supercomputer. Indeed, a supercomputer was used in their analysis (Derby and Brown, 1986).

Heat loss by radiation from the crystal side surface and heat received by the crystal by radiation from the exposed surface of the crucible play significant roles in the process, as shown by Kobayashi (1972) and Rea (1981). A detailed model for the temperature distribution in the crystal including the radiation interaction between the various surfaces present in the crystal growth apparatus was developed by Ramachandran and Dudukovic (1985). In their work, a simple Stefan's model normally used for calculating the radiation heat loss was replaced by the more detailed Gebhart's model from the enclosure theory of radiation (Gebhart, 1961). The above discussion indicates that a complete analysis even for a conduction dominated model is not available. In particular, all the critical elements independently analyzed by various investigators need to be put together for a complete simulation.

B. HYDRODYNAMICS

The flow field in the melt is governed by the Navier-Stokes equation. These equations can be expressed in terms of the vorticity, stream function (ψ, ω) formulation and the azimuthal velocity or in terms of the basic variables (three components of velocity and pressure). A number of studies have focused attention on the hydrodynamics of the melt and these are summarized in Table 1. The special features of these studies are indicated in Table 1 as follows:

A. Radiation is Included

    A1. Simple Stefan's Law to Surroundings at 0°K

    A2. Stefan's Law to Surroundings at $T = T_{amb}$ (specified ambient temperature)

B. Melt-Crystal Interface Shape Determined

C. Unsteady Case Solved

D1. Axial Magnetic Field applied

E. Oxygen Transfer Considered

F. Thermocapillary Flow Considered

G. Non-Axisymmetric, Three-Dimensional Simulation

H. Microgravity

The dimensionless groups shown in Table 1 are defined as follows:

$$Gr = \beta g \Delta T b^3 / \nu^2$$

$$Re_c = \omega_s R_c^2 / \nu$$

$$Re_s = \omega_c R_c^2 / \nu$$

The following symbols and units are used:

R_c crucible radius, cm

g acceleration due to gravity, cm/s^2

ΔT temperature difference (crucible wall and melting point), K

β volume expansivity, K^{-1}

ν kinematic viscosity, cm^2/s

ω_c crucible rotation rate, s^{-1}

ω_s crystal rotation rate, s^{-1}

It is seen that although considerable information is available on the hydrodynamics, studies in the range of parameters of interest in silicon growth are rather limited. In addition, none of the studies shown in Table 1 solves the combined problem of the melt + crystal. Such a study is essential for a quantitative model for the Czochralski process. Kobayashi

TABLE 1

Summary of Studies in Hydrodynamics of CZ Melts

Workers	Year	Numerical Method	Special Features	Parameter Range Gr	Re_c	Re_s	Material
1. Kobayashi & Arizumi	1970	Finite difference with over-relaxation	A1, B	10^3	0	3×10^3	Germanium
2. Kobayashi & Arizumi	1975	Finite difference with relaxation		0	100	400	
3. Langlois & Shir	1977	Finite difference with SOR	A1, C	?	100	400	
4. Langlois	1977	Finite difference (upstream differencing)	A1, C	3.2×10^6	2×10^4	3×10^4	
5. Langlois	1984	Finite difference	A2, D1, C	2×10^9	7×10^5	1×10^6	Silicon
6. Langlois	1980	Finite difference	A1, C, F, H				$A\ell_2O_3$
7. Lee, Langlois & Kim	1984	Finite difference	A2, D1, E. F, C	2×10^9	1×10^6	1×10^6	Silicon
8. Mihelcic et. al.	1981	MAC "Marker & Cell"	C		50	250	1:1 water glycerine
9. Mihelcic et. al.	1982	MAC	C	6×10^6	50	250	liquid copper
10. Mihelcic, Wingerath & Pirron	1984	MAC	C, G	4×10^5	50	250	liquid copper
11. Crochet et. al.	1983	Finite element 9-noded elements	C	10^7	375	1000	Gallium arsenide
12. Dorsey et. al.	1985	Finite element 8-noded elements	F	2×10^5	10	200	Silicon
13. Mihelcic & Wingerath	1985	MAC	C, D1	1.3×10^8	1×10^6	25×10^6	Silicon

and Arizumi (1970, 1981) were the only investigators who made some attempts to solve the combined problem but this was for a limited range of parameters.

III. MODEL DEVELOPMENT/COMPUTER ALGORITHM

In this section an efficient computational scheme is presented for solving the case of conduction dominated heat-transfer in the melt. Temperature profiles in the melt and crystal, position and shape of the melt-crystal interface and the required crystal pull-rate are all determined. The finite element method with triangular cells is applied separately to solve the heat transfer problem both in the crystal and the melt. The two systems are coupled through the energy balance at the melt-crystal interface. The complete problem is then solved in an iterative manner. At each iteration the crystal and melt temperature profiles are updated along with the interface shape and the crystal pulling rate. A detailed radiation model accounting for both direct and reflected radiation is used to model the radiative heat exchanges in the system. This algorithm should be readily extendable to treat the hydrodynamics of the melt without significant reprogramming. This approach will also be suitable for complete transient simulation of the crystal pulling process to predict the entire history of the growth process. The effect of various process parameters on interface shape and pulling rate is investigated in detail. The former is tied to crystal quality and the latter determines the puller productivity. Thus, the present work updates the results of Kobayashi (1981); Derby and Brown (1986); Ramachandran and Dudukovic (1985), and provides a complete simulation for the conduction dominated model for the melt. A new computational scheme based on sequential modular simulation is also introduced thus providing easy replacement of the conduction dominated model for the melt with other more detailed models.

The governing equations describing the heat transport in the melt and the crystal are farily well established and will be discussed briefly. The model is based on the following assumptions.

i. Conduction is the dominant heat transfer mechanism in both the crystal and the melt.

ii. Pseudo-steady state is achieved with respect to temperature gradients, i.e., the crystal is pulled at sufficiently low speed so that the gradients are not changing significantly at a given instant of time.

iii. Both direct and reflected radiation exchange occurs among all the exposed surfaces at various temperatures in the crystal puller enclosure.

iv. The melt-gas interface can be described by an approximate analytical solution (available in the literature). This includes the shape of the meniscus at the crystal-melt-gas line of contact.

The differential equation describing the heat flow in the crystal is as follows:

$$\frac{1}{r}\frac{\partial}{\partial r}\left(r\,k_s\,\frac{\partial T}{\partial r}\right) + \frac{\partial}{\partial z}\left(k_s\,\frac{\partial T}{\partial z}\right) - v\rho_s C_{ps}\frac{\partial T}{\partial z} = 0 \tag{1}$$

Here r is the radial position; z is the axial position measured from the bottom of the crucible; T is the temperature at position (r,z); ρ_s is solid density; k_s is solid thermal conductivity, C_{ps} is specific heat of the solid and v is the pulling rate.

The governing differential equation for the melt is:

$$\frac{1}{r}\frac{\partial}{\partial r}\left(r\,k_\ell\,\frac{\partial T}{\partial r}\right) + \frac{\partial}{\partial z}\left(k_\ell\,\frac{\partial T}{\partial z}\right) = 0 \tag{2}$$

where k_ℓ is the thermal conductivity of the melt. The model definition is complete once the boundary conditions are specified. Symmetry at r = 0, for both crystal and melt, requires:

$$\frac{\partial T}{\partial r} = 0 \tag{3}$$

On the cylindrical surface of the crystal conduction is balanced by radiation and convection losses:

$$- k_s \left(\frac{\partial T}{\partial z}\right)_s = h \ (T - T_a) + q_R \tag{4}$$

Here q_R is the net heat loss by radiation for an element of the crystal surface per unit area, h is the convective heat transfer coefficient and T_a is the average temperature of the argon gas that surrounds the crystal. Assuming that the argon flow in the enclosure is laminar, the value of h is given by:

$$h = a \ (T - T_a)^{1/4} \tag{5}$$

Here a is an empirical correlating constant. The value of a in a vacuum is zero and can be calculated for other cases using the correlations given in texts such as McAdams (1954). The complete solution of the heat transfer problem involving gaseous convection requires the simultaneous solution of the gas hydrodynamics in order to calculate precisely heat losses by convection. Such a calculation is not necessary since the convection contribution to heat loss is considerably less than the loss due to radiation.

On the crystal top surface conduction is also balanced by radiation and convection losses:

$$- k_s \left(\frac{\partial T}{\partial z}\right)_s = h \ (T - T_a) + q_R \tag{6}$$

On the melt free surface the same condition holds:

$$- k_\ell \left(\frac{\partial T}{\partial n}\right)_\ell = h \ (T - T_a) + q_R \tag{7}$$

Here n is the outward normal on the melt free surface.
The crucible surface is assumed to be at constant temperature:

$$T = T_c \quad , \text{ on the crucible surface} \tag{8}$$

- 14 -

The crystal-melt interface is determined by the melting point isotherm:

$$T = T_m \quad , \quad \text{on the melt-crystal interface} \tag{9}$$

On the crystal-melt interface the conduction flux from the melt and the energy released by solidification are balanced by conduction in the crystal.

$$Q_s = Q_\ell + Q_f \tag{10}$$

where:

$$Q_s = - k_s \left(\frac{\partial T}{\partial n}\right)_s = - k_s \left(\frac{\partial T}{\partial z}\right)_s \overline{\sqrt{m^2 + 1}} \tag{10a}$$

$$Q_\ell = - k_\ell \left(\frac{\partial T}{\partial n}\right)_\ell = - k_\ell \left(\frac{\partial T}{\partial z}\right)_\ell \overline{\sqrt{m^2 + 1}} \tag{10b}$$

$$Q_f = \rho_s v \Delta H / \overline{\sqrt{m^2 + 1}} \tag{10b}$$

Here n refers to the outward normal from the melt at the interface, m is the slope of the crystal-melt interface and ΔH is the latent heat of fusion. The shape of the melt-gas meniscus is given by the Laplace-Young equation.

$$g z_2 (\Delta\rho) = \sigma_{ST} \left(\frac{1}{R_1} + \frac{1}{R_2}\right) \tag{11}$$

Here σ_{ST} is the surface tension of the melt; $\Delta\rho$ is the difference between densities of the fluid (melt) forming the meniscus and the ambient fluid (argon); g is the gravitational acceleration and z_2 is the vertical coordinate at the melt surface measured from the crucible bottom; R_1 and R_2 are the principle radii of curvature of the meniscus (which can be related to the first and second derivatives, with respect to radius, of the melt-gas interface position). In this work an approximate analytical equation proposed by Hurle (1983) is used to model the shape of the melt-gas meniscus. (This equation is very lengthy and is not reproduced here). This analytical solution compares very well with the rigorous numerical

solution of the Laplace-Young equation (Hurle, 1983). Both the analytical solution and the numerical solution require the contact angle at the melt-crystal interface to characterize the melt-gas interface shape. The melt volume constraint introduced by Derby and Brown (1986) is expressed as:

$$\int_{o}^{R} 2\pi r \, z_1(r)dr + \int_{R}^{R_c} 2\pi r \, z_2(r)dr = V_m \tag{12}$$

Here $z_1(r)$ and $z_2(r)$ refer to the vertical coordinate of the melt-crystal and melt-gas interface, respectively; R and R_c are the crystal and the crucible radii.

Equations (1) to (12) describe the complete model for the crystal and the melt necessary to calculate the temperature field in the crystal and the melt along with the interface shape and the crystal pulling rate. Next we review the method introduced by Ramachandran and Duduković (1985) for the calculation of radiation heat losses from any crystal or melt surface accounting for both direct and reflected radiation.

A. ESTIMATION OF RADIATION HEAT LOSSES

The radiation heat loss per unit area for a surface k at temperature T_k, can be calculated as (Gebhart, 1961):

$$\begin{aligned} q_{R,k} &= \epsilon_k \, \sigma T_k^4 - \frac{1}{A_k} \sum_{i=1}^{N} G_{ik} \, \epsilon_i \sigma T_i^4 A_i \\ &= \epsilon_k \, \sigma \, (T_k^4 - T_{e,k}^4) \end{aligned} \tag{13}$$

where

$$T_{e,k} = [\frac{1}{A_k \, \epsilon_k} \sum_{i=1}^{N} G_{ik} \epsilon_i T_i^4 A_i]^{1/4} \tag{14}$$

G_{ik} = radiation factor representing the fraction of the radiation emitted by surface i which is absorbed by surface k.

- 16 -

N = total number of radiating surfaces present in the system.

ε_i = emissivity of the i-th surface.

Here, $T_{e,k}$ can be viewed as the effective temperature to which the surface k loses heat by radiation.

As a simplified model, the radiation heat loss term can be calculated assuming that an element of crystal or melt loses heat only to the surroundings (say wall of the enclosure). Then

$$q_{R,k} = \varepsilon_k \sigma (T_k^4 - T_{eff}^4) \tag{15}$$

where

T_{eff} = an effective temperature of the surroundings to which radiation heat loss takes place. (This can also be treated as an assumed model parameter).

This simplified model (Equation 15) is referred to as the Stefan's model while the general model (Equation 13), which includes the detailed radiation exchange, is referred to as the Gebhart's model.

The procedure for calculating the G-factors (G_{ik}; i, k = 1, 2,..., N, where N is total number of radiating surfaces present in the system) is described in standard textbooks on radiation, and only the final set of equations will be presented here (see for example Gebhart, 1961; Siegal and Howell, 1972). For any surface k these equations are:

$$G_{ik} = F_{ik} \varepsilon_k + \sum_{j=1}^{N} F_{ij} (1-\varepsilon_j) G_{jk} \tag{16}$$
$$i = 1, 2,..., N$$

Where F_{ij} is the view factor from surface i to j. The above set of linear equations for G_{ik}; i = 1, 2,...,N, can be solved by Gaussian elimination. Repeating the calculations for all the surfaces by changing k, we obtain all the radiation factors. These equations are based on the assumption

that the reflectivity of any surface k is equal to $(1-\epsilon_k)$, which is valid

for opaque gray surfaces.

In our computation the entire enclosure containing the CZ puller

apparatus is divided into surfaces as indicated below, and each surface is

assumed to be at uniform temperature for the purpose of calculation of

the G-factors.

1. NT surfaces for the crystal top = Number of finite element divisions

   in the crystal in r direction.

2. NC surfaces for the crystal side = Number of finite element divisions

   in the crystal in the z direction.

3. NM surfaces for the melt surface = Number of finite element divisions

   in the melt in the r direction.

4. One surface for the crucible wall.

5. One surface for the enclosing walls.

   Total number of surfaces N = NT + NC + NM + 2

The calculation procedure for the view factor matrix $F(i,j)$:

i, j = 1, 2,..., N, is straightforward when the melt free surface is

assumed to be flat. The closed form expressions for all the required view

factors are available in the literature (Siegal and Howell, 1972; Rea,

1975; Minnig, 1979; Howell, 1982). The estimation of the view factors

for the curved melt free surface (meniscus) is accomplished by approximating

the melt free surface near the crystal by a straight line with the correct

slope as required by contact angle consideration. This does not cause

significant errors since the curvature is rather steep and confined to a

very small region near the crystal edge. This approximation is valid

particularly for silicon since the three phase contact angle for silicon is

very small (Brown and Ettouney, 1983). The view factors from the various

surfaces to other surfaces can then be calculated in terms of known view

- 18 -

factors by applying suitable view factor algebra. Radiation view factors for short crystals during necking and shoulder growth have been reported for the first time by our group. Table 2 summarizes the entire calculations of the view factors needed for the CZ puller.

The above method for calculation of radiation interchange is computationally equivalent to that introduced by Rea (1981) in his one-dimensional model for the crystal. This has been proved in the book by Siegal and Howell (1972). However, the current procedure is more suitable in iterative calculations and also when interactions among large number of surfaces needs to be considered. (The G-factors need to be calculated only once at the start of the iteration if the slight changes in G-factors due to the temperature dependence of emissivity are ignored).

B. SOLUTION PROCEDURE

A sequential modular type of approach is used for the calculation of the thermal field in the crystal and melt, the crystal-melt interface shape, the melt meniscus, and the crystal pulling rate for a fixed crystal radius. The shape of the melt-gas meniscus is calculated in the beginning using the analytical solution of Hurle (1983) for the desired crystal radius. The Galerkin finite element method with triangular basic cells is applied separately to the Laplace Equations (1) and (2) for the crystal and the melt along with the appropriate boundary conditions. A typical finite element mesh used for the system is shown in Figure 3. The isotherm boundary condition defined by Equation (9) is used for the finite element formulation of Equations (1) and (2). At each iteration Equations (9) and (12) along with the known shape of the melt meniscus (from Equation (11)) are used to update the crystal-melt interface and the crystal pulling rate. The procedure for updating the crystal-melt interface is discussed in Appendix 1.

Table 2

View Factor Calculation in a Czochralski Puller

| VIEW FACTOR	REFERENCES
I. Long Crystal (Crystal Top is Outside the Crucible) with Flat Melt Surface	
1. Crystal to Melt	Siegal and Howell (1972), Rea (1975)
2. Crystal to Crucible	Rea (1975)
3. Melt to Crucible	Minning (1979)
4. Crucible to Crucible	Howell (1982)
II. Short Crystal (Crystal Top is Inside the Crucible) with Flat Melt Surface	
1. Crystal to Melt	Siegal and Howell (1972), Rea (1975)
2. Crystal to Crucible	Rea (1975)
3. Melt to Crucible	Srivastava et. al. (1986)
4. Crucible to Crucible	Srivastava et. al. (1986)
III. Modifications for Curved Melt Surface	
1. Crystal to Melt	Srivastava et. al. (1986)
2. Crystal to Crucible	Rea (1975)
3. Melt to Crucible	Srivastava et. al. (1986)
4. Crucible to Crucible	Srivastava et. al. (1986)
5. Melt to Melt	Srivastava et. al. (1986)
IV. Neck Growth	
V. Shoulder/Initial Bulk Growth	
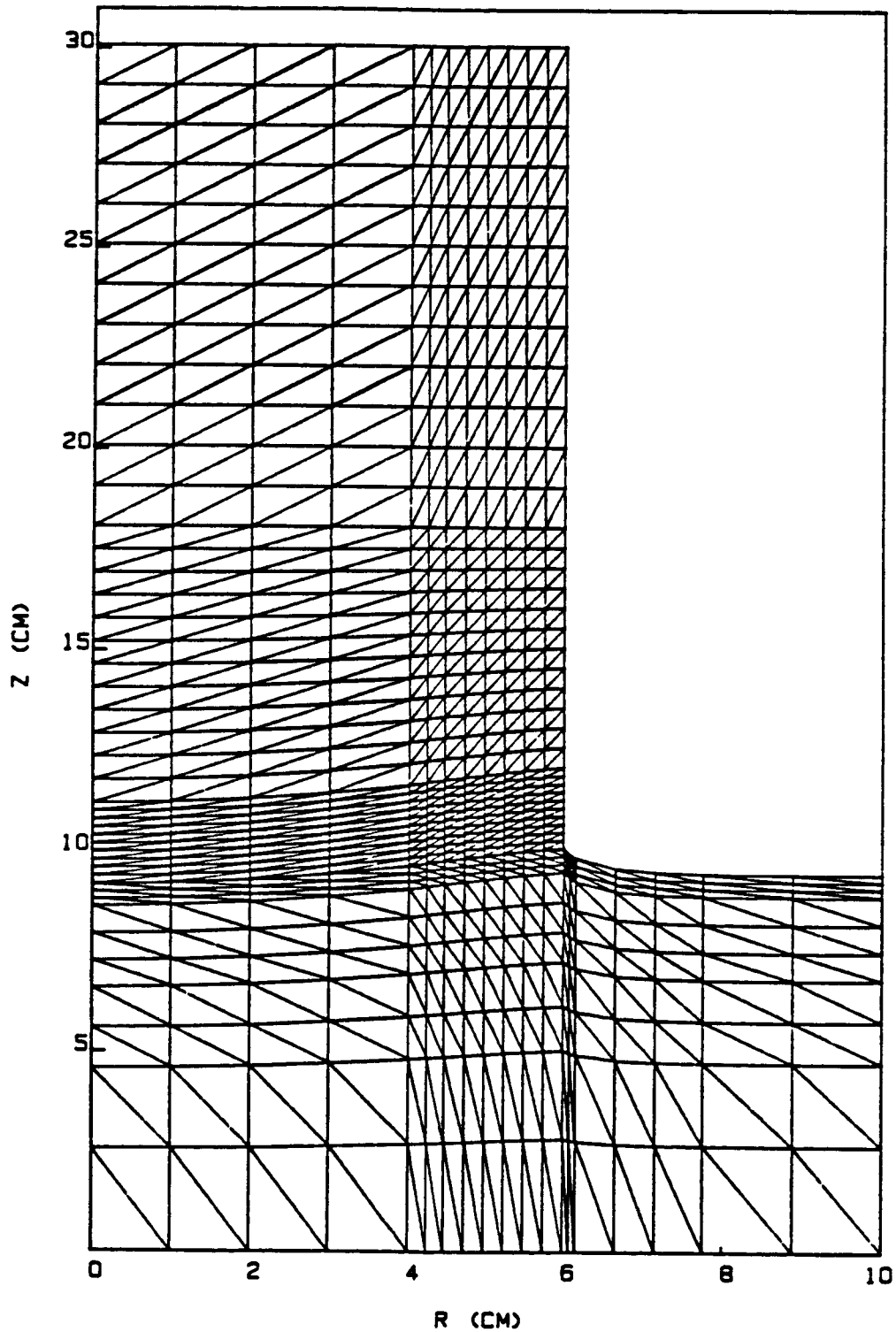
Figure 3. A Typical Finite Element Mesh with Triangular Basic
Cells for Crystal + Melt.

In brief, the overall simulation procedure is as follows:

1. Calculate the melt meniscus shape.

2. Assume a crystal-melt interface shape and calculate its location (z-coordinate) from Equation (12).

3. Calculate view factors for all the surfaces to account for slight changes resulting from the volume constraint (every 5 iterations).

4. Calculate G-factors for all the surfaces to account for the effect of temperature on emissivity (every 5 iterations).

5. Calculate $T_{e,k}$ for all the surfaces from Equation (14).

6. Do one iteration of the crystal temperature profile calculations.

7. Do one iteration of the melt temperature profile calculations.

8. Calculate Q_{si} and $Q_{\ell i}$ at the interface for each node from Equations (10a, b).

9. At this stage Equation (10) is not satisfied and therefore the pulling rate is updated and the interface is deformed such that energy balance Equation (10) is satisfied at all nodes. The procedure for doing this is discussed in Appendix 1.

10. Continue iteration (steps 3 to 9) until the temperature profiles, the interface shape and the pulling rate converge within a specified tolerance.

The delayed application of the Wegstein accelerator (after every 5 iterations) to the interface shape and the pulling rate leads to rapid convergence of the problem. The Wegstein method is a modified secant method for multivariable problems (Westerberg and Motard, 1979). Most of the simulations using this approach converged within 10 to 15 iterations. This approach also enables the easy replacement of the conduction dominated model of the melt with a more detailed model which includes other heat transport

- 22 -

effects, such as natural and forced convection as well as thermocapillary flow and the effect of a magnetic field.

The computation scheme proposed by Derby and Brown (1986) predicts the crystal diameter for a specified crystal pulling rate. It is often desirable to simulate the complete crystal growth cycle and determine the necessary crystal pulling rate adjustments as the growth takes place in order to produce an ingot of a desired diameter. Derby's and Brown's scheme (1986) is not convenient for such simulation of the complete transient behavior of the full growth cycle of the CZ process, since it solves for the crystal radius and keeps the pulling rate fixed. The other disadvantage of calculating the crystal radius at a fixed pulling rate is that the Laplace-Young equation describing the melt meniscus has to be solved simultaneously, at each iteration, along with all other model equations since the meniscus shape is a function of the crystal diameter. On the other hand, if the crystal diameter is fixed and the pulling rate estimated (as in our case) then one needs to solve the meniscus equation only once in the beginning of the simulation procedure to predict the shape of the meniscus.

IV. PARAMETRIC STUDIES

One of the objectives of this work was to study the effect of various parameters of the CZ process on the crystal-melt interface and on the pulling rate (the production rate). These results will be presented now. The physical properties such as emissivity, melting point, latent heat, thermal conductivity, etc., are set beforehand. The standard values of these properties used for simulation are listed in Table 3. The process parameters for the conduction dominated model are the following: coefficient of convective heat transfer from the crystal and melt to the gas, crystal radius, exposed crucible height, melt volume, and crucible temperature. As discussed earlier, the growth rate is not explicitly specified, because it is uniquely determined by the energy balance equation at the interface.

The effects of process parameters on the interface shape and the pulling rate were examined, because the interface shape is primarily controlled by these factors. Only one process parameter is varied at a time in order to isolate its effect on the interface shape. The values of the process parameters are listed in the Table 4. the extent of convexity or concavity of the interface shape is defined by the following parameter:

$$\Delta r = z_1 - z_{nr} = z (r = 0) - z (r = R) \qquad (17)$$

This parameter can be viewed as the measure of the deivation of the interface shape from planarity as follows:

For $\Delta r < 0$, the interface is convex and the crystal penetrates into the melt.

For $\Delta r > 0$, the interface is concave and the melt penetrates into the crystal.

TABLE 3

Values of Physical Properties Used for the Simulations

Melting Point   1693.15 K

Latent Heat   2160.0 J/cm^3

Emissivity

     Crystal   0.64 if T < 1000 K

                   $0.9016 - 2.616 \times 10^{-4} T$ if T > 1000 K

     Melt   0.30

     Crucible   0.59

     Wall   1.0

Thermal Conductivity

     Crystal $0.9889240 - 9.4286595 \times 10^{-4} T + 2.889 \times 10^{-7} T^2$, W/cm K

     Melt   0.64 W/cm K

Specific Heat

     Crystal   1.0 J/g K

     Melt   1.0 J/g K

Density

     Crystal   2.33 g/cm^3

     Melt   2.42 g/cm^3

Contact Angle   11°

Surface Tension   720 dyne/cm

TABLE 4

Values of Process Parameters Used for the Simulations

Coefficient of convective heat transfer	$1.66 \times 10^{-4} (\Delta T)^{1/4}$ W/cm^2 K
Crystal radius	3 to 9 cm
Crystal length	30 cm
Crucible radius	12 to 18 cm
Total crucible height	16 cm - 25 cm
Melt volume	4524 cm^3 6000 - 20,000 cm^3 (for Eqs. (31) & (37))
Crucible temperature	1700 - 1900 K
Wall area	1500 cm^2 30,000 cm^2 (for Eqs. (31) & (37))
Wall temperature	300 K
Average argon temperature	500 K
Nozzle diameter	0.1 cm
Aspect ratio of the jet (d/D)	60

In the following discussion the words 'more concave' also mean 'less convex'. Similarly less concave also implies more convex. All the simulations were performed using the detailed radiation model except where mentioned.

A. EFFECT OF MELT MENISCUS

To examine the effect of the melt meniscus in detail, the crystal and melt temperature profiles are simulated for both a flat and a curved melt surface for a 12 cm diameter crystal. The flat melt surface results from assuming a contact angle of 90° while the curved melt surface was generated using a contact angle of 11°. All other parameters are kept the same. The temperature profiles (isotherms) in the crystal and the melt are shown in Figures 4 and 5.

These figures reveal that the incorporation of the melt meniscus shape into the model leads to the increase in both pulling rate (from 4.1 cm/hr for a flat melt surface to 7.5 cm/hr for the curved melt surface) and to increased concavity of the interface. In fact, for the test case, the interface for the flat melt free surface is convex (less concave) (Figure 4) in contrast to a more concave interface when the melt free surface forms a meniscus (Figure 5). This is due to the following reasons:

1. Incorporation of the melt meniscus shape into the model leads to an increase in the melt depth below the crystal. The increase is of the order of 0.5 cm for this case. As explained by Kobayashi (1981), such an increase in melt depth leads to an increase in the pulling rate as well as to increased concavity of the interface. This is caused by the reduction in the axial heat transfer from the melt to the interface. This effect is also observed experimentally (Billig, 1955; Mil'Vidskii and Gotavin, 1961).

2. The formation of the melt meniscus leads to an increase in the surface area of the melt free surface, particularly near the crystal-melt interface.
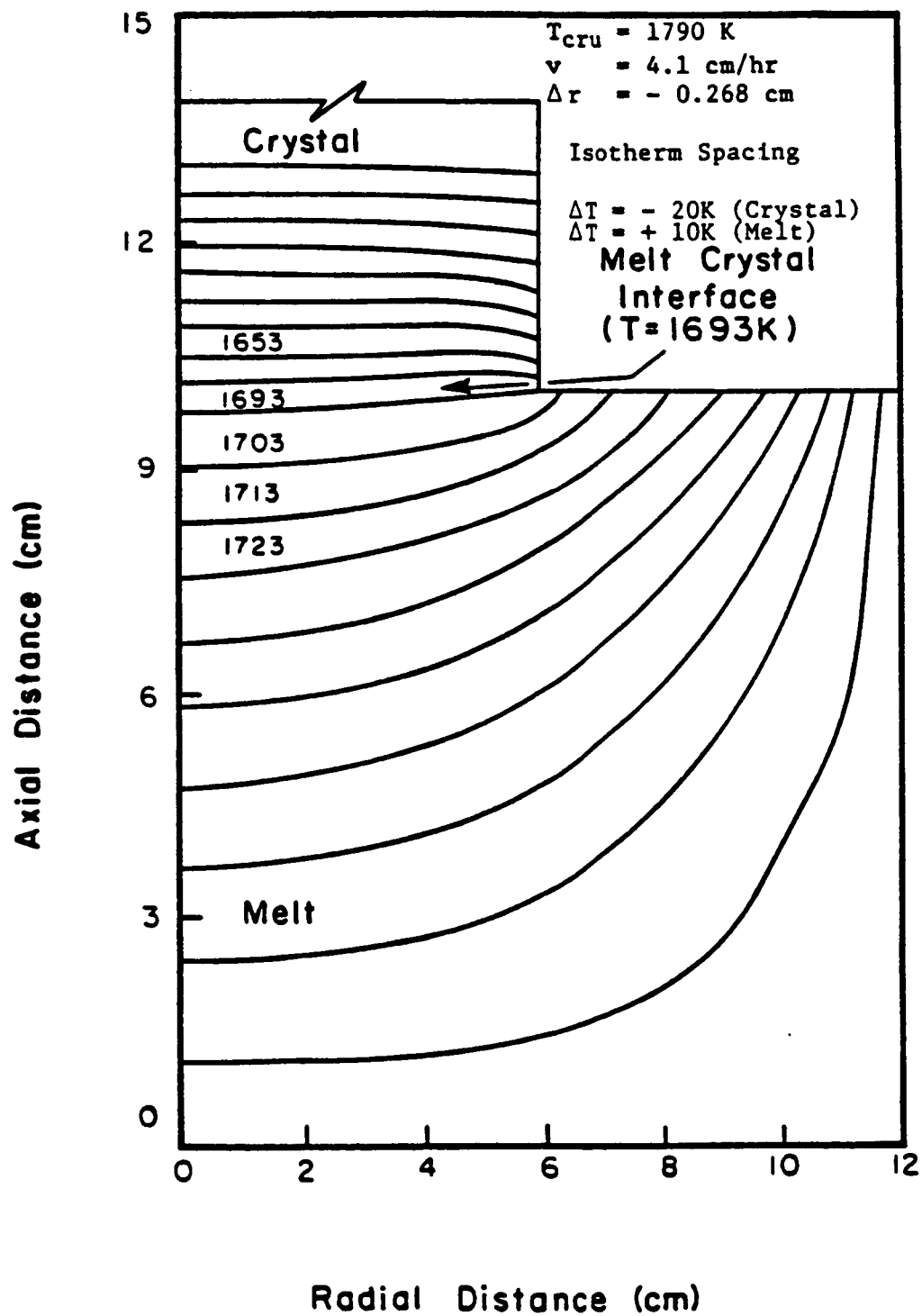
Figure 4. Temperature Field in the Crystal and Melt.
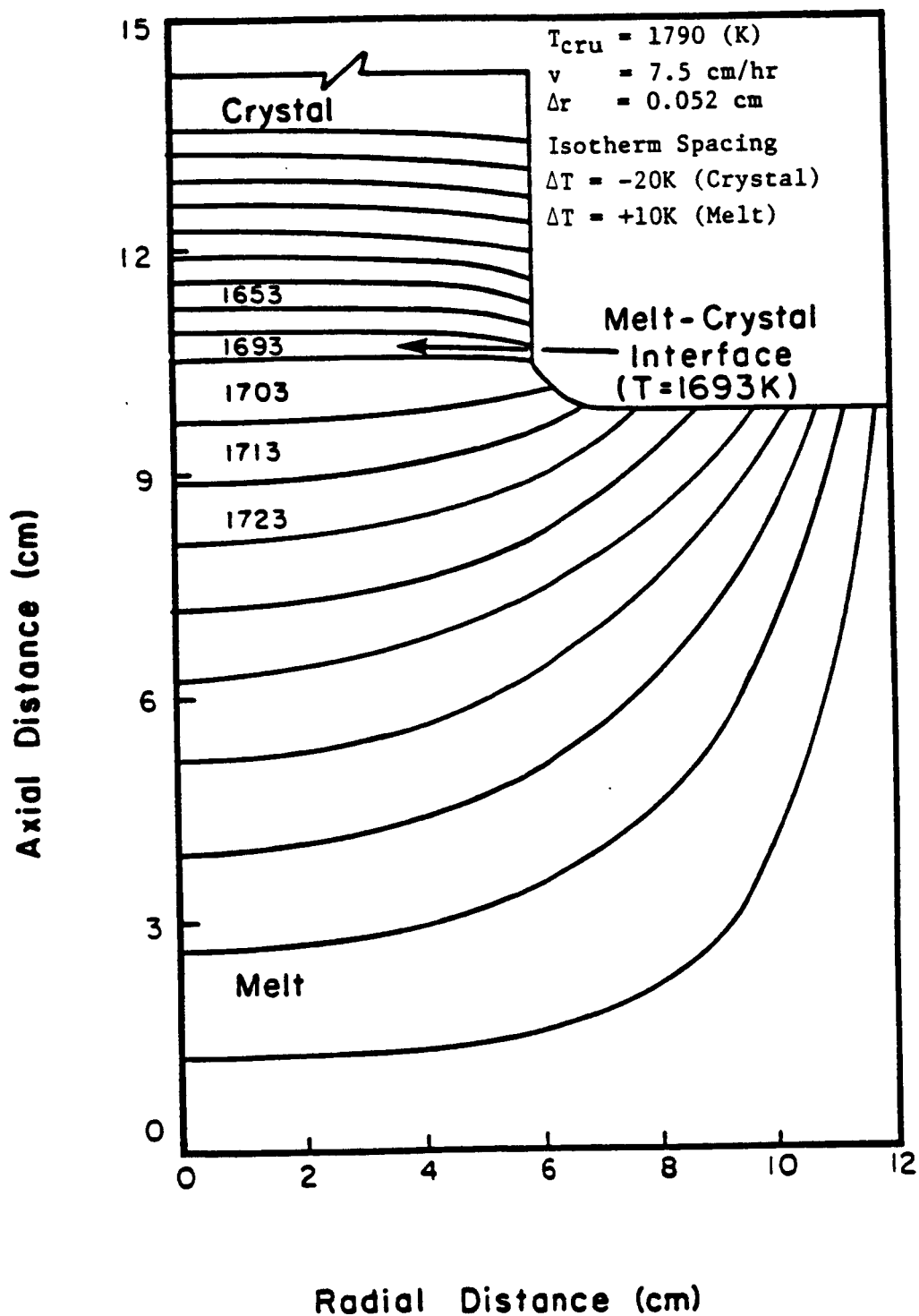(Flat Melt — Gas Interface).

Figure 5.   Temperature Field in the Crystal and Melt.
(Curved Melt-Gas Interface).

me of this area is almost 'vertical' (especially for a low contact angle of 11° such as silicon). This allows for radial heat transfer (both convection and radiation) from the melt to the surroundings near the melt-crystal interface and thus reduces the net radial heat transfer from the melt to the interface. This leads to an increase in the pulling rate and increased concavity of the interface. The flat melt free surface does not allow for any radial heat transfer from the melt to the surroundings.

Similar behavior of the pulling rate and the interface shape is observed for various crucible temperatures (see Figures 6 and 7). Brown and Derby (1986) also examined the effect of the melt meniscus on the interface shape and crystal radius. They reported an increase in crystal radius as well as increase in concavity of the interface due to the melt meniscus at a fixed pulling rate. This is equivalent to an increase in pulling rate at a fixed crystal diameter as shown here. It appears that the melt meniscus has a considerable effect on the heat transfer near the interface especially for silicon due to the small contact angle. Thus, the simplifying use of a flat melt free surface leads to erroneous results.

B. EFFECT OF CRUCIBLE TEMPERATURE

The interface shape is shown as a function of crucible temperature for both flat and curved melt-free surfaces in Figures 6 and 7, respectively. To avoid clustering of the results the y axis is not the same for curves 1 to 5. The proper y axis for each of the various cases is defined by the parameter H in these figures. This shifting of the y axis for each curve applies to the other figures as well and lends clarity to the presentation of the figure. In both cases, for flat and curved meniscus, the interface shape changes from concave to convex as the crucible temperature is increased. This is due to the following two factors:
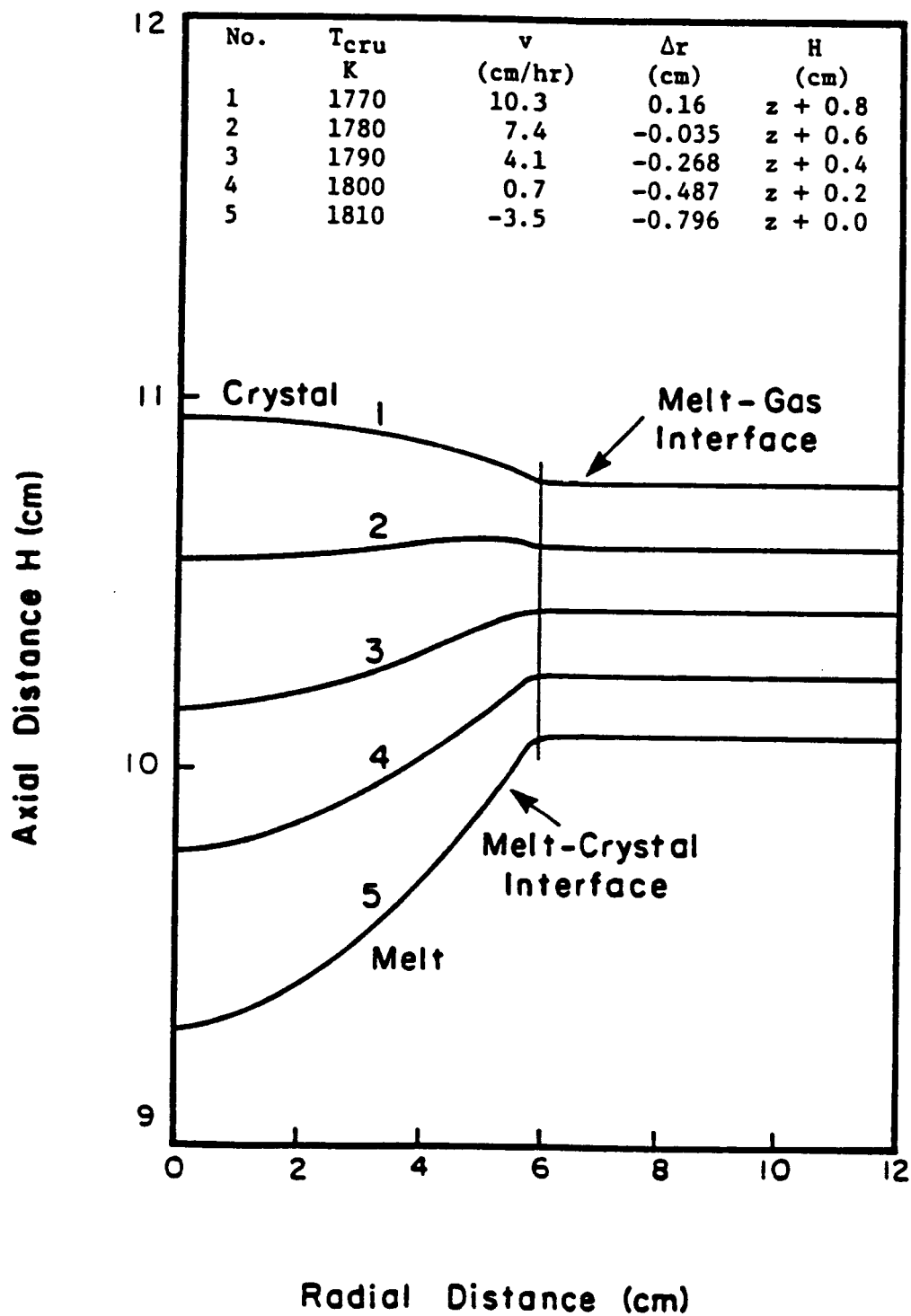
No.	T_{cru} K	v (cm/hr)	Δr (cm)	H (cm)
1	1770	10.3	0.16	z + 0.8
2	1780	7.4	-0.035	z + 0.6
3	1790	4.1	-0.268	z + 0.4
4	1800	0.7	-0.487	z + 0.2
5	1810	-3.5	-0.796	z + 0.0

Figure 6. Effect of Crucible Temperature on Interface Shape.
(Flat Melt- Gas Interface).

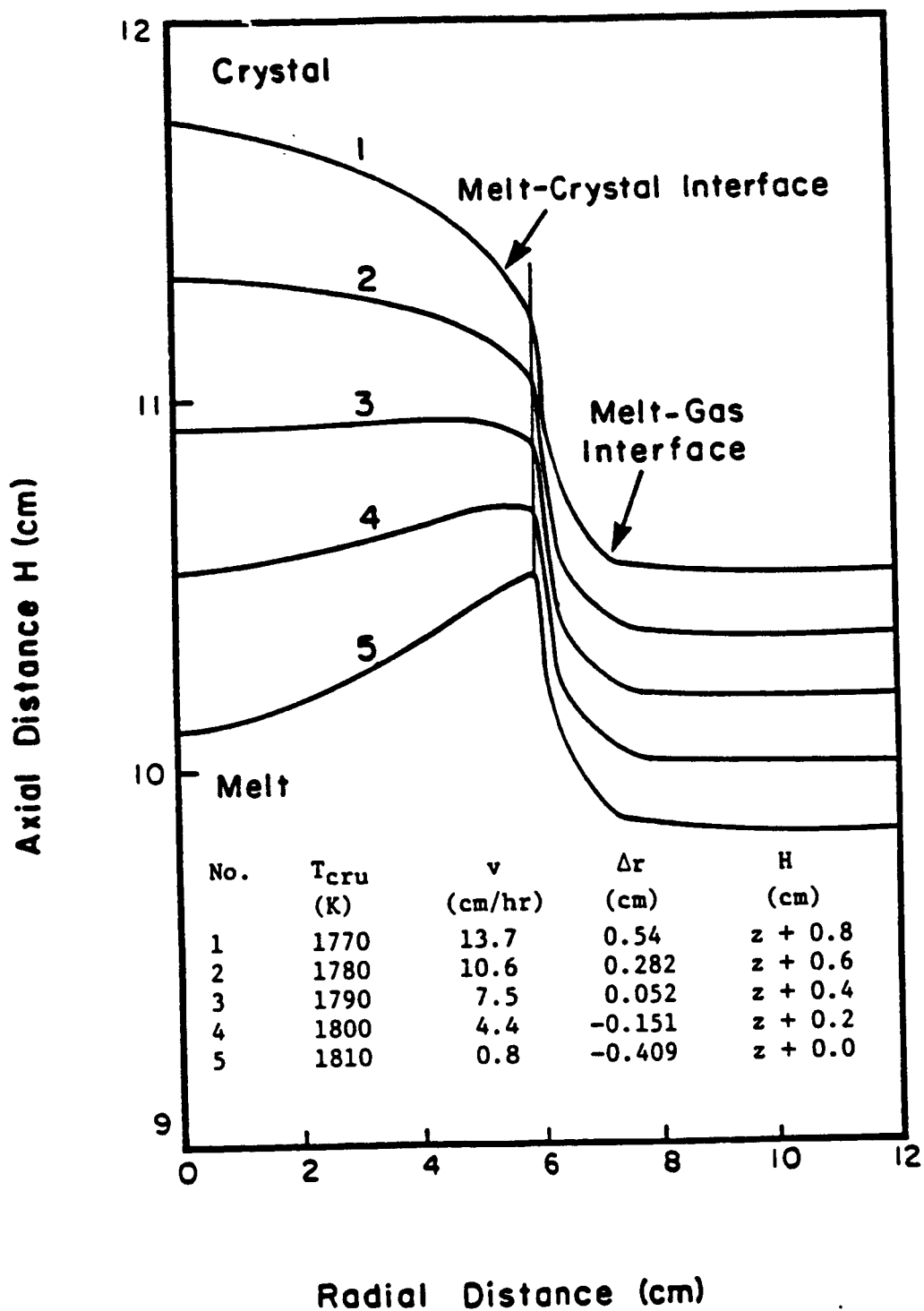| No.	T_{cru} (K)	v (cm/hr)	Δr (cm)	H (cm)
1	1770	13.7	0.54	z + 0.8
2	1780	10.6	0.282	z + 0.6
3	1790	7.5	0.052	z + 0.4
4	1800	4.4	-0.151	z + 0.2
5	1810	0.8	-0.409	z + 0.0

Figure 7. Effect of Crucible Temperature on Interface Shape.
(Curved Melt— Gas Interface).

1. A higher crucible temperature leads to an increase in the radial heat transfer from the melt to the interface i.e., to an increase in isotherm slope.

2. At a higher crucible temperature radiative heat losses from the crystal portion near the interface are decreased, and heat transfer in the crystal in the vicinity of the interface becomes mainly axial. This is due to the significant radiation interchange between the exposed portion of the crucible wall and the lower part of the crystal. These two factors force the crystal to penetrate into the melt and lead to an increasingly convex interface as the crucible temperature increases. In addition, the increased crucible temperature requires a reduction of the pulling rate if the crystal diameter is to remain constant, as shown in Figures 6 and 7. The diminishing growth rate is again caused by the two factors mentioned above. Negative growth rate, implying the remelting of the crystal for a flat melt surface (Figure 6) at a high crucible temperature (1810 K) is predicted. In this case, the heat transfer from the melt to the interface overcomes the axial heat dissipation from the interface to the crystal, leading to the remelting of the crystal. At high crucible temperatures, excessive radial heat transfer from the melt to the interface takes place and at the same time radiative heat losses from the crystal portion in the vicinity of the interface are significantly reduced due to the radiative exchange with the exposed crucible wall. Remelting does not occur at this crucible temperature (1810 K) when the melt interface (meniscus), is curved as shown in Figure 7. The thin layer of the melt at the meniscus allows sufficient radial heat transfer from the melt to the surroundings so that no remelting occurs. Higher crucible temperatures would be required for remelting. The effect of crucible temperature on the interface shape

can also be explained qualitatively on the basis of the dimensionless group ψ introduced in the paper by Ramachandran and Duduković (1985). This parameter represents the dimensionless heat flux to the interface and can be defined for the present problem as:

$$\psi = \frac{[- k_\ell \, (\frac{dT}{dn})_{interface} + v \, \rho_s \Delta H] \, R}{k_s \, [T_m - T_a]}$$

(18)

Ramachandran and Duduković (1985) showed that any decrease in parameter ψ tends to make the interface more convex. An increase in crucible temperature increases the first term of the RHS of Equation (18), while the simultaneous decrease in the pulling rate necessary to keep the same diameter decreases the second term. The result of these two opposing effects is a net decrease in the parameter ψ with the increasing crucible temperature. This makes the interface more convex as shown in Figures 6 and 7.

C. EFFECT OF CRYSTAL RADIUS

Interface shapes for various crystal radii at the crucible temperature of 1800 K are shown in Figure 8. The degree of concavity increases first with increasing crystal radius up to a radius of 3.0 cm, and then rapidly decreases as the crystal radius approaches the crucible radius. For a larger crystal radius (7.5 cm), the interface shape is highly convex, because the radial heat transfer from the melt to the interface becomes significant. In addition, the view factor from the crucible wall to the crystal increases significantly (since crucible radius is used in the simulations). The result is similar to the effect of an increased crucible temperature, namely, the transition from increasing concavity to increasing convexity of the interface also depends on the
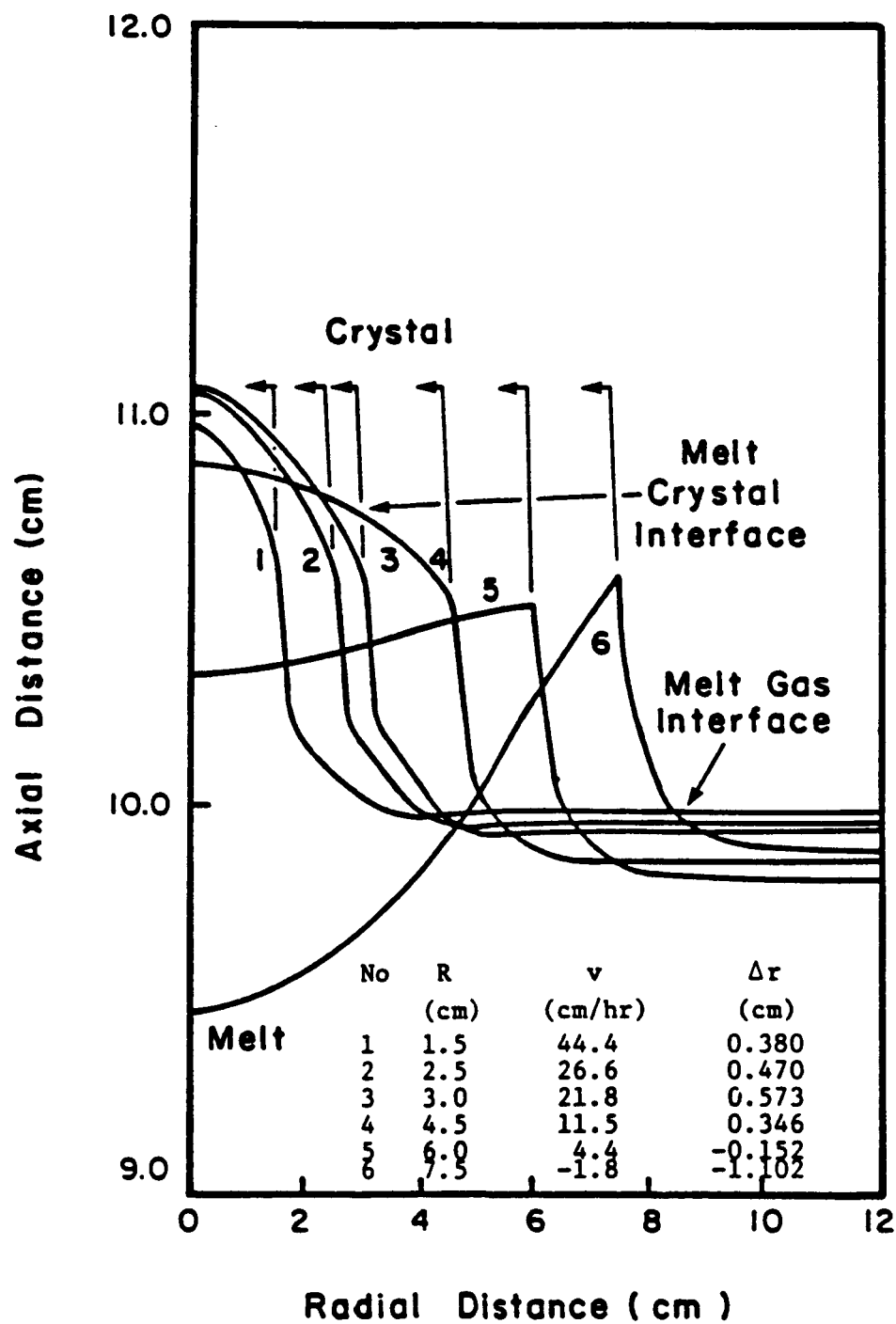
Figure 8. Effect of Crystal Radius on Interface
Shape.

crucible temperature. For high crucible temperatures, the transition will occur at a smaller crystal radius since the radial heat transfer rapidly increases with the increasing crucible temperature.

The increasing concavity of the interface shape, up to the radius of 3.0 cm, can be explained on the basis of the increasing Biot number. The earlier work of Wilcox and Duty (1966) showed that the interface shape becomes more concave as the Biot number is increased provided the pull rate is also simultaneously adjusted in order to keep a constant radius.

However, for larger crystal radii, the Biot number is no longer a measure of the interface shape, since the radial gradients in the melt become significant, and the crystal portion near the interface starts absorbing radiative heat from the exposed crucible wall. Experimentally, as the crystal radius is increased, the interface shape becomes less concave and sometimes changes from concave to convex (Inoue, 1976; Brice, 1973). This is in agreement with the theoretical predictions.

D. EFFECT OF EXPOSED CRUCIBLE WALL

The exposed crucible wall plays an important role in the crystal growth process in a batch CZ puller. The effect of the crucible wall continuously increases as the growth proceeds, since more and more area of the crucible wall is exposed to the crystal as the melt level drops. Basically the exposed crucible wall reduces the crystal capacity to lose heat by radiation in the vicinity of the interface. This phenomenon is best studied by defining the radiation heat transfer efficiency of the crystal side surface as follows:

$$\text{efficiency } (\eta) = \frac{\text{actual heat exchange by radiation}}{\text{maximum possible heat loss by radiation}} \tag{19}$$

$$= \frac{\sigma \varepsilon \, (T^4 - T_e^4)}{\sigma \varepsilon \, T^4}$$

- 36 -

where T_e is the effective temperature for radiative heat loss at any position of the crystal surface as defined by Equation (14).

In Figure 9 the radiation efficiency of the crystal side surface is shown for various heights of the exposed crucible wall. The radiation efficiency rapidly becomes smaller as the crucible wall exposed height, h_c, increases. For h_c greater than 5.5 cm the efficiency becomes negative over a region close to the interface. In this region the crystal is receiving heat by radiation rather than losing heat. This significantly hampers the growth rate of the crystal. As expected an increase in h_c leads to decreasing growth rate of the crystal and increasing convexity of the interface. The results obtained here are similar to the results of Arizumi and Kobayashi (1981).

E. COMPARISON WITH THE SIMPLE RADIATION MODEL

The results obtained by using the detailed radiation model, (Gebhart's model) incorporating direct and reflected radiation, were compared with the simple radiation model (Stefan's model). The crystal surface temperatures obtained for the Gebhart's model and for the Stefan's model for several assumed effective radiative temperatures in the heat loss term from the crystal (see Equation 15)) are shown in Figure 10. An attempt was made to match the calculated crystal temperature profile based on Gebhart's method by the appropriate choice of the effective temperature in the simple Stefan's model. The entire temperature profile cannot be matched using a single value for the effective temperature in the simple model. Low values of effective temperatures (such as 500 K) can match the temperature in the top region; however, a very high crystal growth rate as well as a highly concave interface shape is predicted for this situation. The match near the interface is also very poor. On the other hand, high

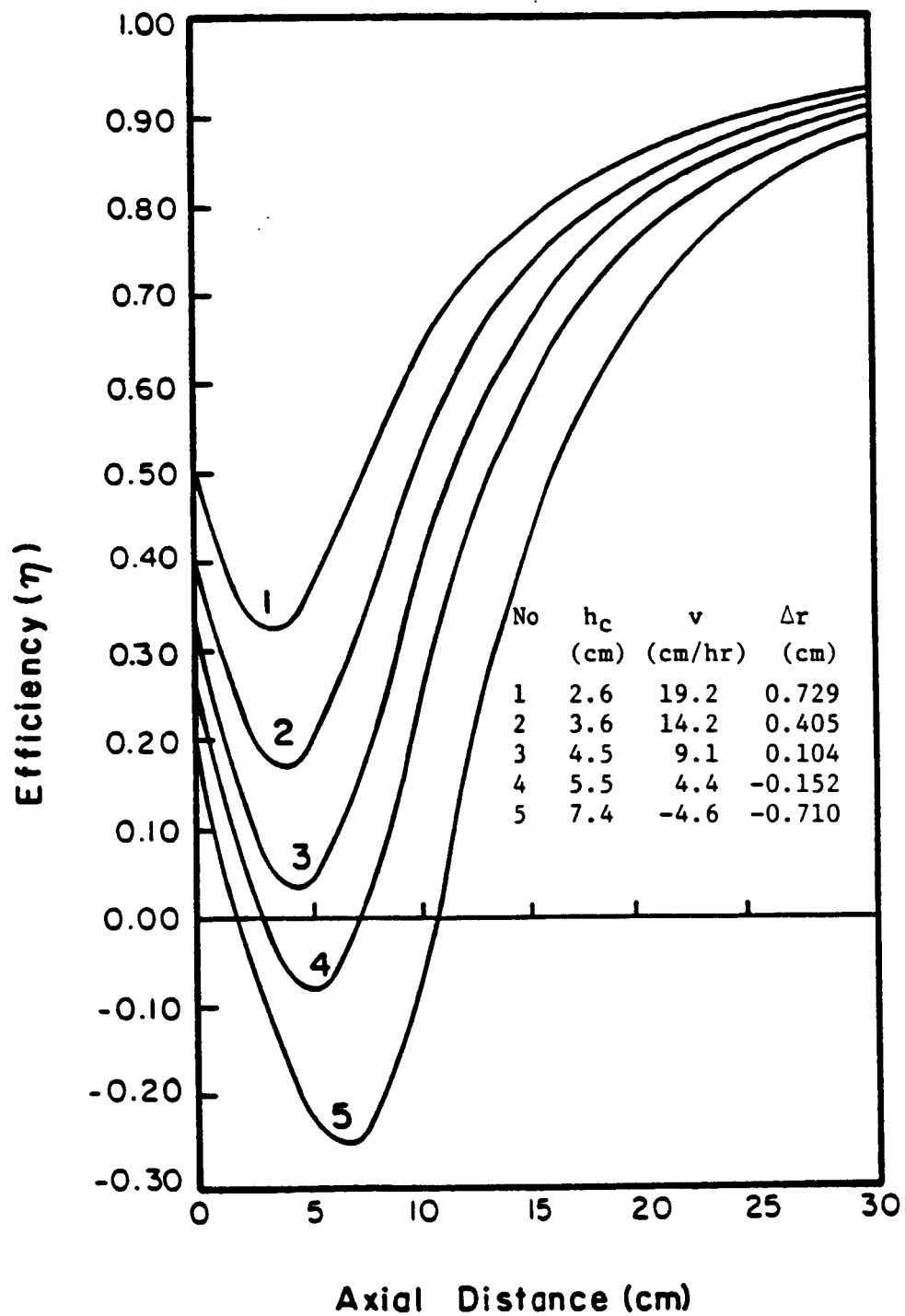| No	h_c (cm)	v (cm/hr)	Δr (cm)
1	2.6	19.2	0.729
2	3.6	14.2	0.405
3	4.5	9.1	0.104
4	5.5	4.4	-0.152
5	7.4	-4.6	-0.710

Figure 9. Efficiency of Radiation of the Crystal
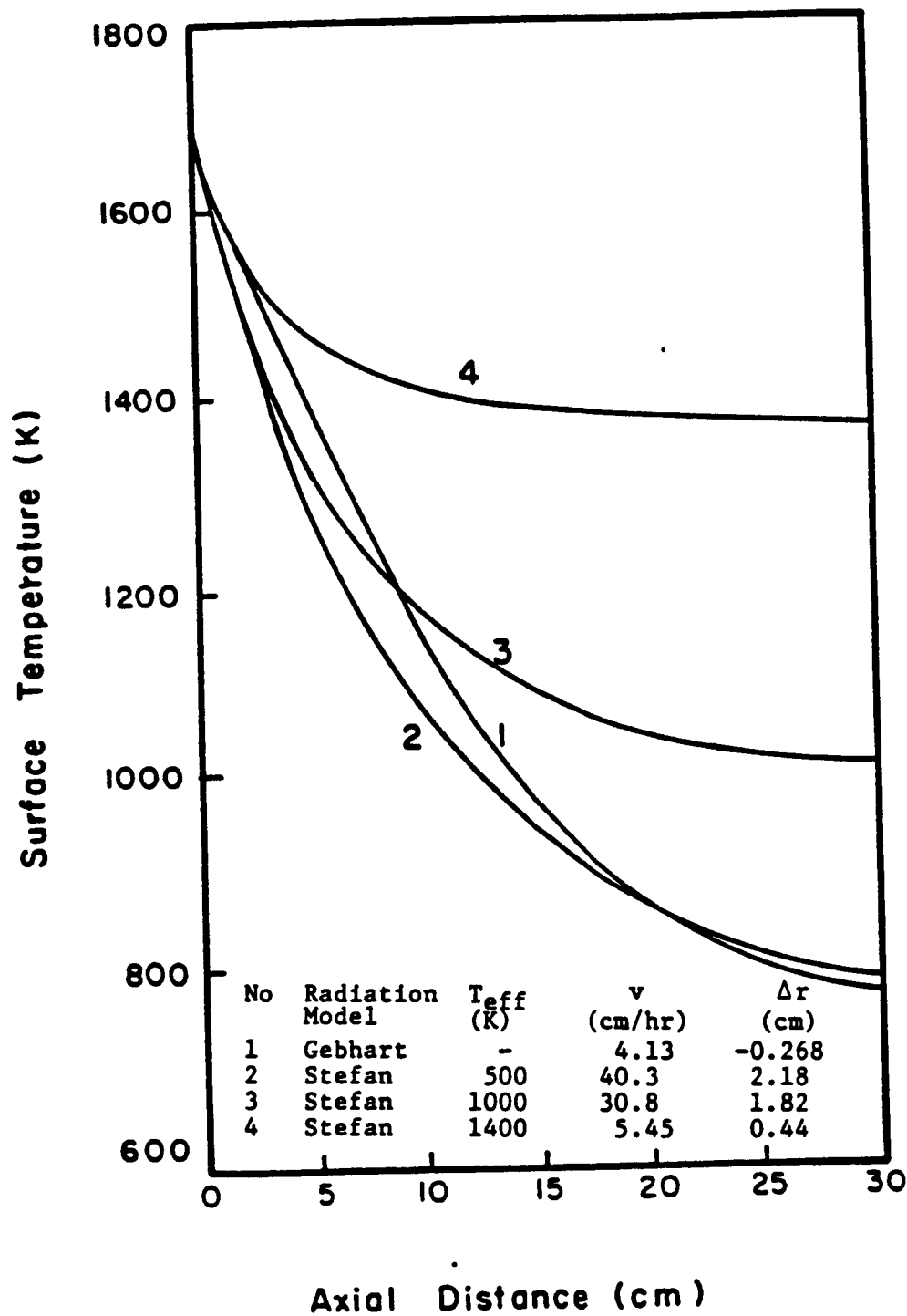Side Surface.

Figure 10.   Temperature Profile on Crystal Surfaces:
Effect of Radiation Interactions.

effective temperatures (such as 1400 K) can match the profile near the interface and predict the growth rates to a reasonable extent, but higher temperatures are predicted in the top region. In either case, it is not possible to match the interface shape. It appears that a linearly increasing effective temperature from the crystal top to the bottom should be used to predict the thermal behavior of the crystal if a simple radiation model is to be used. In any case, such an approach loses its predictive abilities and the detailed model, which includes all the radiation interactions, is to be recommended for correlating experimental data.

The details of this work are also presented in our recent publication (Srivastava, et. al., 1985).

V. DEVELOPMENT OF SIMPLE MODELS

In addition to the detailed modeling studies there is considerable incentive to develop a simple correlating equation for predicting the pulling rate and the interface shape. Although several studies of the hydrodynamic and heat transfer problems including modeling are underway, very little attention has been focused on developing some simple models or empirically correlating the results in terms of important process parameters of the system.

It is well established that the thermal environment changes continuously as the crystal growth takes place. This is due to the effects of the diminishing melt level and the increasing height of the exposed crucible wall. Thus, the pulling rate and the crucible temperature need to be adjusted to grow crystals of uniform diameter with a nearly planar interface. The detailed models coupled with the finite element solution technique cannot readily be used on-line with the growth process to predict the changes in the pulling rate and the crucible temperature required for strict control of crystal diameter and interface shape, since these models are fairly complex and require an excessive amount of computing time due to a convergence problem. Hence, the development of a simple model to represent the system is desireable. Kim et. al. (1983) at IBM have proposed a simple mathematical model, which describes the different crystal growth phases including neck-in, shoulder growth and constant diameter bulk growth. This model basically correlates the crystal diameter with the pulling rate and the crucible temperature using two parameters. Experimentally, they observed that the crystal radius, R, is inversely proportional to the crystal pulling rate, v, and the temperature difference ΔT of the system. Here ΔT is the difference between the crucible wall temperature, T_c, and the

melting point, T_m, of the crystal. On this basis they proposed the following relationship:

$$R = \frac{1}{v + A} + \frac{B}{\Delta T} \qquad (20)$$

where A and B are constants determined from the experimental data. These authors were able to match this model with the actual operating data. However, this model has limited utility because it is based on a single set of operating conditions and does not account for the decreasing melt level and the increasing height of the crucible wall during the growth cycle, both of which have significant influence on the growth rate and the interface shape. Further, no model or correlation was proposed for the prediction of the interface shape.

The objective of this part of the study was to develop a simple model, based on semi-quantitative arguments, which can predict both the pulling rate and the interface shape as a function of the important process variables of the system. The development of the model is based on first principles of heat transfer and energy balance considerations. The accuracy of the simple model is compared with results obtained from the finite element solution of the detailed model described in Section III and in the reference (Srivastava et. al., 1985b).

In the following sections, first a simple model is proposed and tested with a large set of data over a wide range of operating conditions encountered during the growth process. The model is further updated to account for various other effects in the system. The operating conditions used for this study are given in Tables 3 and 4. Although the form of the equations developed in this study are general, the empirical constants evaluated are applicable only to the data of Tables 3 and 4.

A. MODEL FOR GROWTH RATE

1. Equation Development

The solidification of the melt to form the crystal takes place at the crystal-melt interface. Therefore, the growth rate of the crystal is governed by the heat balance consideration at the interface. The heat balance at the interface is as follows:

$$\Delta H \frac{dm}{dt} = Q_c - Q_m \tag{21}$$

where

dm/dt = rate of solidification of melt at the interface $\alpha\ vR^2$

Q_c = rate of heat loss from the interface

     = rate of heat loss from the crystal side surface $\alpha\ R$

Q_m = rate of heat input to the interface from the melt $\alpha\ R^2\Delta T$

Hence, the following relationship is obtained between the v, R and ΔT:

$$v = \frac{A}{R} - B\Delta T \tag{22a}$$

This relationship implies that the pulling rate is inversely proportional to the crystal radius, R, and directly proportional to $\Delta T = T_c - T_m$. This is similar to the experimental results of Kim et. al., (1983). Further, when $\Delta T = 0$, the melt is maintained uniform at its melting point temperature and under these conditions the maximum pulling rate is obtained.

$$v_{max} = \frac{A}{R} \tag{22b}$$

Equation (22a) neglects the heat losses from the crystal top surface and the melt free surface. Further, the heat loss from the crystal side surface, Q_c, is assumed to be proportional to R. This implies that the crystal surface temperature is weakly dependent on the crystal radius.

Based on a one-dimensional model of a long crystal, Billig (1955) showed that the temperature gradient at the interface is inversely proportional to the square root of crystal radius. Therefore, according to Billig we have

$$Q_c \propto \pi R^2 \left(\frac{dT}{dz}\right) \text{ and } \frac{dT}{dz} \propto R^{1/2} \text{ so that } Q_c \propto R^{3/2} \tag{23}$$

This analysis implies that the crystal surface temperature increases in proportion to the square root of the crystal radius. Then, Equation (22a) has the following form if the analysis of Billig is used.

$$v = \frac{A}{\sqrt{R}} - B\Delta T \tag{23a}$$

and the maximum pulling rate is

$$v_{max} = \frac{A}{\sqrt{R}} \tag{23b}$$

The analysis of Billig thus implies that the growth rate is inversely proportional to the square root of the crystal radius. The question is whether Equation (22a) or (23a) provides a suitable starting point for correlating experimental data for CZ growth. It will now be shown by comparison with a detailed model that Equation (22a) provides a more suitable model. It may also be noted that Equation (22a) provides the same dependency on radius as predicted by Kim et. al. (1983) although the actual model equations are different. (Compare Equation (20) and (22a)).

2. Verification of the Model

The simple models described by Equations (22a) and (23a) are now compared with the results of the detailed model to check their accuracy. For this purpose the simulations were carried out over a wide range of crystal radii (3 to 9 cm) and crucible temperatures (1760 to 1800 K). The crucible radius was kept constant at 12 cm.

Figure 11 shows the variation in pulling rate with changes in crucible temperature at various crystal radii. As expected, the pulling rate varies linearly with ΔT at all the crystal radii. The accuracy of the linear approximation is also given in Figure 11 for all the crystal radii. Therefore, at a constant crystal radius

$$v = v_{max} - B\Delta T \tag{24a}$$

Here v_{max} is the value of the maximum pulling rate and B is the corresponding constant in Equation (22a) or (23a). Further, note from the tabular inset in Figure 11 that B varies considerably with the crystal radius. The variation of v_{max} and B with respect to the crystal radius R is discussed next in order to complete the model equation.

First, as required by Equation (22b) and (23b), respectively, v_{max} is fitted with respect to $1/R$ and $1/\sqrt{R}$, to determine the constant A. The results are given in Figure 12. The relationship of Equation (22b) fits the data much better than the relationship of Equation (23b). The maximum deviation in the pulling rate is only 5 cm/hr for Equation (22b) compared to the maximum deviation of 21 cm/hr for Equation (23b). Also the value of the root mean square deviation (variance) is much lower when the data is fitted with respect to $1/R$. Based on this analysis, we conclude that the pulling rate is inversely proportional to the crystal radius. Similar conclusions have been reported earlier by Derby and Brown (1986); and Derby et. al. (1985). We, therefore, use Equation (22a) for further discussion in this report.

A new feature of the extensive comparison of the simple model and the detailed numerical solution is the finding that constant B depends on crystal radius. Figure 12 gives the variation of B with R. The
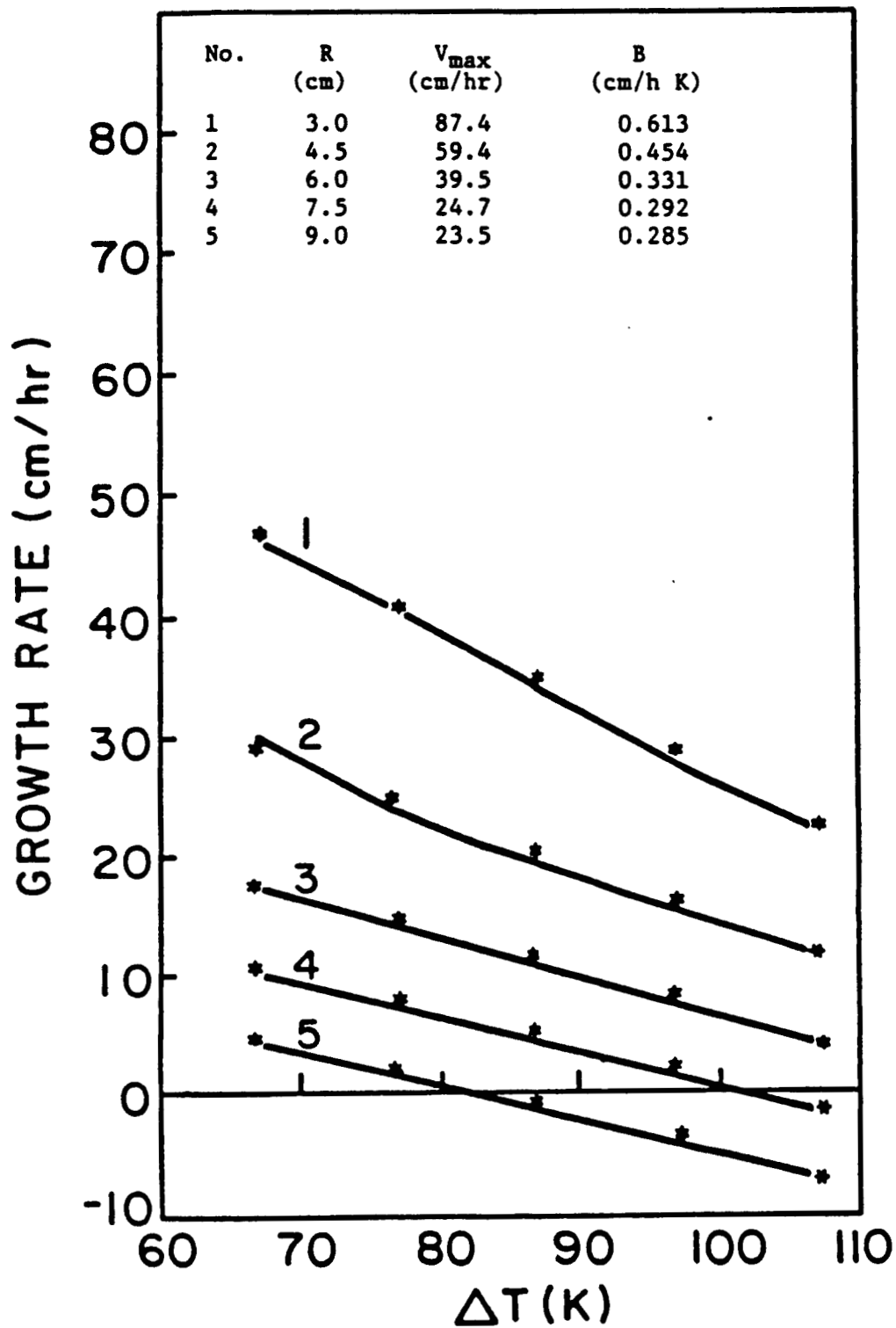
- 45 -

Figure 11.   Variation of Growth Rate with Respect to Crucible
             Temperature. ____ : Detailed Model;
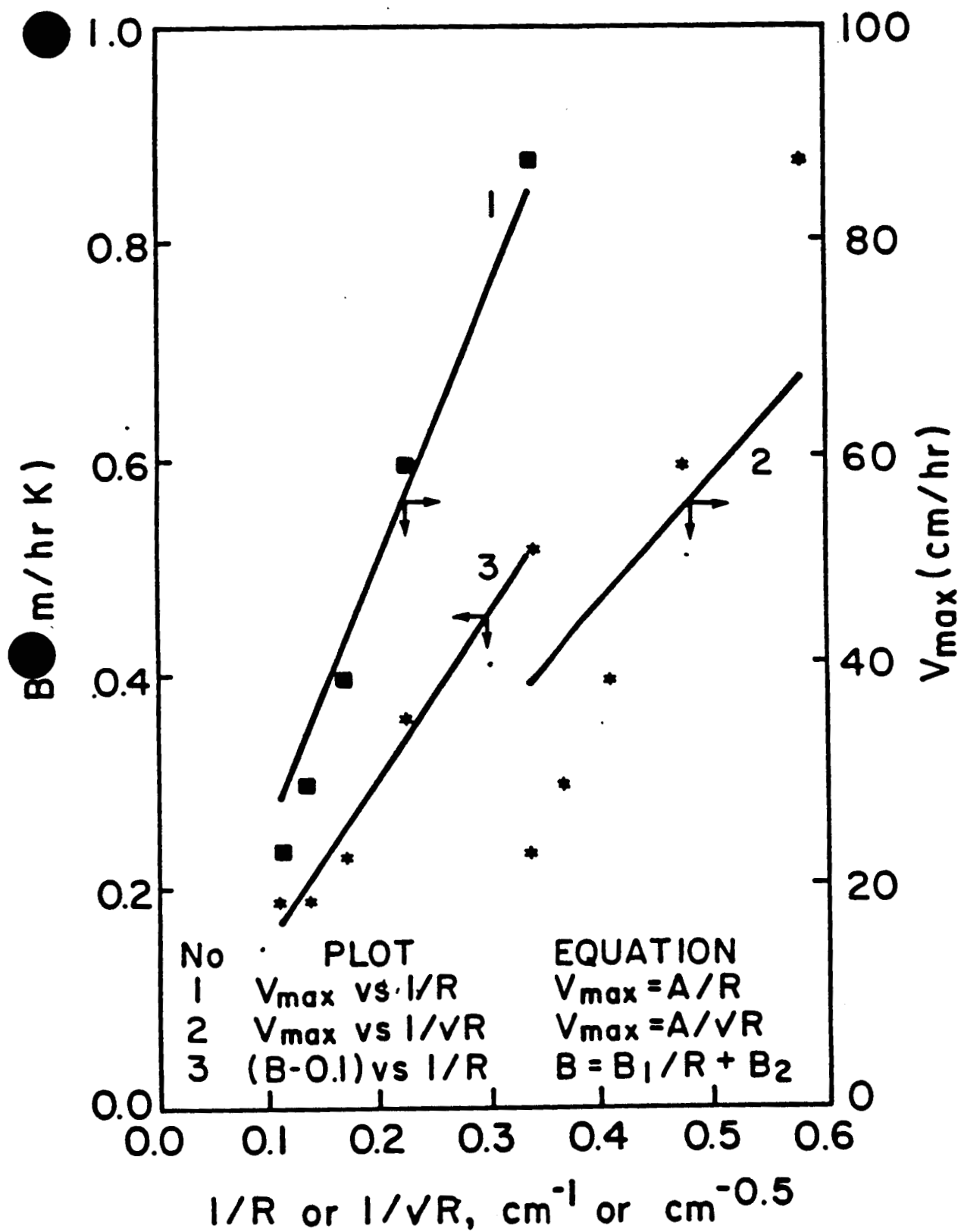   **: Linear Model.

Figure 12. Variations of V_{max} and B with Crystal Radius.
____ : Simple Model; ■ ,*: Detailed Model
Numerical Solution.

- 47 -

dependency of B on R can be fitted with the following form (see Figure 12):

$$B = \frac{B_1}{R} + B_2$$

Therefore, Equation (22a) is reduced to the following form:

$$v = \frac{A}{R} - \frac{B_1 \Delta T}{R} - B_2 \Delta T \tag{25}$$

Equation (25) can be explained on the basis of heat transfer from the exposed portion of the crucible wall to the crystal. As established by the earlier studies of Kobayashi and Arizumi (1972) and Srivastava et. al. (1985), the crucible wall plays the role of an after heater and impairs the heat losing capacity of the crystal. In our simulations, the height of the exposed portion of the crucible wall, h_c, was kept constant at 6 cm. Heat gained by the crystal from the crucible wall can be assumed to be proportional to ΔT (the difference between the crucible temperature and the melting point of the crystal) and to the radius of the crystal. The net heat loss from the crystal side surface will then be

$$Q_c \, \alpha \, (R - \beta R \Delta T)$$

where β is a numerical constant which includes physical properties, and other design parameters. The first term on the right hand side describes the heat loss from the crystal to the surroundings and the second term accounts for the heat received by the crystal from the hot crucible wall.

The above form of Q_c can be shown to yield a relationship for the pulling rate of the form of Equation (25). The parameters A, B_1 and B_2 were then re-estimated simultaneously by a least-squares technique using the entire set of data. The values obtained are:

$A = 252 \text{ cm}^2/\text{hr}; \ B_1 = 1.036 \text{ cm}^2/\text{hr/K}; \ B_2 = 0.188 \text{ cm/hr/K}$

3. Effects of Crucible Wall and Melt Level

The model developed up to this point neglects the changes in the melt level and in the exposed height of the crucible wall during the growth. The model is modified as follows to include these effects.

The crystal growth in the Czochralski process takes place in the batch mode. Therefore, as the crystal grows the melt level drops continuously and correspondingly the height of the exposed portion of the crucible wall increases. The decreasing melt level results in increasing axial heat transfer from the melt to the interface and at the same time the increasing height of the crucible wall impairs the ability of the crystal to lose heat, since now a larger section of the crystal is surrounded by the crucible wall. On the other hand, the increasing crystal length provides for a larger heat transfer area. However, the effect of increasing crystal length on the pulling rate and the interface shape is small, (Kobayashi, 1981; Srivastava et. al., 1985), since major heat transfer activity takes place near the interface. Therefore, the net effect of decreasing melt level, coupled with the increasing height of the exposed crucible wall, is the reduction in the growth rate. Therefore, if the crystal is being grown at constant pulling rate the crucible temperature needs to be lowered progressively to offset the effects of the depleting melt level and increasing height of the exposed crucible wall. Then, the growth rate is balanced with the pulling rate and the crystal diameter can be kept constant. A few modifications of Equation (25) are proposed in order to incorporate these effects.

The variation in the pulling rate with the height of the exposed portion of the crucible wall at constant melt level is presented in

- 49 -

Figure 13. The relationship between the pulling rate and h_c is linear.
This linear relationship has also been reported by Kobayashi (1975).
This is because the heat received by the crystal can be considered to
be proportional to $Rh_c\Delta T$. Note that h_c is also the length of the crystal
which is surrounded by the crucible wall at temperature T_c. Therefore,
the net heat loss from the crystal is

$$Q_c \propto (R - \beta'Rh_c\Delta T)$$

and Equation (25) can be updated to include the effects of the exposed
crucible wall.

$$v = \frac{A'}{R} - \frac{B_1'h_c\Delta T}{R} - B_2'\Delta T \qquad (26)$$

Figure 13 also shows the required changes in the pull rate with
decreasing melt level as predicted by the rigorous model. Other para-
meters are kept constant to isolate melt level effects on the pulling rate.
In Figure 13, at high melt level (initial growth period) the effect on the
pulling rate is small, however, at lower values of the melt level the
growth rate drops rapidly with the diminishing melt level. This variation
of v with respect to h can be approximated by the following equation:

$$v = c_1 - \frac{c_2}{h} \qquad (27)$$

Equation (27) fits well the data in Figure 13. The second term in Equation
(27) describes the heat transfer from the melt. It appears that the rate
of heat transfer from the melt to the interface can be considered to be
inversely proportional to the melt level, h. This is consistent with heat
conduction theory.

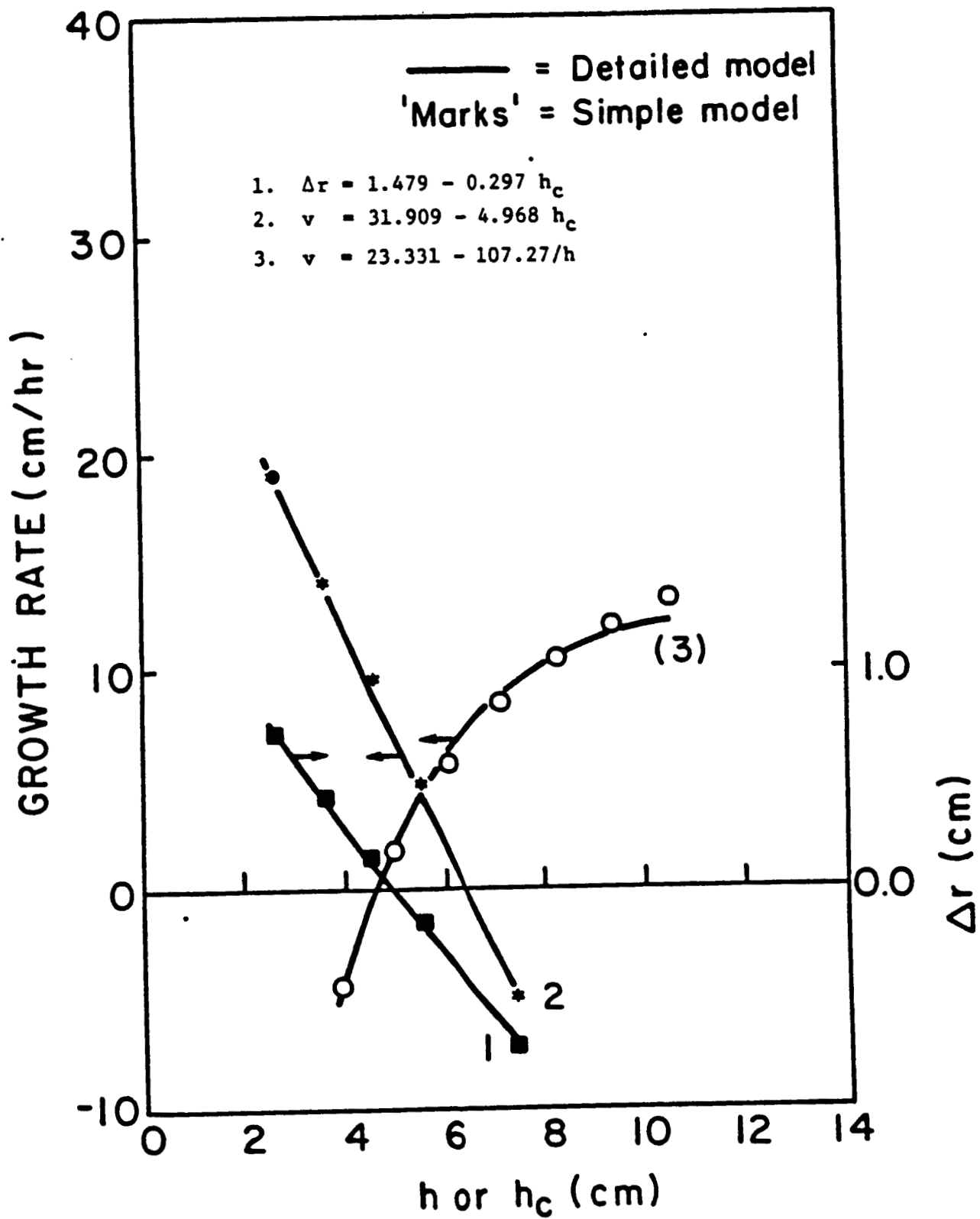In order to develop a simple model which is valid over the entire

Figure 13.   Variation of Growth Rate with h and h_c and
Variation of Interface Shape with h_c.

growth cycle, the influence of the melt level (or melt volume) and the effect of the height of the exposed crucible wall were compared. This should determine which effect is the dominant one. In the first set of computations h_c was arbitrarily kept constant at 6 cm regardless of the melt volume. The variation of the melt volume did not produce significant changes in the pulling rate as shown by the dotted lines in Figure 14. In the second set of computations the height of the exposed crucible wall was changed simultaneously with the melt volume as required by the mass balance shown below.

$$h_c = \frac{1}{\pi R_c^2} (V_c - V_m) \tag{28}$$

Here V_c is the volume of the crucible and R_c is the radius of the crucible. These results are shown as solid lines in Figure 14. It is evident that the effect of the melt level can be neglected in developing a simple model and only the effect of the exposed crucible wall height needs to be included. It is, however, more convenient to express Equation (26) in terms of melt volume.

$$v = \frac{A'}{R} - \frac{B_1'}{\pi R_c^2} \left(\frac{V_c - V_m}{R} \right) - B_2' \Delta T \tag{29}$$

For a fixed crystal radius this is reduced to the form below:

$$v = \alpha_1 + \alpha_2 V_m \Delta T - \alpha_3 \Delta T \tag{30}$$

It should be emphasized that in Equation (30) the term V_m really represents the effect of the exposed portion of the crucible wall and not the direct effect of the changing melt volume.

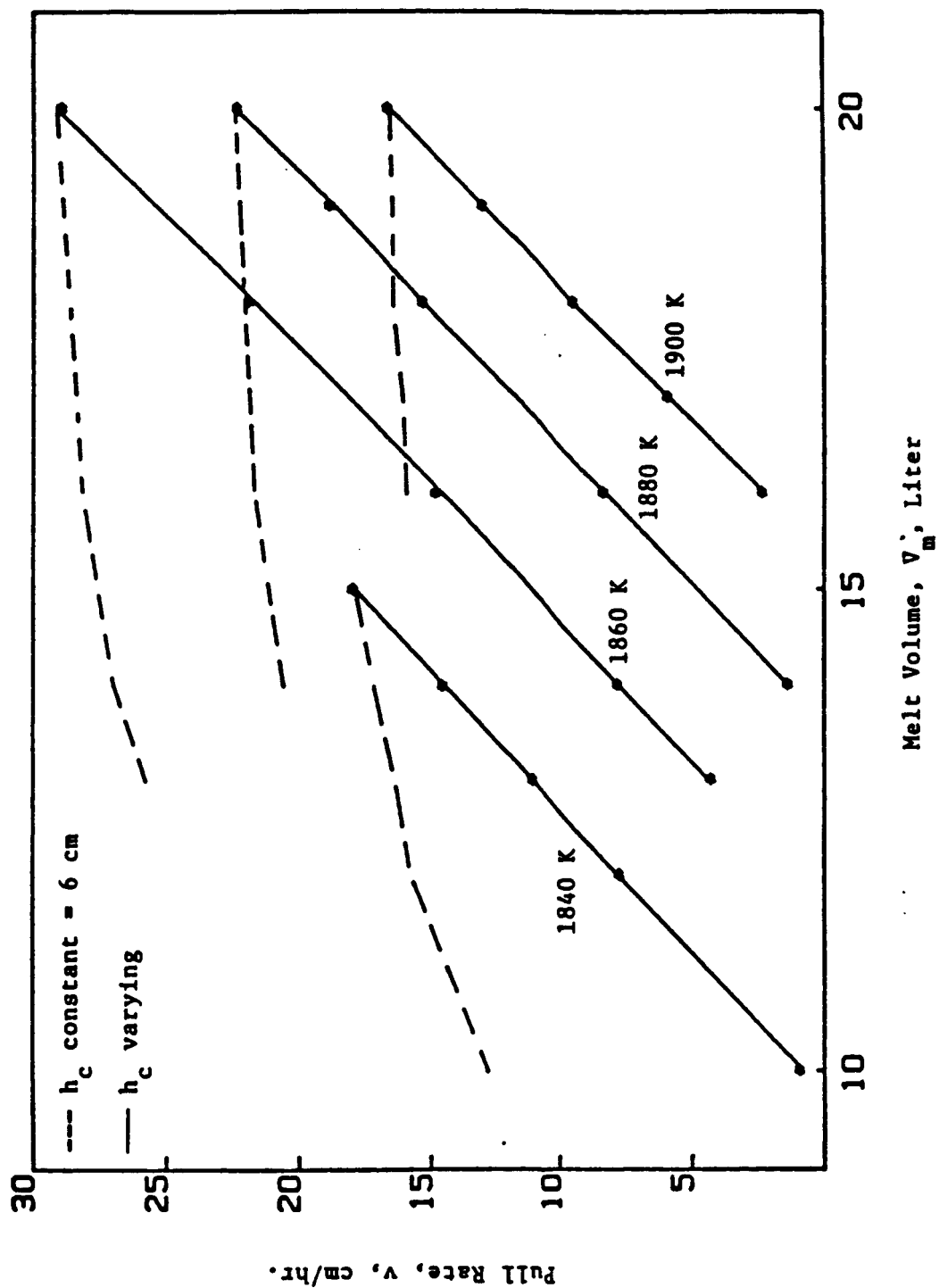The correlating equation, given by Equation (30), was fitted to the

Figure 14. Effect of increasing the height of exposed crucible wall on the pull rate; * denotes the simple model while the full lines denote numerical solution.

simulated data and a satisfactory agreement was obtained with a root-mean-square error in the pulling rate of ± 0.37 cm/hr. Further, it was found that the accuracy of the model could be increased considerably by adding one more term to the equation. For this improvement, we assume α_1 to be linearly dependent on h_c, which means that α_1 can be expressed as a linear function of V_m (due to Equation (29)). Therefore, the correlating equation is now defined in the following manner:

$$v = \alpha_1' + \alpha_2' V_m + \alpha_3' V_m \Delta T - \alpha_4' \Delta T \tag{31}$$

The justification for including a linear dependence on h_c for the term α_1 is as follows. For $\Delta T \rightarrow 0$ the melt is at a uniform temperature close to the melting point and we are in the maximum pulling rate situation. Even in this case the pulling rate should depend on the height of the exposed crucible walls and therefore it is proper to include a linear dependence of α_1 on h_c (or on V_m). Equation (31) was found to give a better fit to the data than Equation (30) with a root mean square error of 8.62×10^{-2} cm/hr. The following values of parameters were obtained:

$\alpha_1' = 23.713$ cm/hr

$\alpha_2' = 2.927$ cm/hr L

$\alpha_3' = 4.174 \times 10^{-3}$ cm/hr K L

$\alpha_4' = 0.3985$ cm/hr K

The model can now be used to simulate a complete growth cycle and to adjust the operating policy. The crystal length, melt volume and pull rate are related by the following relationship:

$$L = \Sigma v_i \Delta t_i \tag{32}$$

$$V_m = V_{m_o} - \frac{\rho_s}{\rho_m} (\pi R^2) L \tag{33}$$

V_{m_o} is the initial melt volume.

B. MODEL FOR THE INTERFACE SHAPE

1. General Discussion

For the purpose of developing a simple model which can predict both the nature (convex or concave) and the magnitude (extent of convexity or concavity) of the crystal-melt interface shape, a parameter Δr is defined which measures the deviation of the interface from planarity.

$$\Delta r = z \ (r=0) - z \ (r=R)$$

$$= z \ (center) - z \ (edge)$$

The sign of Δr indicates the nature of the interface. A negative sign for Δr means that the interface is convex and a positive sign means that the interface is concave. The magnitude of Δr measures the extent of concavity or convexity of the interface. The equation for the parabolic shaped interface is given by $z_I = \Delta r \ (1 - \dfrac{r^2}{R^2})$.

The interface shape, Δr, is plotted in Figure 15 as a function of the crystal radius for various crucible temperatures. At a constant crucible temperature, as the crystal radius increases, the concavity of the interface increases first and then starts decreasing as the crystal radius approaches the crucible radius. Similar results were also obtained by Kobayashi (1981). The shape of the interface is basically determined by the shapes of the isotherms (radial heat transfer) in the crystal and the melt. As discussed earlier, the radial heat transfer from the crystal is proportional to the crystal radius R, and the heat transfer from the melt to the interface is proportional to R^2. Therefore, a suitable correlating equation for the interface shape at constant crucible temperature can be defined as:

$$\Delta r = aR - bR^2 \tag{34}$$

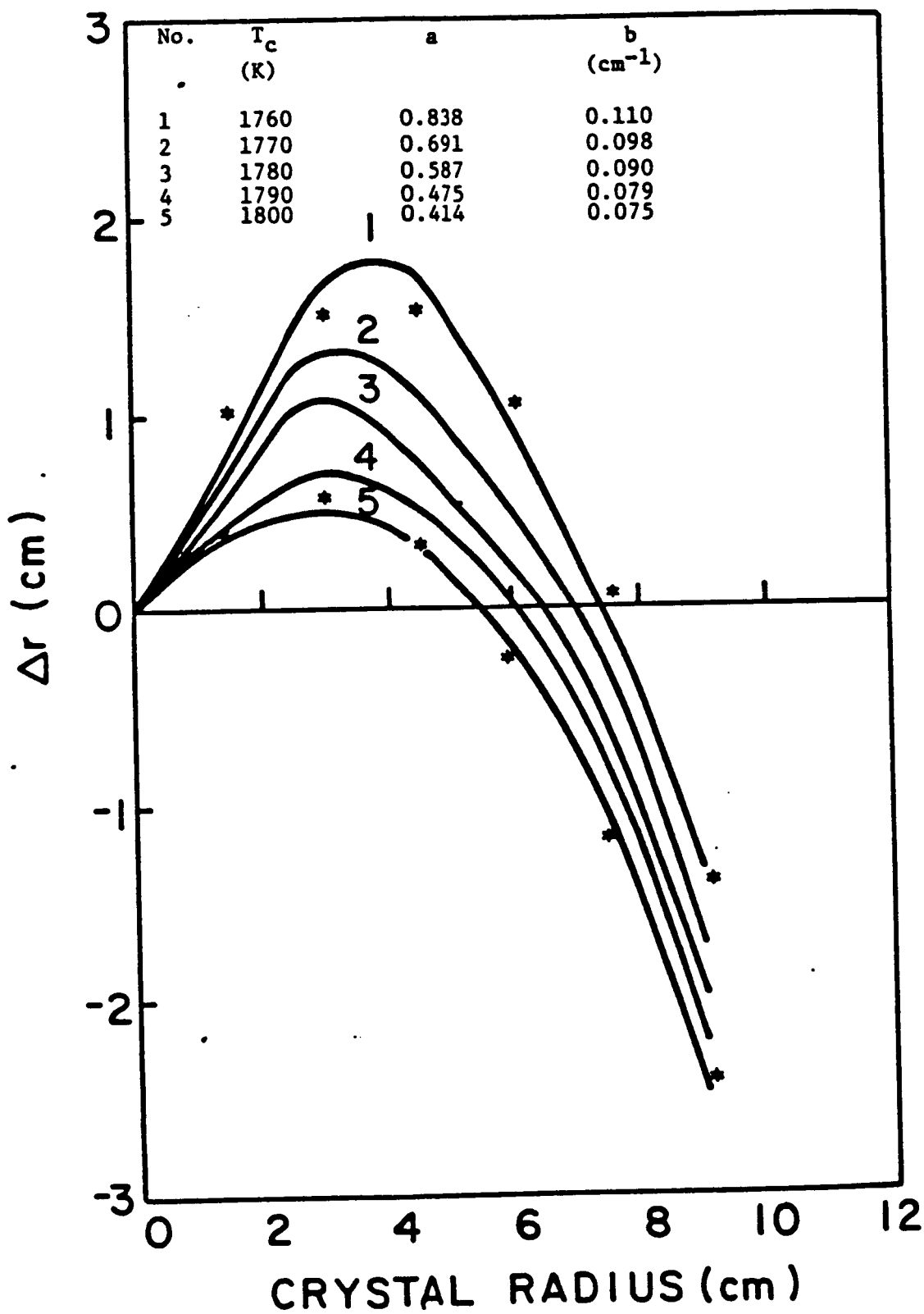| No.	T_c (K)	a	b (cm^{-1})
1	1760	0.838	0.110
2	1770	0.691	0.098
3	1780	0.587	0.090
4	1790	0.475	0.079
5	1800	0.414	0.075

Figure 15. Variation of Interface Shape with Crystal Radius.
_____: Detailed Model; **: Simple Model.

In Equation (34) the first term contributes to the concavity of the interface and the second term to the convexity of the interface. The values of the constants for each crucible temperature are shown in Figure 15. The agreement between the equation and the computer results is excellent. This indicates that Equation (34) is a suitable correlating equation.

Figure 16 shows the variation in the interface shape with the crucible temperature (defined as ΔT) at various crystal radii. The variation of Δr with ΔT is linear at all the crystal radii. Similar results were also obtained by Kobayashi (1981). This linear relationship between ΔT and Δr is expected since at constant radius the radial heat transfer from the melt to the interface increases linearly with ΔT. Therefore, at constant crystal radius

$$\Delta r = \Delta r_0 - c\Delta T \tag{35}$$

and the Δr_0 gives the interface shape under the maximum pulling rate conditions when the melt is maintained at the melting point. Note that under these conditions the interface shape is always concave since there is no radial heat transfer from the melt. In this region, the concavity of the interface (Δr_0) starts decreasing as the crystal radius approaches the crucible radius. This is due to heat transfer effects from the crucible wall.

To obtain the combined relationship between the interface shape Δr, R and ΔT, Equations (34) and (35) are combined. The coefficients a and b of Equation (34) are seen to obey a linear relationship with respect to ΔT. Therefore, the equation for the interface shape Δr, as a function of ΔT and R, can be written as:
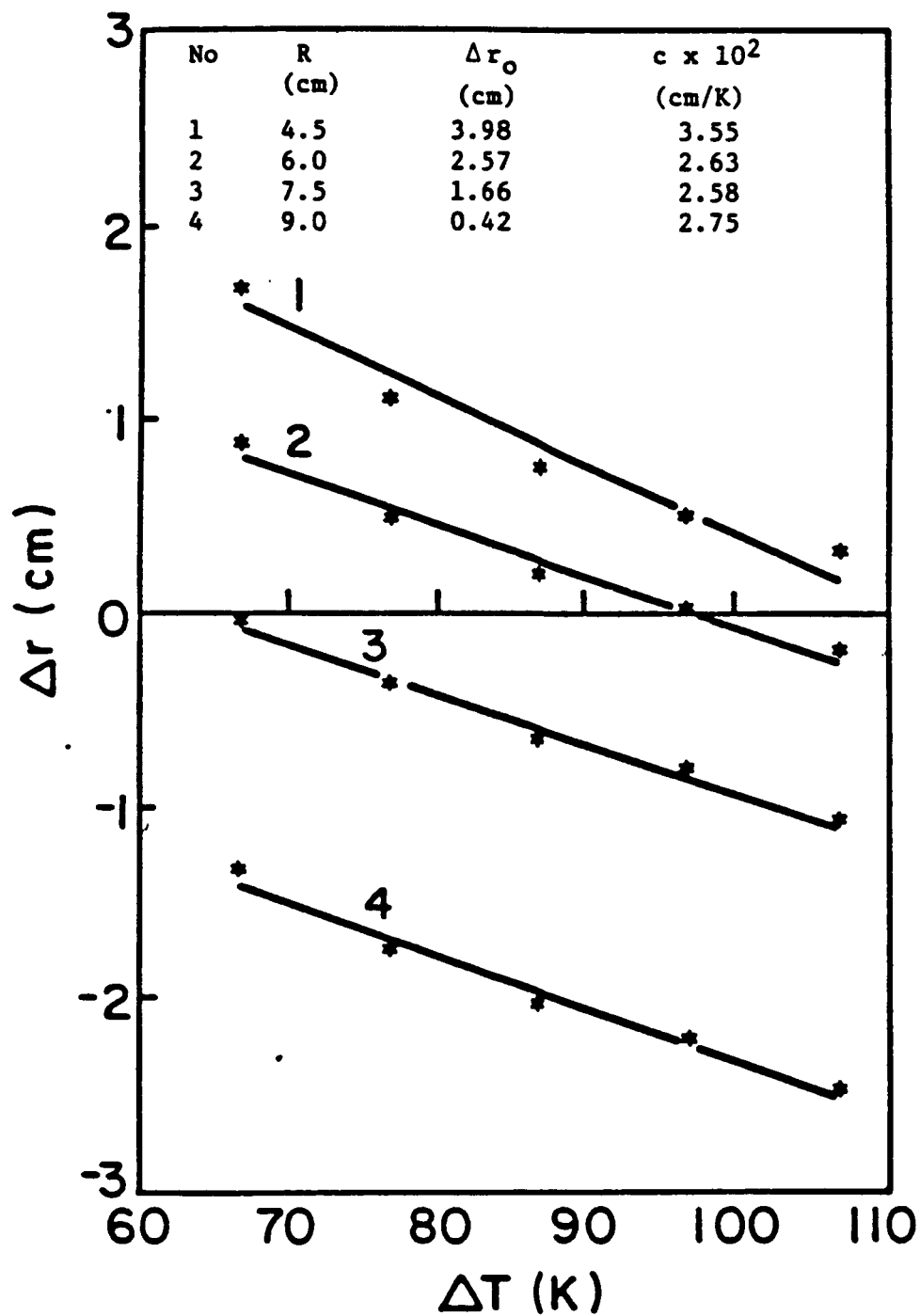
Figure 16.   Variation of Interface Shape with Crucible
             Temperature.   _____: Simple Model;
             **:   Detailed Model.

$$\Delta r = (a_1 - a_2 \Delta T) R - (b_1 - b_2 T) R^2 \tag{36a}$$

$$= (a_1 R - b_1 R^2) - (a_2 R - b_2 R^2) \Delta T \tag{36b}$$

$$= \Delta r_0 - (a_2 R - b_2 R^2) \Delta T \tag{36c}$$

Thus four parameters are needed to describe the relationship between the interface shape Δr, R, and ΔT. In Equation (36c), the first term (Δr_0) can be looked upon as the interface shape under the maximum pulling rate conditions. In this case ΔT is zero and there is no heat transfer from melt to the interface. This term describes the shape of the isotherms in the crystal generated by the radial heat transfer from the crystal side surface to the surroundings. This term contributes to the concavity of the interface. The second term $(a_2 R - b_2 R^2) \Delta T$ describes the effects of the crucible wall $(a_2 R \Delta T)$ and the radial heat transfer from the melt to the interface $(b_2 R^2 \Delta T)$ and contributes to the convexity of the interface. The form of Equation (36) was further verified by observing the variation of coefficients Δr_0 and c in Equation (35) with respect to the crystal radius R. It was seen that both coefficients can be described by a second order relationship of the form $(a'R - b'R^2)$. This approach also leads to the form given in Equation (36).

Having chosen a suitable correlating form, Equation (36), the coefficients a_1, b_1, a_2, and b_2 were also estimated simultaneously using the least-squares technique and the values obtained are: $a_1 = 1.556$, $b_1 = 0.172$; $a_2 = 1.088 \times 10^{-2}$, $b_2 = 9.199 \times 10^{-4}$ with R and Δr in cm and ΔT in K. Thus, Equation (36) is a suitable representation for the interface shape for the conditions given in Tables 3 and 4. The values of the correlating constants are, of course, only valid for these conditions and are also based on the conduction dominated, rigorous model. These constants can also be obtained for other operating conditions.

- 59 -

2. Effects of Crucible Wall and Melt Level

The increasing height of the crucible wall results in increasing convexity of the interface. The effects of h and h_c on the interface can be expressed in terms of melt volume alone via Equation (28). The effect of melt volume alone (dashed lines) as well as the coupled effects of melt volume and the height of the exposed crucible wall (solid lines) are shown in Figure 17. The effect on the interface shape of melt volume alone is small and can be neglected in the simple model. On this basis, the correlating equation for the interface (during the entire period of growth of a constant diameter crystal) is reduced to the following form:

$$\Delta r = \beta_1' - \beta_2' V_m + \beta_c' V_m \Delta T - \beta_4' \Delta T \tag{37}$$

Equation (37) was found to give the best fit of the simulated data and the parameters are as follows:

$$\beta_1' = 2.733 \text{ cm}$$

$$\beta_2' = 0.1335 \frac{cm}{L}$$

$$\beta_3' = 4.48 \times 10^{-4} \frac{cm}{K \, L}$$

$$\beta_4' = 3.039 \times 10^{-2} \frac{cm}{K}$$

The accuracy of the simple model is thus improved by including the effect of the height of the exposed crucible wall. Both the pulling rate and interface shape are correlated in a satisfactory manner by these equations.

C. OPERATING STRATEGY

We now demonstrate the use of the simple model to determine the operating strategy during a growth cycle. The various stages of growth can be characterized by the remaining melt volume present in the crucible.
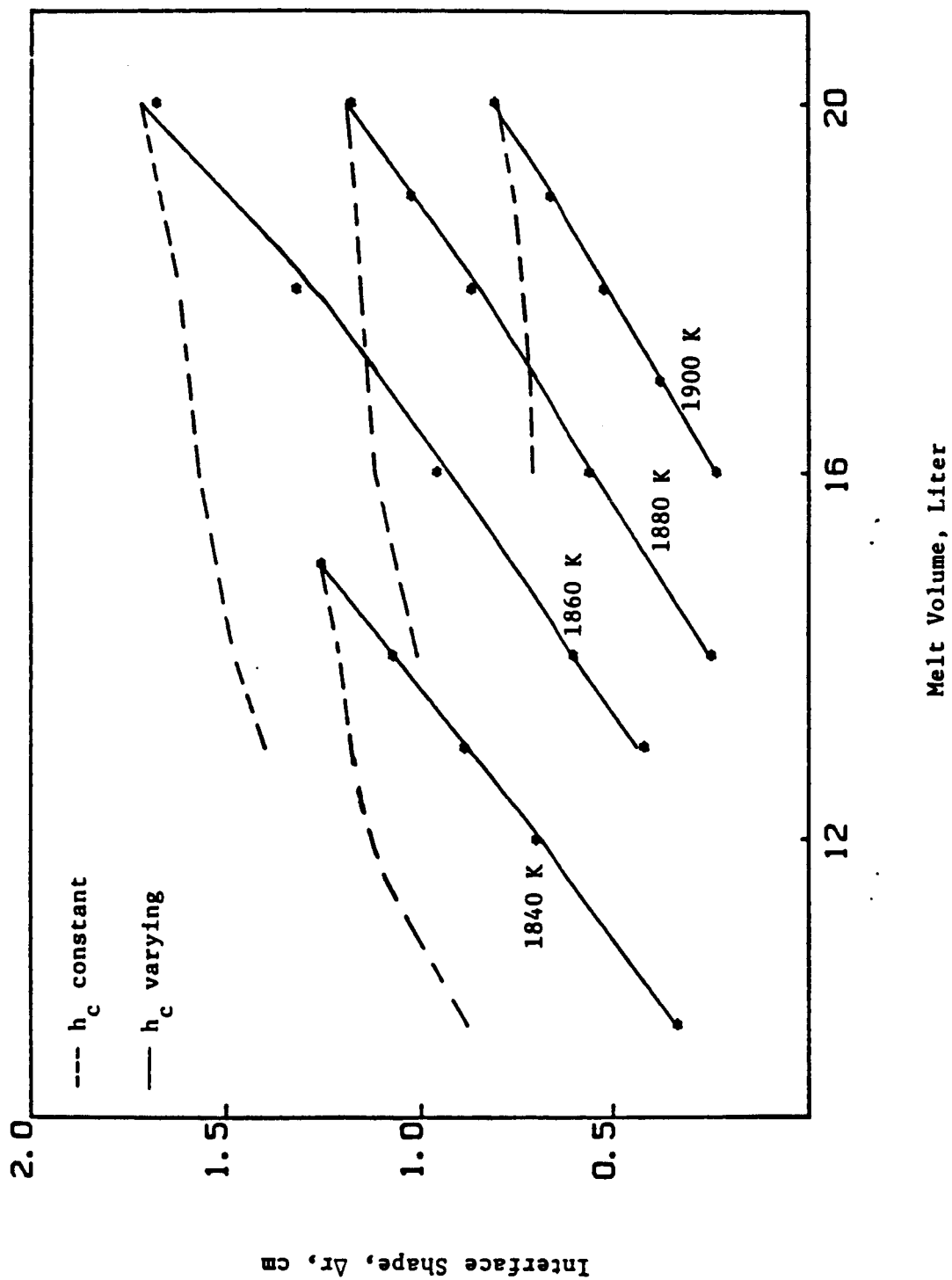
Figure 17. Effect of increasing height of crucible wall on interface shape.

Equations (31) and (37) are then used to calculate the pulling rate and crucible temperature needed for operating at a constant crystal radius. Various operating strategies can be readily examined. We shall discuss a few of these.

1. Constant Pull Rate, Varying Crucible Temperature Strategy

This is the scheme used in some of the earlier crystal growth processes. Here ΔT is determined from Equation (31) as a function of V_m as

$$\Delta T = \frac{v^* - \alpha_1 - \alpha_2' V_m}{\alpha_3' V_m - \alpha_4'} \tag{38}$$

and the corresponding values of Δr can be calculated from Equation (37).

Here v^* is the set pull rate. Note that the interface cannot be controlled by this strategy. This strategy is shown in Figure 18 for three values of v^* of 5, 10 and 15 cm/hr. It is seen that the crucible temperature should be progressively decreased with decreasing melt volume to keep the diameter constant. This means that crucible temperature is decreased with time. As a result the concavity of the interface will increase from the seed to the tail end of crystal, as shown in Figure 18.

2. Constant Crucible Temperature Varying Pull Rate Strategy

This can be analyzed in a similar manner. Here the pull rate for a set temperature ΔT^* can be calculated from Equation (31). The pull rate has to be decreased progressively with time (or decrease in melt volume) to offset the increasing radiation heat transfer to the crystal from the exposed portion of the crucible wall. This strategy is therefore not suitable for the complete growth cycle as the pull rate may drop below unacceptable levels after some time. Therefore, one modification is to fix the lower and upper limits to the pull rate and keep the temperature constant as long as the pull rate stays within these limits. If these limits
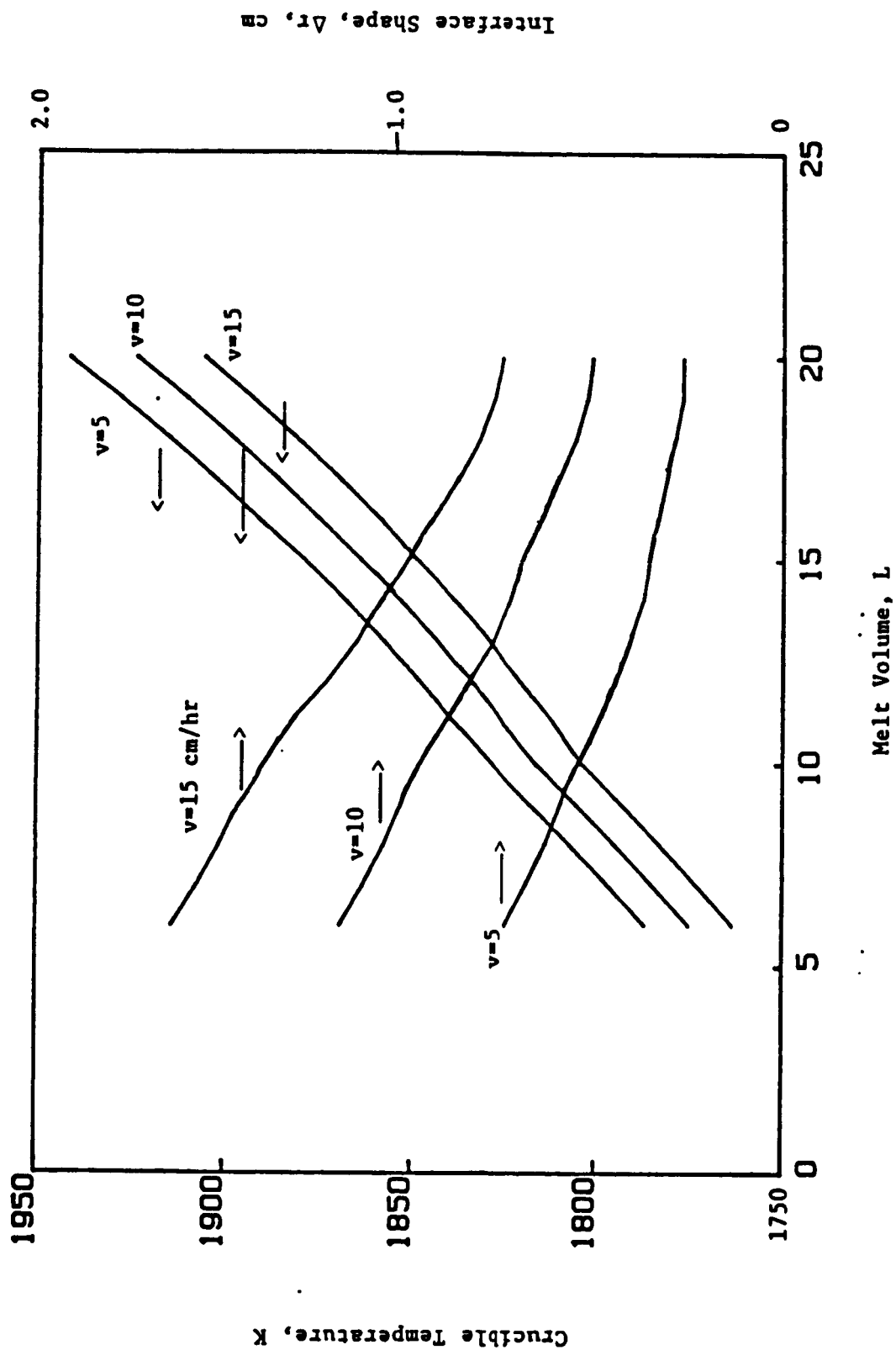
Figure 18. Operational strategies of varying the crucible temperature at various fixed pull rates and the corresponding interface shape.

are exceeded, a new crucible temperature (lower temperature to increase the pull rate) is set so that the pull rate is now back within the prescribed limits. Again, the interface shape varies in accordance with Equation (37) and cannot be controlled independently.

3. Varying Pull Rate and Crucible Temperature Strategy

In this strategy we have two degrees of freedom and therefore both the crystal radius and interface shape can be controlled simultaneously. The importance of controlling the interface shape during the growth process has been emphasized by several investigators. The quality of the growing crystal is closely associated with the nature of the interface shape maintained during growth. This strategy can be executed in the following manner. For a desired Δr, calculate ΔT from Equation (37) at any given stage of growth, i.e., for a given value of V_m. Now calculate the corresponding v from Equation (31). The strategy is plotted in Figure 19. Both pull rate and crucible temperature are now decreased with time (decreasing melt volume). The numerical results are only valid within the range of simulated parameters given in Tables 3 and 4 and for a conduction dominated situation. The concepts behind the simple model and the operating strategy shown in Figure 19 are, however, general and can be readily applied to practical CZ growth. The details of this study are published in a recent article (Srivastava, et. al., 1986).
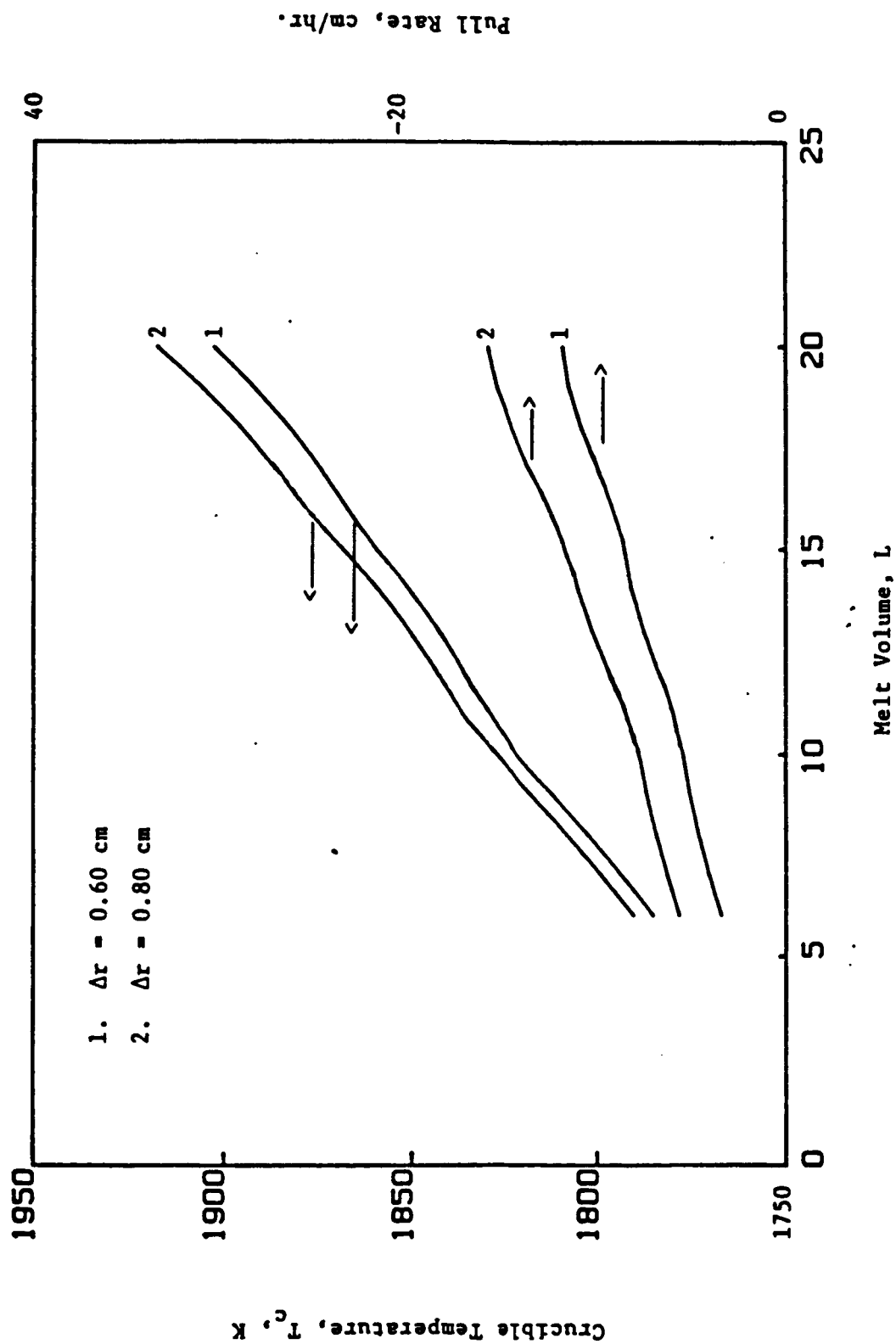
Figure 19. Constant diameter and interface shape control by simultaneous adjustments in pull rates and crucible temperatures.

VI. EFFECTS OF JET COOLING ON CZ CRYSTAL GROWTH

As discussed previously, the crystal growth process is primarily governed by the energy balance at the crystal melt-interface.

$$\rho_s v \, \Delta H \cos \alpha \quad (- k_s \frac{dT}{dn}) - (-k_\ell \frac{dT}{dn}) \qquad (39)$$

The above equation determines the growth rate (productivity of the puller) and shape of the crystal-melt interface (indicates the quality of the growing crystal) for a fixed radius of the crystal (Srivastava, et. al., 1985a). On the other hand, for a fixed pull rate, this energy balance equation can be used to determine the crystal diameter and the interface shape (Derby and Brown, 1986).

In general, the growth process can be monitored by controlling any of the three terms in Equation (39). Examples of this are: (1) by continuously adjusting the pulling rate of the crystal, the pulling rate can be kept equal to the growth rate and hence the crystal with a desired constant diameter can grow; (2) the pulling rate can be kept constant during the growth and the second term on the right hand side of Equation (39) can be adjusted by changing the heater power (crucible temperature) so that the growth rate is balanced by the pulling rate. This is often done in practice.

The first quantity on the right hand side of Equation (30) represents the heat loss from the crystal and is automatically fixed by the furnace design and the operator does not have any control over it. This is because the main portion of this heat loss from the crystal to the surroundings takes place by radiation (heat loss by convection is small). One approach which provides control over the heat loss from the crystal to the ambient is to change the dominant mode of heat transfer from radiation to convection (locally near the region of interest). This can be accomplished by suitably blowing an inert gas jet on to the crystal surface near the crystal-melt

- 66 -

interface. This is the idea that we pursue in the present study. Gas

jets for cooling applications are extensively used in industry, such as

in annealing of non-ferrous sheets and in the tempering of glass. Jet

cooling is particularly attractive in view of its low cost and fine degree

of control which is achievable. The application of an impinging jet

increases the convective heat transfer coefficient by an order of magnitude

compared to the values usually associated with gaseous heat media (Gardon

and Akfriat, 1966). By controlling the gas flow rate through the jet, the

value of the heat transfer coefficient and hence the rate of heat loss

from the crystal can be controlled. This scheme is especially suitable

for control of the diameter of crystals of materials which have low thermal

conductivity and which are opaque to infra-red radiation. Brice and co-

workers (1970, 1971) were able to grow good quality crystals of barium

strontium nitrate of constant diameter by blowing a gas jet over the growing

crystal. Both the transverse and the axial gas jet positions were in-

vestigated by these authors. Completely satisfactory control of the crystal

diameter by only changing the gas flow rate through the jet was demon-

strated. The diameter stability was also much improved and about 70% of

the attempts provided samples of useful size.

Against this background, the main objective here was to investigate

the effects of jet cooling on crystal growth using a detailed model of the

CZ growth process. The detailed model and the solution procedure used for

this analysis are described in the first and second quarterly reports and

also in Srivastava, et. al. (1985, 1986). The detailed modeling of the

heat transfer characteristics of the jet region was not attempted for this

study. The correlations available in the literature (Gardon and Akfriat,

1966; Ylachopoulos and Tomich, 1971), which are based on experimental

data, were used for estimating the convective heat transfer coefficient. In the following sections the effects of jet cooling on various aspects of crystal growth are presented.

A. PREDICTION OF HEAT TRANSFER COEFFICIENTS FROM JETS

The gas blowing through a jet onto the crystal surface provides the necessary turbulence in the vicinity of the crystal side surface. This increases the convective heat transfer coefficient between the crystal surface and the surrounding gas. For the purpose of calculating the heat transfer coefficient, the jet region is generally divided into two parts. The region directly opposite to the jet nozzle is referred to as the impingement zone and the maximum heat transfer coefficient is obtained in this region. The properties of this region are primarily determined by the direct interaction of the oncoming jet and the recipient surface. the impingement region is the region where the static pressure is greater than the ambient pressure. Gardon and Akfriat (1966) proposed the following correlation, based on experimental data for estimating the heat transfer coefficient in the impingement region:

$$Nu_o = 1.2 \ (Re_o)^{0.58} \ (d/D)^{-0.62} \tag{40}$$

Here d is the distance between the nozzle and the surface and D is the nozzle diameter. The Reynolds number, Re_o, is defined on the basis of nozzle diameter and the gas velocity at the nozzle exit. The Nusselt number, $Nu_o = h_a D/k_a$, is based on the thermal conductivity of the blowing gas and h_a is the heat transfer coefficient.

After the flow leaves the impingement region, the flow stream lines are approximately parallel to the surface of the flat plate and the static pressure is very nearly equal to the ambient pressure. In this

region, known as the wall jet region, the flow is essentially that of a tangential wall jet. The heat transfer coefficient in the wall jet decreases with the increasing distance from the impingement region. The heat transfer coefficient in this zone is given as a function of distance z from the impingement region by the following correlation proposed by Vlachopoulos and Tomich (1971):

$$Nu_z = 0.04 \ (Re_z)^{0.8} \ (z/D)^{-0.3} \tag{41}$$

In Equation (41), both the Reynolds number and the Nusselt number are calculated with respect to the distance, z, from the impingement point.

In the present study the horizontal (transverse) position of the jet was studied in detail. The curvature of the crystal was neglected so that the above correlations could be used. Since we are interested in the preliminary assessment of jet effects, this simplification is justified. The location of the jet was assumed to be just above the crucible wall. The height of the exposed portion of the crucible wall was assumed to be 6 cm. Therefore, the jet strikes the crystal side surface at about 6 cm from the crystal-melt interface. The aspect ratio of the jet (d/D), i.e. the ratio of the distance from the crystal to nozzle diameter, was fixed at 60. The performance of the jet was studied at various Reynolds numbers, i.e., at various gas jet velocities. Figure 20 shows the variation in the convective heat transfer coefficient along the crystal surface for different Reynolds numbers (Equations (40) and (41)). The maximum point on each curve corresponds to the impingement region. Curve 1 represents natural convection in the laminar region without the jet. Here the heat transfer coefficient is calculated by the standard correlations available in the literature (McAdams, 1954). Figure 20 reveals that the convective

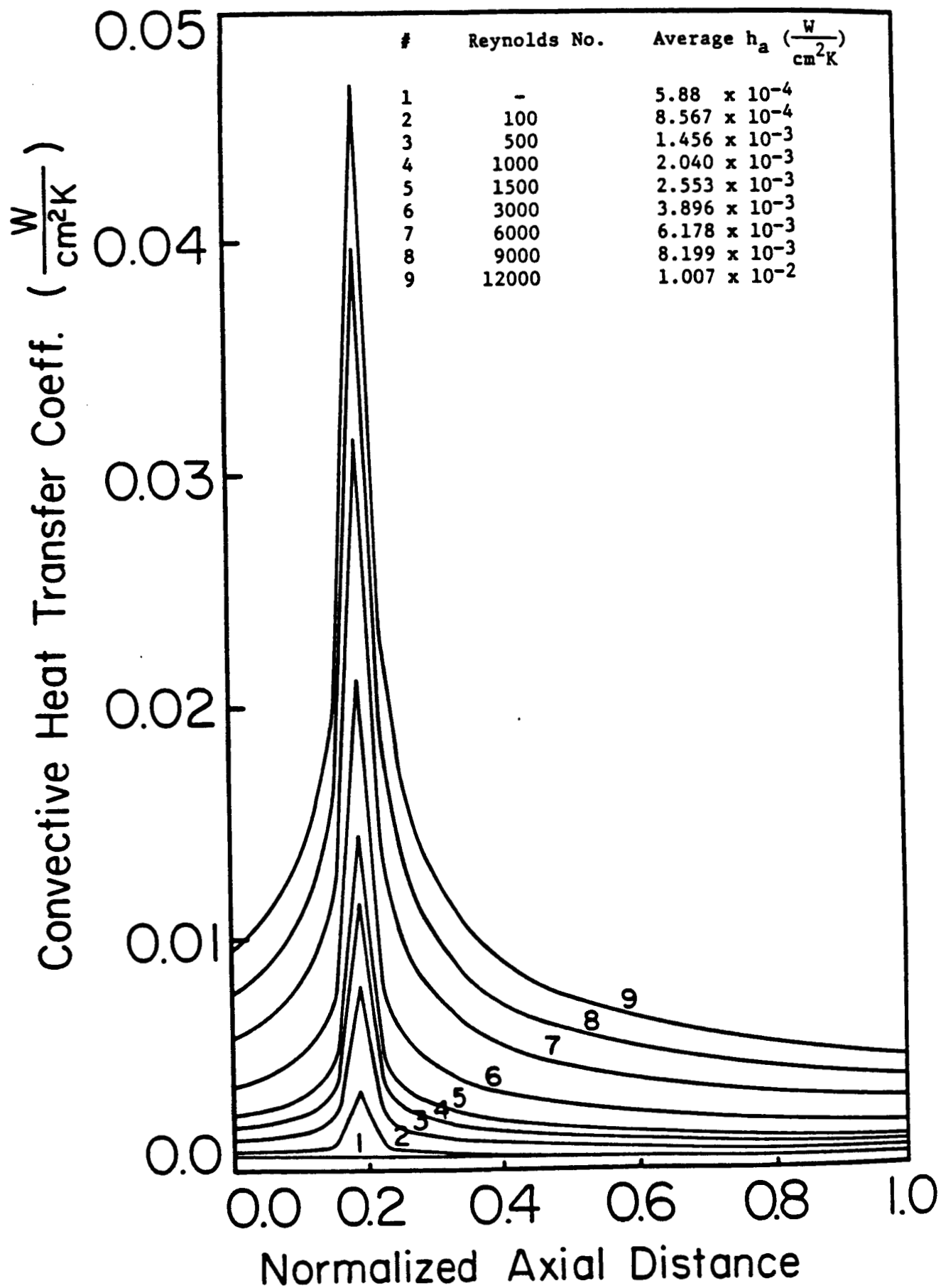| #	Reynolds No.	Average h_a ($\frac{W}{cm^2 K}$)
1	–	5.88×10^{-4}
2	100	8.567×10^{-4}
3	500	1.456×10^{-3}
4	1000	2.040×10^{-3}
5	1500	2.553×10^{-3}
6	3000	3.896×10^{-3}
7	6000	6.178×10^{-3}
8	9000	8.199×10^{-3}
9	12000	1.007×10^{-2}

Figure 20. Effects of Jet Cooling on the Convective Heat Transfer
Coefficient.

heat transfer coefficient is increased considerably due to the jet.

It was assumed that there is no enhancement of the heat transfer coefficient from the flat melt surface. This is a reasonable assumption as the jet impingement direction is parallel to the melt surface. However, the small region of the melt free surface near the crystal-melt-gas contact point is assumed to be almost 'vertical' due to the very small contact angle of silicon (11°). In this region the convective heat transfer coefficient between the melt and the surroundings is calculated using the correlation in Equation (41). the remaining portion of the melt free surface (away from the crystal-melt-gas point of contact) is assumed to lose heat by natural convection in the laminar regime. The heat transfer coefficient is calculated using the standard correlation (McAdams, 1954).

B.   CONTROL OF CRYSTAL DIAMETER

The important operating variables affecting crystal growth are the pulling rate, the crucible temperature and the convective heat transfer coefficient from the crystal side surface to the surroundings. This co-efficient can be adjusted by changing the parameters of the jet. As discussed earlier, the change in any of these variables will influence the respective terms in the energy balance, Equation (39), and thus the thermal field around the crystal-melt interface will change. This will directly affect the crystal diameter and the shape of the crystal-melt interface. The output variables which are required to be controlled in order to produce a dislocation free crystal are the crystal radius, R, and the shape of the crystal melt-interface, Δr. The parameter is defined in Equation (17). It has been well established that to have uniform radial distribution of the dopants in the crystal a planar interface ($\Delta r = 0$) should be maintained during the crystal growth.

Based on the above discussion, the growth process can be represented by a block diagram as shown in Figure 21. (At this point it should be mentioned that during crystal growth in commercial practice, the crucible and the crystal are rotated in opposite directions to provide radial homogenity of the melt and the crystal. The rotation has a significant influence on the melt hydrodynamics and hence on the thermal field in the melt due to the interaction of forced and natural convection. However, for the purpose of this study, the effects of melt hydrodynamics were neglected and conduction was assumed to be the dominant mode of heat transfer in the melt (Srivastava, et. al., 1985)). Next, the effects of jet cooling on the pulling rate for a fixed crystal diameter (or on the crystal diameter for a fixed pulling rate) are examined.

In this study the crucible temperature was maintained at 1800 K and the effects of jet cooling were examined at different crystal radii (3 cm to 9 cm). Figure 22 shows the changes in the pulling rate at various levels of jet cooling. The variation of h_a along the crystal length for these cases is as shown in Figure 20. Figure 22 reveals that as the level of jet cooling increases, the crystal is able to lose more heat to the surroundings and this results in a corresponding increase in the growth rate. Thus the puller can be operated at higher pull rates which increases the productivity.

As proposed by Kim et. al. (1983) and Srivastava et. al. (1986), the relationship between v and R at constant crucible temperature can be described as

$$v = \frac{A}{R} - B \tag{42}$$

where A and B are constants. The term A/R represents the heat loss from the crystal per unit area of the interface and the term B is porportional
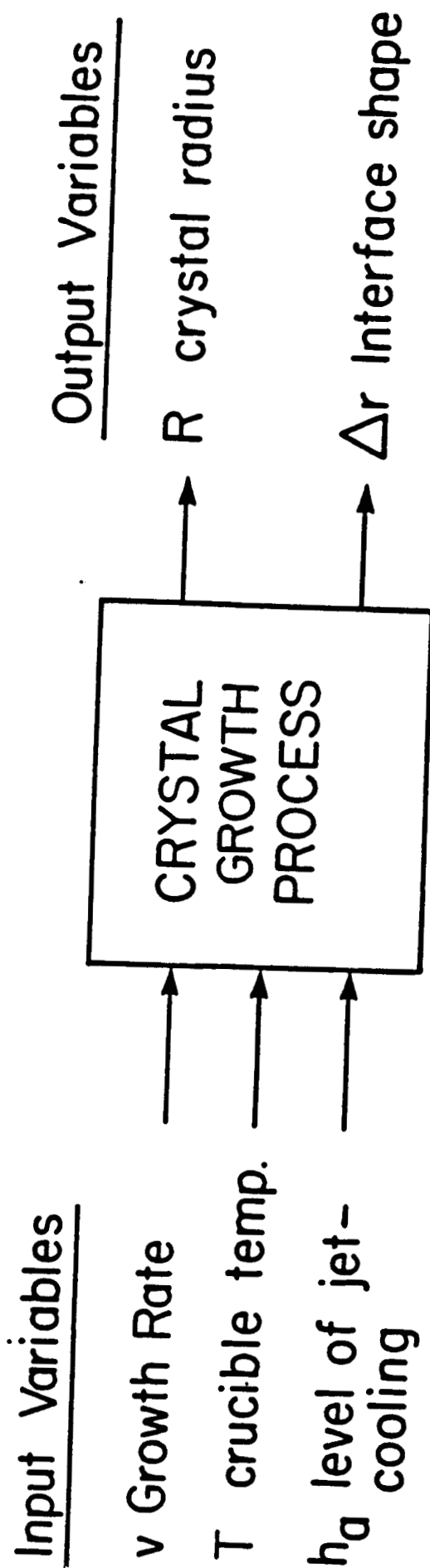
Figure 21. Important Input/Output Process Variables Affecting Crystal Growth by the CZ Process.

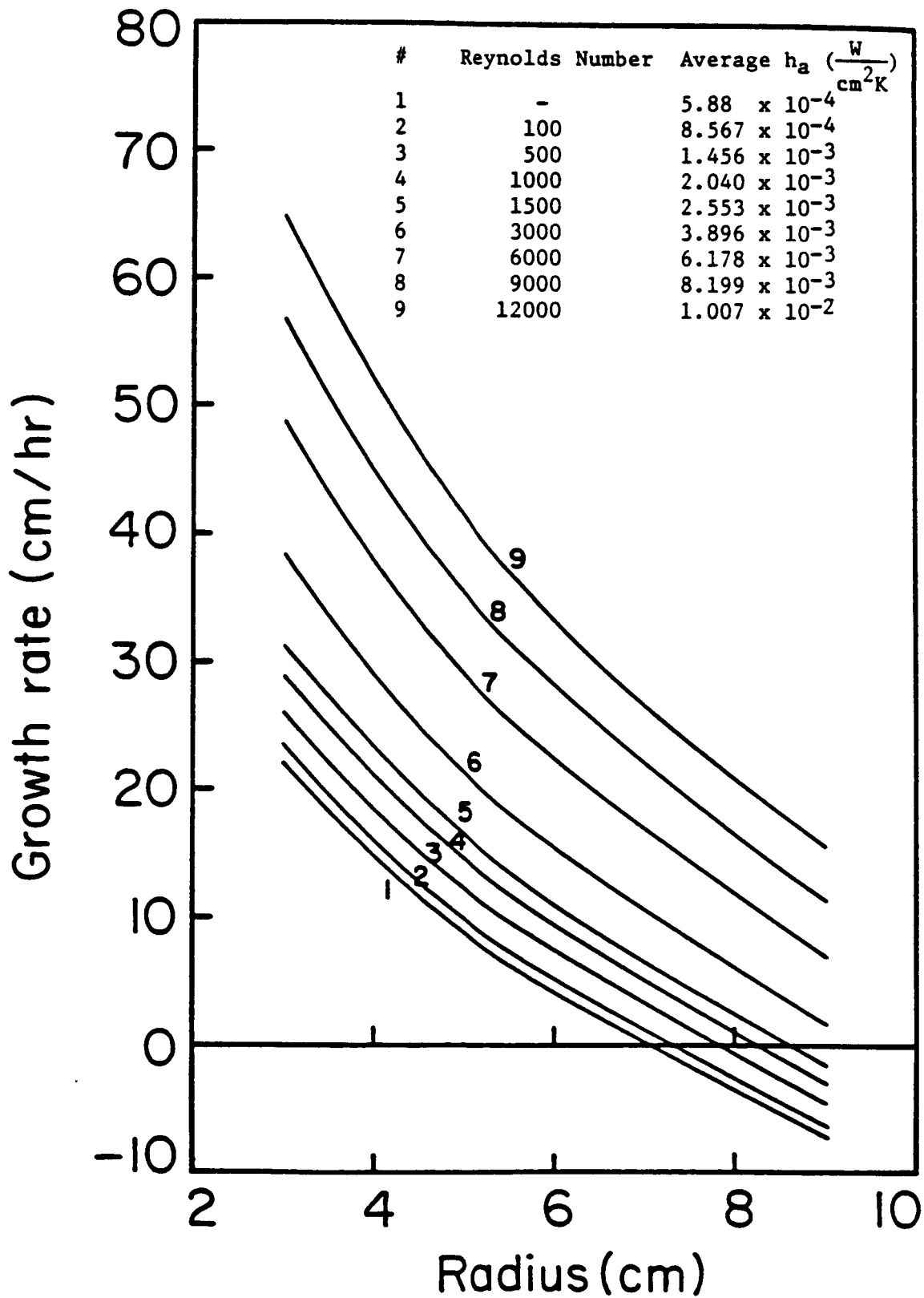| #	Reynolds Number	Average h_a $(\frac{W}{cm^2 K})$
1	–	5.88×10^{-4}
2	100	8.567×10^{-4}
3	500	1.456×10^{-3}
4	1000	2.040×10^{-3}
5	1500	2.553×10^{-3}
6	3000	3.896×10^{-3}
7	6000	6.178×10^{-3}
8	9000	8.199×10^{-3}
9	12000	1.007×10^{-2}

Figure 22.   Variation cf Growth Rate with Crystal Radius at Different Levels of Jet-Cooling.

to heat input from the melt to the interface per unit area. The various cases in Figure 22 were approximated by the relationship given in Equation (42) and the results are shown in Figure 23. The comparison of the approximate predictions obtained by Equation (42) and the exact simulated behavior of v vs. R shows good agreement. The accuracy of the approximation is measured by the root mean square deviation, e_{rms},

$$e_{rms} = \frac{\sqrt{\Sigma \ (y_t - y_p)^2}}{N}$$ (43)

where y_t and y_p are the true and predicted values of a variable y respectively and N is the number of data points. The values of e_{rms} for all the cases are given in Figure 23. The values of the parameter A represent the effects of jet cooling on the crystal surface and are a measure of the convection heat transfer coefficient generated by the jet action. The changes in parameter B for various Reynolds numbers are caused by the effect of jet cooling on the melt meniscus near the crystal edge and by the resulting complex radiation interactions. As the level of jet-cooling increases, the portion of the melt-free surface close to the crystal is able to lose more heat to the surrounding and thus the heat input (B) to the crystal-melt interface decreases. The detailed mathematical dependence between A and h_a or the jet parameters, such as the gas velocity through the jet nozzle, is difficult to establish as A also contains the contribution from the radiative heat transfer. In addition, both h_a and the radiative heat losses vary considerably over the length of the crystal.

1. Control of Diameter Via Pull Rate

One approach to growing crystals with constant diameter is to operate the furnace at constant heater power and at fixed level of jet cooling,
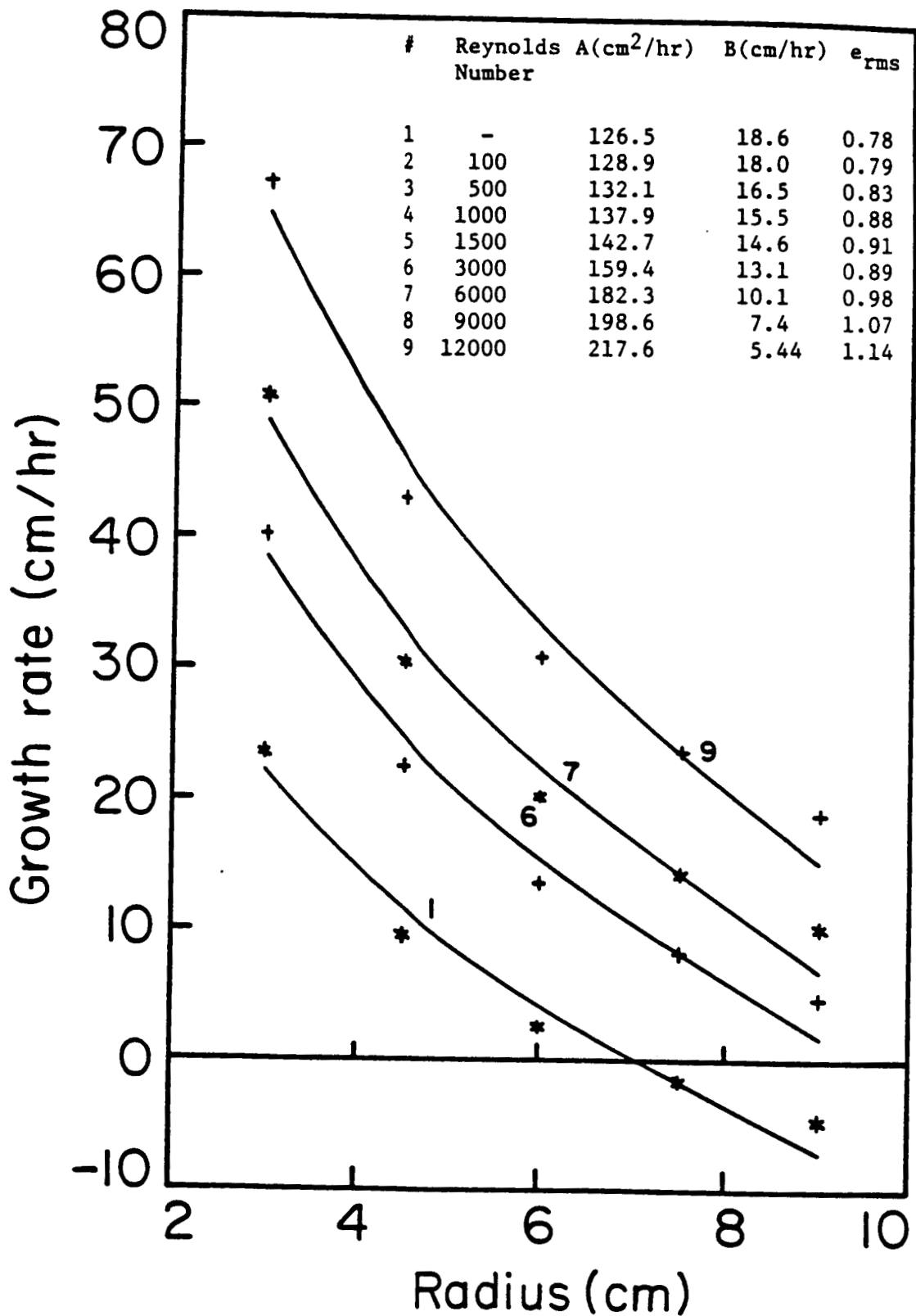
#	Reynolds Number	$A(cm^2/hr)$	$B(cm/hr)$	e_{rms}
1	–	126.5	18.6	0.78
2	100	128.9	18.0	0.79
3	500	132.1	16.5	0.83
4	1000	137.9	15.5	0.88
5	1500	142.7	14.6	0.91
6	3000	159.4	13.1	0.89
7	6000	182.3	10.1	0.98
8	9000	198.6	7.4	1.07
9	12000	217.6	5.44	1.14

Growth rate (cm/hr) vs Radius (cm)

Figure 23. Comparison of Pulling Rate versus Crystal Radius (v vs. R) at Different Levels of Jet Cooling, —— Detailed Simulation, ***, + + + Simple Model.

while the adjustments in the pulling rate are made to control the diameter. In order to consider the sensitivity of the radius change due to changes in pulling rate, Equation (42) is expressed in differential form as:

$$dR = - (\frac{R^2}{A}) \, dv \quad \text{(at constant } T_c \text{ and } h_a) \tag{44}$$

Now, if the crystal pulling rate is used to control the diameter, then the pulling rate has to be adjusted such that it balances the growth rate which is determined by the heat balance considerations. Here dv can be looked upon as the error in the pulling rate. Note that dv will be zero if the pulling rate is exactly equal to the growth rate and thus the crystal diameter will remain constant. Since the values of A (a measure of h_a) are increasing with increasing intensity of the jet cooling, it can be seen that the same error in the pulling rate will produce a smaller change in the crystal diameter at higher levels of jet cooling on the crystal side surface. In other words the crystal diameter will be more stable in this region. Similar conclusions were reported by Brice et. al. (1970, 1971) based on their experimental investigations.

2. <u>Control of Diameter Via Gas Jet</u>

In the case where crystal growth at constant pulling rate and constant crucible temperature is desired, the gas flow rate through the jet can be used to control the diameter changes in the crystal. The changes in the gas flow rate through the jet will change the convective heat transfer coefficient and hence the extent of heat losses from the crystal. Thus, the growth rate of the crystal can be balanced with a set pulling rate. As mentioned earlier, the parameter A is proportional to the value of the heat transfer coefficient or the effects of the jet cooling. Therefore, for crystal growth at a constant pulling rate and a constant crucible temperature,

the change in crystal radius due to changes in the level of jet cooling
can be derived from Equation (42) and is given by:

$$dR = (\frac{R}{A}) \; dA \; \text{(at constant v and } T_c) \tag{45}$$

In the above equation the changes in parameter B due to variations in
jet-cooling have been neglected. According to Equation (45), the
crystal diameter will increase with increases in jet cooling at a constant
pulling rate and constant crucible temperature. This is expected since
with the increase in cooling of the crystal, the solidification rate at
the crystal-melt interface will increase. This will result in the formation
of a larger diameter crystal unless the pulling rate is increased. Further,
Equation (45) indicates that the crystal diameter will be more stable
during growth at high values of A (high levels of jet cooling). Notably,
in this case (Equation (45)) the changes in diameter are proportional to
R. On the other hand, in Equation (44) the changes in diameter are
proportional to R^2. This implies that diameter control with adjustments
in the gas flow rate through the jet would be easier than with adjustments
in the pull rate.

3. Control of Diameter Via Crucible Temperature

The currently used growth process is generally controlled by adjusting
the crucible temperature. The effects of the changes in the crucible
temperature on growth rate and interface shape at various levels of jet
cooling are now examined.

Figure 24 shows the variation in growth rate with respect to changes
in the crucible temperature. The crystal radius is kept constant at 6 cm.
The growth rate continuously decreases as the crucible temperature increases.
This relationship between the growth rate and the crucible temperature
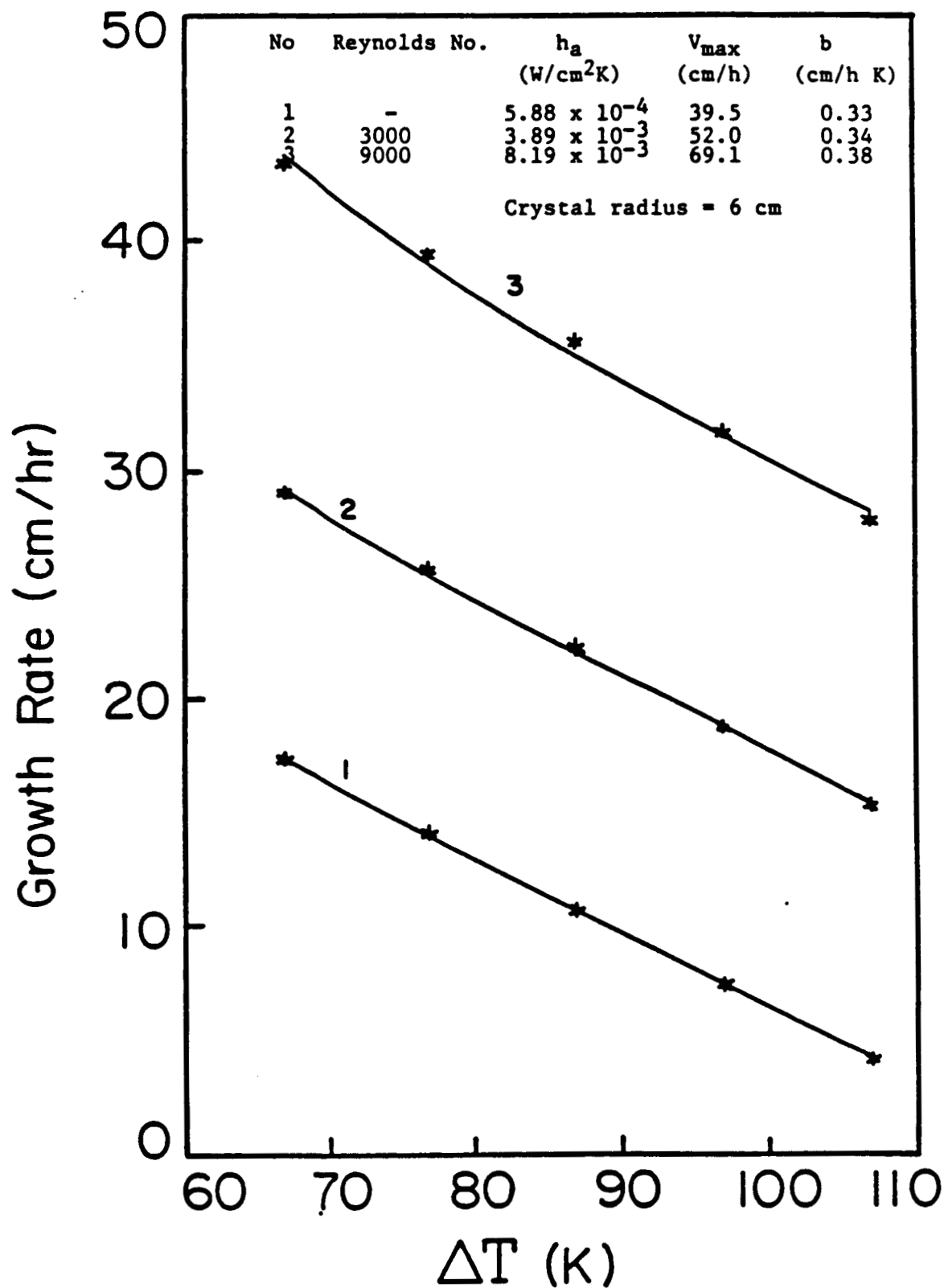
No	Reynolds No.	h_a (W/cm^{2}K)	V_{max} (cm/h)	b (cm/h K)
1	–	5.88×10^{-4}	39.5	0.33
2	3000	3.89×10^{-3}	52.0	0.34
3	9000	8.19×10^{-3}	69.1	0.38

Crystal radius = 6 cm

Figure 24. Effect of Crucible Temperature on Interface Shape at Various Levels of Jet Cooling. ___: Detailed Model; ***: Linear Model.

- 79 -

$(\Delta T = T_c - T_m)$ can be assumed to be linear. The accuracy of the linear approximation and the values of the parameters of the linear model are given in Figure 24 for various levels of jet cooling. The dependence of growth rate on ΔT can be written as:

$$v = v_{max} - b\Delta T \tag{46}$$

The parameter b is a measure of the heat transfer coefficient from the melt side to the interface and changes little (lines are parallel) with the increasing cooling of the crystal by the jet. This is expected since the term $b\Delta T$ in Equation (46) represents the heat transfer from the melt to the interface and this is independent of the effects of the jet cooling on the crystal side surface. Small changes in the parameter b are due to the fact that the effects of jet cooling on the melt meniscus were incorporated into the study. The growth rate under the conditions when there is no heat transfer from the melt to the interface ($\Delta T = 0$) and the melt is at a uniform melting temperature is given by v_{max}. In these limiting conditions the growth rate is primarily controlled by the extent of heat loss from the crystal and hence increases with the increased cooling of the crystal by the jet (Figure 24). Now, if the growth takes place at constant pull rate and at a fixed level of jet cooling and the diameter is controlled by adjustments in the crucible temperature, then the change in crystal radius with the changes in T_c can be expressed as:

$$dR = (\frac{\partial R}{\partial T_c})_{v,h_a} \, dT_c \quad \text{(at constant v and } h_a) \tag{47a}$$

$$= - (\frac{\partial R}{\partial v})_{T_c} (\frac{\partial v}{\partial T_c})_R \, dT_c \tag{47b}$$

$$= - \frac{R^2 b}{A} \, dT_c \tag{47c}$$

In Equation (47c) parameter b (the heat transfer coefficeint from the melt to the interface) can be assumed to be independent of R. Since b is also independent of the effects of the jet cooling, the change in the crystal diameter is proportional to R^2/A (same as in Equation (44)). Therefore, a small fixed error in the crucible temperature will produce a smaller change in the crystal diameter at higher levels of jet cooling. Thus, in the environment of increased jet cooling of the crystal, the crystal diameter will be more stable. This can also be understood from Equation (39), since to balance the changes in the heat transfer from the melt to the interface due to the changes in the crucible temperature, a small change in the crystal diameter will occur at high values of h_a to balance the energy balance. On the other hand, for small values of h_a, a large change in diameter will be required to balance Equation (39).

Comparing Equations (44), (45), and (47), it appears that the best control of the diameter will be achieved when jet velocity is used for controlling the diameter, since in this case the changes in the diameter are proportional to only R as compared to R^2 in the other two cases when either pulling rate or crucible temperature is used as manipulative variables.

The effects of jet cooling on interface shape and the unique possibility of control of the crystal diameter and interface shape in presence of jet cooling are reported in our recent publication (Srivastava et. al., 1986b).

VIII. MODELING OF MELT HYDRODYNAMICS

The hydrodynamics and heat-transfer in the melt can be described mathematically by the equations of continuity, motion and energy. This system of equations can be cast into a number of different formulations. Two of these are particularly popular for use in numerical simulations. The first is the velocity-pressure formulation, where the equations are solved in terms of the primitive variables, i.e. the velocity components and the pressure. The second is applicable for two-dimensional problems including those which are axisymmetric. In this case a stream function is defined and solved along with the vorticity transport equation. The advantage of this formulation is that as continuity is automatically satisfied, the number of equations is reduced by one. The disadvantage is that boundary conditions are more difficult to apply. At solid boundaries, it is required that the stream function be a constant and that its normal derivative be set to the tangential velocity of the surface. This can only be accomplished by determining the appropriate boundary condition for the vorticity at the surface. One method for doing this is given by Langlois and Shir (1977).

For the preliminary hydrodynamics model, the velocity-pressure formulation was selected to avoid the boundary condition complications associated with the stream function-vorticity formulation. The simpler boundary conditions will be particularly advantageous when extending the model to irregular geometries.

The following assumptions are frequently made when deriving a mathematical model for the hydrodynamics and heat transfer in Czochralski melts:

1) Bulk flow approximation (described below)

2) Boussinesq approximation

3) Pseudo-steady-state

4) Constant temperature at the crucible wall

5) Thermally insulated melt-gas interface

6) Thermally insulated crucible bottom

7) Negligible viscous dissipation

The bulk flow approximation is the assumption of flat melt-crystal and melt-gas interfaces. In general, these interfaces will not be flat and the solution obtained will not be valid in their vicinity. The solution, should however, be reasonably accurate in the bulk fluid.

The Boussinesq approximation is outlined in Bird, Stewart and Lightfoot (1960). Density differences are neglected in all terms of the equation of motion except the body force term. Here the density is expanded in a Taylor series in temperature which is truncated after the linear term:

$$\rho_m = \bar{\rho}_m (1 - \beta (T - \bar{T})) \tag{48}$$

The quantity β is the coefficient of volume expansion and the bars denote reference quantities. This form of the Navier-Stokes equations is frequently used in solving problems involving natural convection.

During the process, the melt is depleted as the crystal grows. Since the volume of the melt changes with time, no real steady-state exists. If one considers that the growth rate is of the order of 1 mm/min, however, it is obvious that the volume of the melt changes at a very slow rate. Therefore, depletion of the melt will generate a negligible amount of flow compared to the other convection mechanisms.

- 83 -

For this reason, unless one is operating in an oscillatory or turbulent regime, a pseudo-steady-state can be said to exist at any time.

Viscous dissipation gives a negligible contribution to the energy equation. This is due to the low viscosity of molten silicon and to the large (80 - 100 K) temperature variations in the melt.

A. MODEL EQUATIONS

The Navier-Stokes equations with Boussinesq approximation for an axisymmetric system are as follows:

$$V_r \frac{\partial V_r}{\partial r} - \frac{V_\theta^2}{r} + V_z \frac{\partial V_r}{\partial z} = -\frac{1}{\rho_m} \frac{\partial P}{\partial r} + \nu \left[\frac{\partial}{\partial r} \frac{1}{r} \frac{\partial}{\partial r}(rV_r) + \frac{\partial^2 V_r}{\partial z^2} \right] \tag{49}$$

$$V_r \frac{\partial V_\theta}{\partial r} + V_z \frac{\partial V_\theta}{\partial z} + \frac{V_r V_\theta}{r} = \nu \left[\frac{\partial}{\partial r}\left(\frac{1}{r} \frac{\partial}{\partial r}(rV_\theta)\right) + \frac{\partial^2 V_\theta}{\partial z^2} \right] \tag{50}$$

$$V_r \frac{\partial V_z}{\partial r} + V_z \frac{\partial V_z}{\partial z} = -\frac{1}{\rho_m} \frac{\partial P}{\partial z} + \nu \left[\frac{1}{r} \frac{\partial}{\partial r}\left(r\frac{\partial V_z}{\partial r}\right) + \frac{\partial^2 V_z}{\partial z^2} \right] + \beta g(T - \bar{T}) \tag{51}$$

where V_r, V_θ and V_z are the radial, azimuthal, and axial velocities, respectively. These equations must be solved along with the continuity equation,

$$\frac{1}{r} \frac{\partial}{\partial r}(rV_r) + \frac{\partial V_z}{\partial z} = 0 \tag{52}$$

and the energy equation,

$$V_r \frac{\partial T}{\partial r} + V_z \frac{\partial T}{\partial z} = \alpha \left[\frac{1}{r} \frac{\partial}{\partial r}\left(r\frac{\partial T}{\partial r}\right) + \frac{\partial^2 T}{\partial z^2} \right] \tag{53}$$

where the viscous dissipation terms have been neglected, and α is the thermal diffusivity. This is a non-linear, second-order system of five mutually coupled partial differential equations.

B. BOUNDARY CONDITIONS

For the velocities, the no-slip boundary condition is applied at the solid surfaces and the thermocapillary flow condition is applied at the free surface. The symmetry condition holds along the axis of symmetry (r=0). The pressure on the free surface is that of the gas above the melt. The temperature at the growth interface is taken to be that of the melting point of silicon. The derivative of the temperature normal to the free surface and normal to the crucible bottom is set to zero (thermally insulated). The temperature at the crucible wall is assigned some constant value. These boundary conditions will be presented in non-dimensional form in the following section.

It is convenient to non-dimensionalize the equations in order to identify the relevant non-dimensional groups with which the stem can be characterized. It is also desirable to scale the dependent variables such that they lie within some convenient interval (0 to 1 for dimensionless temperature, -1 to 1 for the dimensionless velocities). With this in mind, the following non-dimensionalization scheme was used:

$$r = R_c r^* \tag{54}$$

$$z = R_c z^* \tag{55}$$

$$V_r = V_{\theta max} V_r^* \tag{56}$$

$$V_\theta = V_{\theta max} V_\theta^* \tag{57}$$

$$V_z = V_{\theta max} V_z^* \tag{58}$$

$$P = - \rho_m g z + \rho_m V_{\theta max}^2 P^* \tag{59}$$

$$T = (T_c - T_m) T^* + T_m \tag{60}$$

where the asterisk denotes the non-dimensional variable. The value of $V_{\theta\,max}$, the maximum azimuthal velocity, will be either the velocity at the crystal edge or at the crucible wall, whichever is greater. In cases where there is no rotation, $V_{\theta max}$ has no physical meaning but is simply a scaling factor for the velocities.

Substitution of (54 – 60) into Equations (49 – 53) and dropping the asterisks yields:

$$V_r \frac{\partial V_r}{\partial r} + V_z \frac{\partial V_r}{\partial z} - \frac{V_\theta^2}{r} = -\frac{\partial P}{\partial r} + \frac{1}{Re}\left[\frac{\partial}{\partial r}\left(\frac{1}{r}\frac{\partial}{\partial r}(rV_r)\right) + \frac{\partial^2 V_r}{\partial z^2}\right] \tag{61}$$

$$V_r \frac{\partial V_\theta}{\partial r} + V_z \frac{\partial V_\theta}{\partial z} + \frac{V_r V_\theta}{r} = \frac{1}{Re}\left[\frac{\partial}{\partial r}\left(\frac{1}{r}\frac{\partial}{\partial r}(rV_\theta)\right) + \frac{\partial^2 V_\theta}{\partial z^2}\right] \tag{62}$$

$$V_r \frac{\partial V_z}{\partial r} + V_z \frac{\partial V_z}{\partial z} = -\frac{\partial P}{\partial z} + \frac{1}{Re}\left[\frac{1}{r}\frac{\partial}{\partial r}\left(r\frac{\partial V_z}{\partial r}\right) + \frac{\partial^2 V_z}{\partial z^2}\right] + \frac{Gr}{Re^2}T \tag{63}$$

$$\frac{1}{r}\frac{\partial}{\partial r}(rV_r) + \frac{\partial V_z}{\partial z} = 0 \tag{64}$$

$$V_r \frac{\partial T}{\partial r} + V_z \frac{\partial T}{\partial z} = \frac{1}{PrRe}\left[\frac{1}{r}\frac{\partial}{\partial r}\left(r\frac{\partial T}{\partial r}\right) + \frac{\partial^2 T}{\partial z^2}\right] \tag{65}$$

where

$$Re = \frac{R_c V_{\theta max}}{\nu} \tag{66}$$

$$Gr = \frac{\beta g R_c^3 (T_c - T_m)}{\nu^2} \tag{67}$$

$$Pr = \frac{\alpha}{\nu} \tag{68}$$

Taking advantage of symmetry reduces the three-dimensional problem into a two-dimensional one in the r-z plane. For this preliminary model, the melt-crystal and melt-gas interfaces are considered to be flat (bulk flow approximation).

On the axis of symmetry (r = 0), the following symmetry conditions hold:

$$V_r = 0, \quad V_\theta = 0, \quad \frac{\partial V_z}{\partial r} = 0, \quad \frac{\partial T}{\partial r} = 0 \tag{69}$$

Along the bottom of the crucible (z = 0), the following conditions are in effect:

$$V_r = 0, \quad V_\theta = Br, \quad V_z = 0, \quad \frac{\partial T}{\partial r} = 0 \text{ or } T = 1 \tag{70}$$

On the crucible wall (r = R_c).

$$V_r = 0, \quad V_\theta = B, \quad V_z = 0, \quad T = 1 \tag{71}$$

Along the crystal (z = H/R_c, $0 \leq r \leq R/R_c$).

$$V_r = 0, \quad V_\theta = Ar, \quad V_z = 0, \quad T = 0 \tag{72}$$

At the melt-gas interface (z = H/R_c, $R/R_c \leq r \leq 1$).

$$\frac{\partial V_r}{\partial z} = 0, \quad \frac{\partial V_\theta}{\partial z} = 0, \quad V_z = 0 \quad , \quad \frac{\partial T}{\partial z} = 0 \tag{73}$$

Equation 73 assumes that the gas above the melt is inviscid.

The constants A and B are crystal and crucible rotation parameters, respectively. The restrictions on these parameters are given below:

$$-1 \leq \frac{AR}{R_c} \leq 1 \text{ and } -1 \leq B \leq 1 \tag{74}$$

- 87 -

Either AR/R_c or B must be equal to ± 1 for the characteristic velocity used in the Reynolds number to correspond to the actual maximum azimuthal velocity. The values of AR/R_c and B corresponding to various operating modes is given in Table 5.

The Reynolds number defined by Equation (66) can be related to the crystal and crucible Reynolds numbers defined in Section II by the following expressions:

$$Re_s = \frac{ARe}{2\pi(R/R_c)} \tag{75}$$

$$Re_c = \frac{BRe}{2\pi} \tag{76}$$

The above boundary conditions do not include the effect of thermocapillary flow. To incorporate this effect, one starts with a force balance on the flat melt-gas interface:

$$\mu \frac{\partial V_r}{\partial z} = \frac{\partial \sigma_{ST}}{\partial r} \tag{77}$$

where σ is the surface tension. Introducing the thermocapillary coefficient,

$$C_{tc} = -\frac{1}{\mu} \frac{\partial \sigma_{ST}}{\partial T} \tag{78}$$

into Equation (77) one obtains:

$$\frac{\partial V_r}{\partial z} = -C_{tc} \frac{\partial T}{\partial r} \tag{79}$$

- 88 -

Table 5

Crystal and Crucible Rotation Parameters

Definition:

$$A = \frac{\omega_s R_c^2}{Re} \qquad\qquad B = \frac{\omega_o R_c^2}{Re}$$

Examples:

	$A\dfrac{R_s}{R_c}$	B
No rotation	0	0
Crystal rotation only	$\pm$	0
Crucible rotation only	0	$\pm$
Isorotation of crystal and crucible	+	+
Counter-rotation of crystal and crucible	+	−

Putting Equation (79) into non-dimensional form yields:

$$\frac{\partial V_r}{\partial z} = -\frac{Ma}{RePr} \frac{\partial T}{\partial r}$$

(80)

$$Ma = \frac{C_{tc} (T_c - T_m) R_c}{\alpha}$$

(81)

Here Ma is the Marangoni number, a parameter frequently used to characterize thermocapillary flow.

C. SOLUTION PROCEDURE

The system of Equations (61 - 65) was solved numerically by the Galerkin finite element method. The finite element method was selected because it can readily handle irregular geometries and moving boundaries, which must be considered if non-planar interfaces are to be handled. The finite element method has the additional advantage of a more easily graded mesh than say the finite difference method, which is its chief competitor for flow simulation. In the finite element method, the system of differential equations is approximated by a system of algebraic equations by discretization of the problem domain. A non-linear system of differential equations will result in non-linear algebraic equations, which must be solved by some iterative technique. For details of this method in general, see Rao (1982) and/or Finlayson (1980). For the specific problem of solving the Navier-Stokes equations, there is the excellent book by Taylor and Hughes (1983), and the valuable work of Gresho et. al. (1980).

D. RESULTS

The finite-element code developed in this work is capable of solving steady-state problems of hydrodynamics and heat-transfer in an axisymmetric geometry. Arbitrary boundary shapes may be specified, as

- 90 -

long as the shape of the region remains roughly rectangular. At present only the top surface of the melt is allowed to be non-planar. This corresponds to the CZ-crystal growth geometry.

The full code solves simultaneously for the heat-transfer and hydrodynamics in the melt, which are coupled through the buoyant convection term. Additionally, an isothermal code was developed which has a considerably greater computational efficiency than the full simulation. The isothermal code can be used for the case where forced convection is the dominant mode of momentum transfer. It can also be used to determine the flow field directly adjacent to the crystal, which is of great importance to the mass-transfer in the melt.

Some illustrated results based on the steady-state hydrodynamics code are now presented. We consider each flow mechanism separately at this time to indicate the pertinent features. Subsequently all the factors will need to be assessed together. Also a transient code may be necessary for higher Grashof numbers as the flow may be oscillatory.

1. Natural Convection

Figure 25 shows the case of natural convection alone for $Gr = 2 \times 10^4$. The positive values for the streamlines indicate that the flow is in the counter-clockwise direction. The flow pattern observed is that of a single convective cell with hot fluid rising at the crucible wall and cooler fluid descending in the center of the crucible.

Figure 26 represents the flow obtained for $Gr = 2 \times 10^5$. Increasing the Grashof number results in a shift of the center of the cell towards both the wall and bottom of the crucible. Also as can be seen by the magnitude of the stream function at the center of the cell, the intensity of the vortex increases. As Gr is further increased, Crochet et. al. (1983)
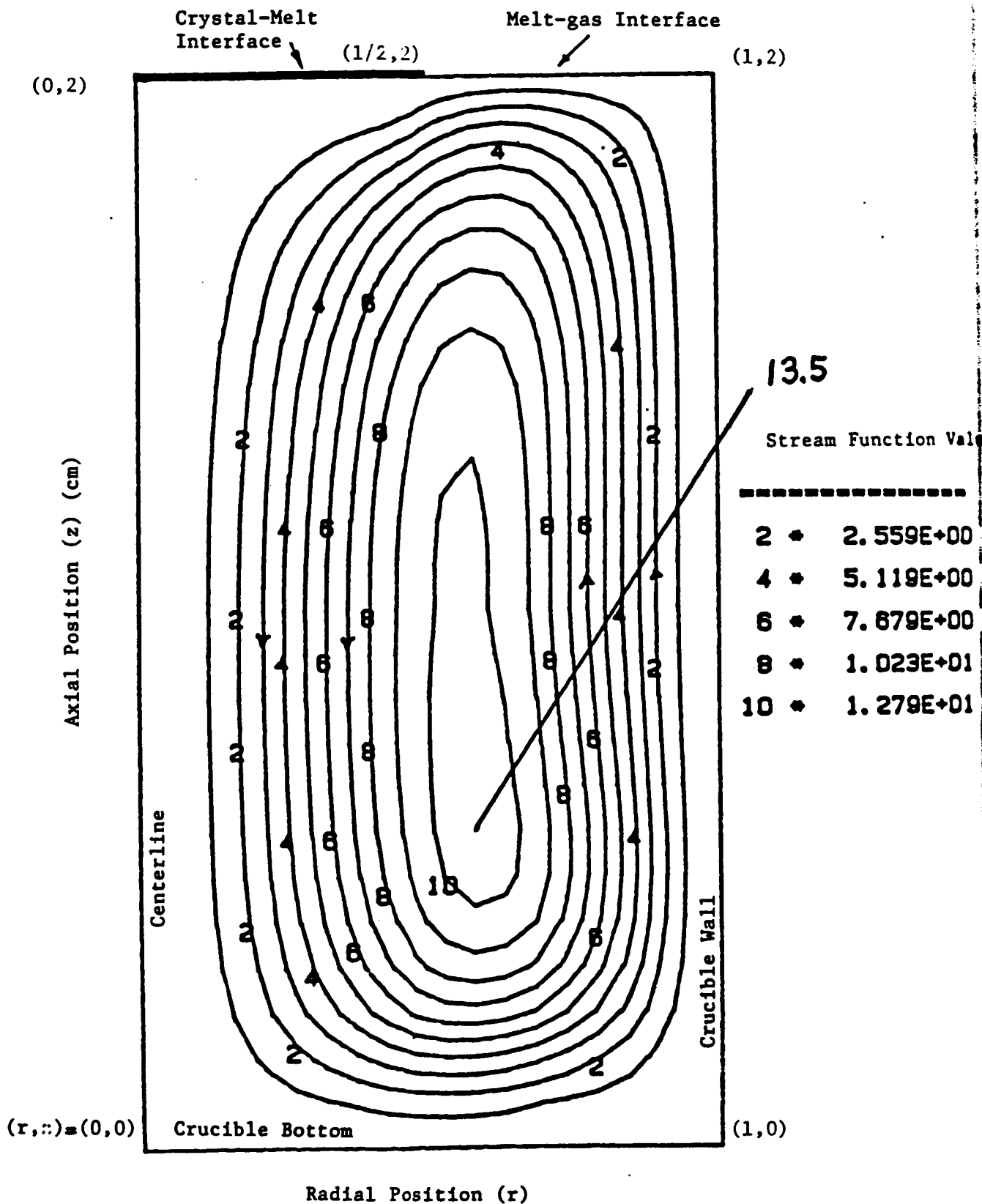
Crystal-Melt Interface

Melt-gas Interface

$(1/2,2)$

$(0,2)$

$(1,2)$

Axial Position (z) (cm)

Centerline

Crucible Wall

Stream Function Val

2 ⊹	2.559E+00
4 ⊹	5.119E+00
6 ⊹	7.679E+00
8 ⊹	1.023E+01
10 ⊹	1.279E+01

13.5

$(r,z)=(0,0)$ Crucible Bottom

$(1,0)$

Radial Position (r)

Figure 25.   Flow Field in the Melt for the Case of Natural
Convection Alone, $Gr = 2 \times 10^4$
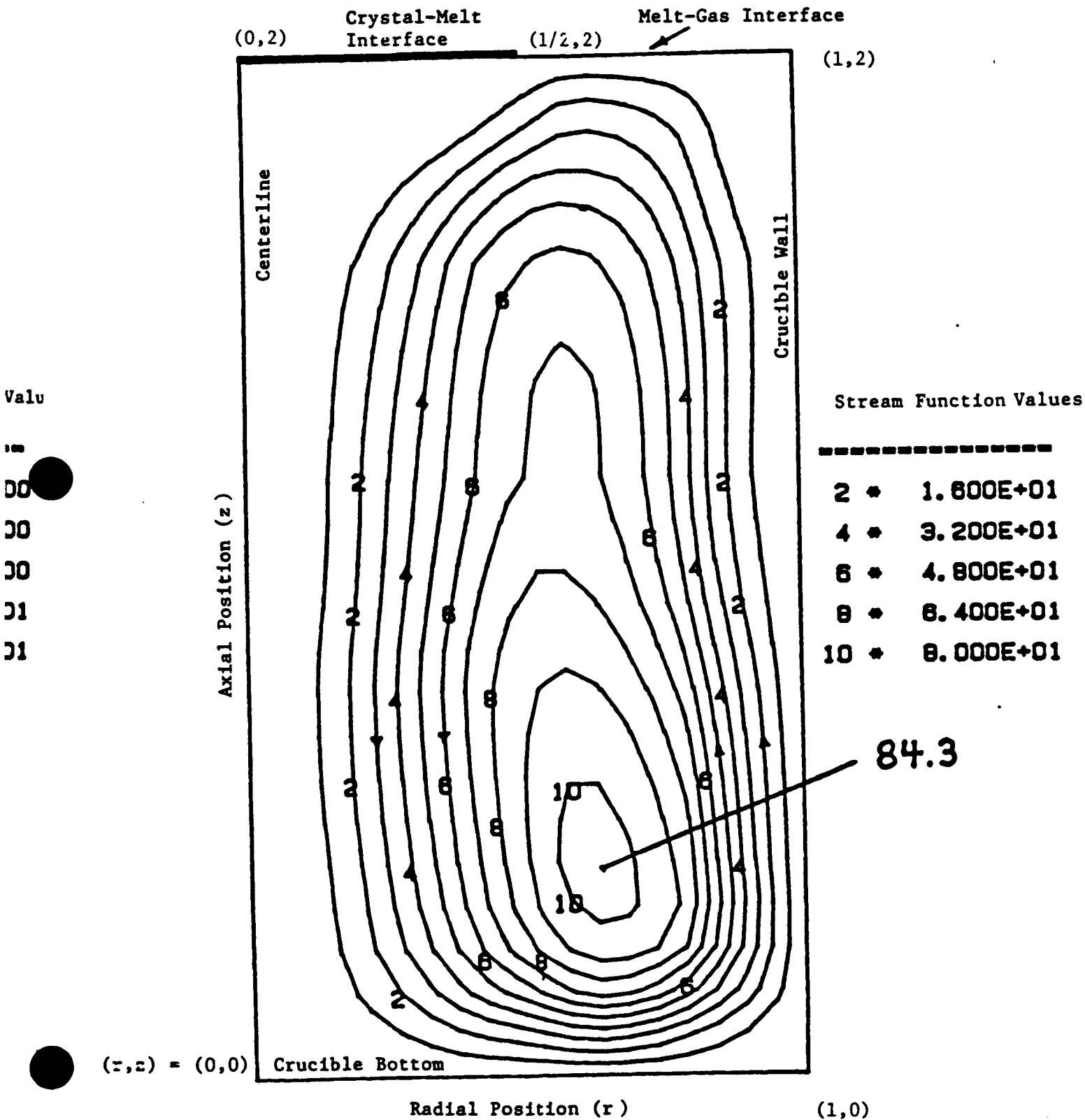
Figure 26.   Flow Field in the Melt for the Case of Natural
Convection Alone, Gr = 2 x 10^5.

have found that the number of convective cells can increase to two or more. After some critical value is reached (Crochet found this to be $Gr = 10^7$ for his geometry and gallium arsenide) an oscillatory regime is encountered.

Natural convection enhances oxygen evaporation from the melt. The oxygen, as soon as it is dissolved from the silica crucible, is immediately convected upwards towards the melt surface, from which it can readily evaporate. Unfortunately this flow pattern results in a very poor radial dopant distribution, as the flow is radially inward at the crystal surface.

The natural convection flow pattern was also simulated using a commercially available hydrodynamics simulation software package (FIDAP). The steady state version of FIDAP gave a stable solution for $Gr = 10^7$. The transient version gave an unstable oscillatory flow for $Gr = 10^9$. However we need to confirm this with further mesh refinement and such work is in progress.

2. Crystal Rotation

The results of crystal rotation is again a single convective cell. Fluid is accelerated outwardly by the rotating crystal and drawn upward in the center of the crystal to conserve mass. As can be seen from both the streamlines and the azimuthal velocity (Figures 27 and 28 respectively) the flow is essentially a boundary-layer flow.

This flow mechanism does an excellent job of reducing radial gradients in dopant concentration. Oxygen evaporation is inhibited, however, because the clockwise vortex near the free surface blocks the transport of oxygen to the melt surface. Simulation studies using higher Reynolds numbers are in progress.
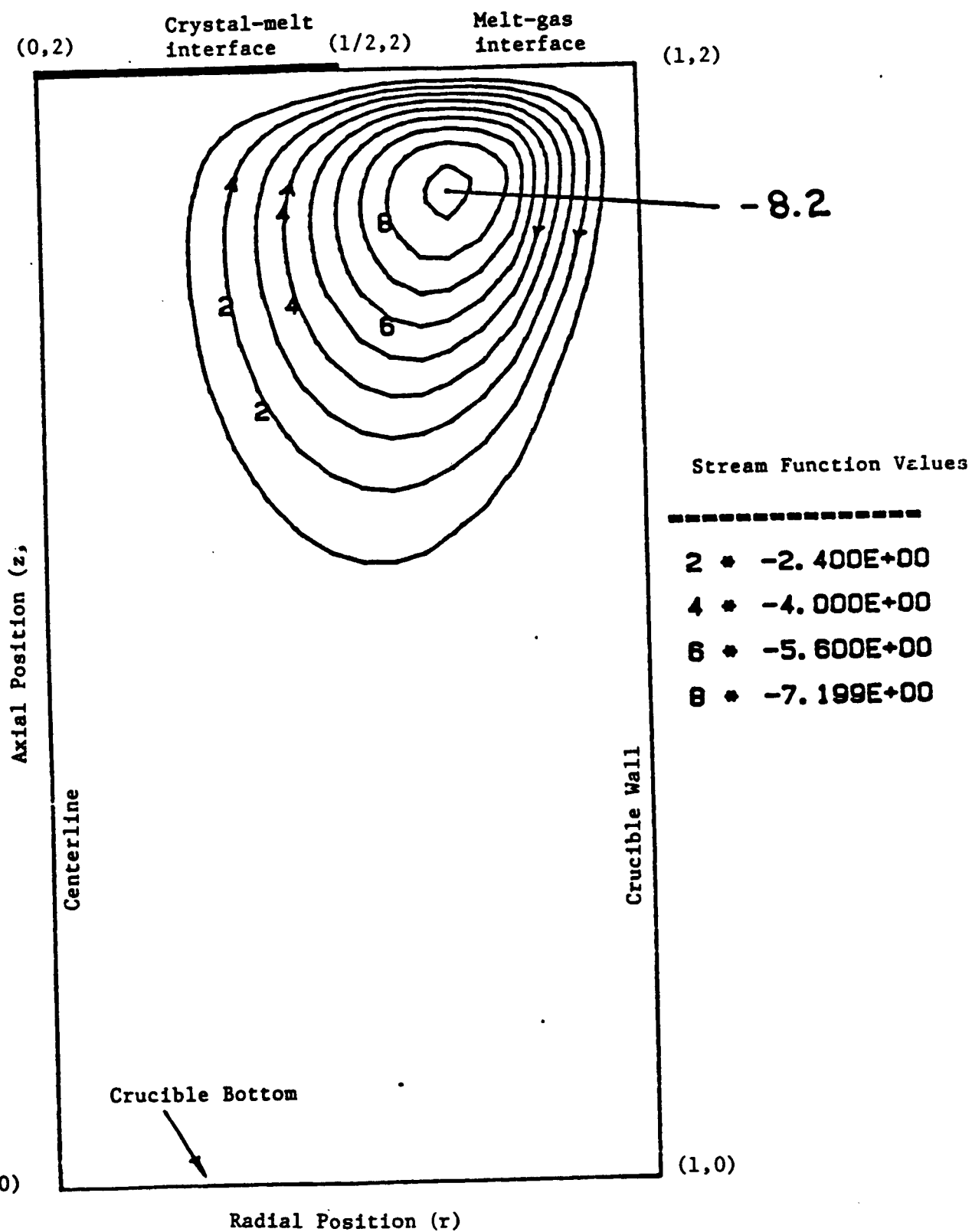
(r,z)

- 94 -

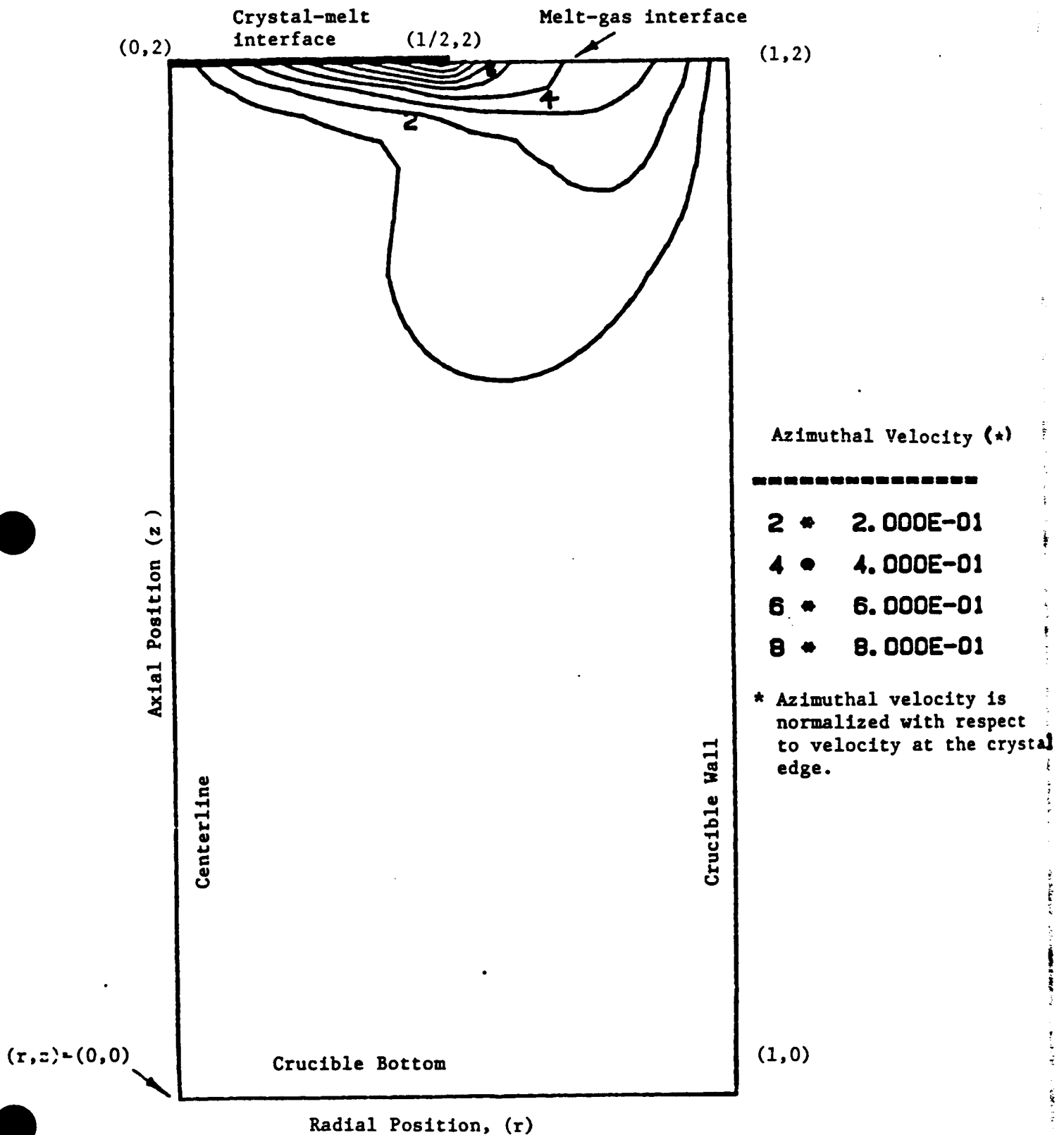Figure 27. Effect of Crystal Rotation on the Melt Flow
Field, Re = 200.

Figure 28. Azimuthal Velocity Field in the Melt Due
to Crystal Rotation, Re = 200.

3. Crucible Rotation

Figures 29 and 30 depict the flow generated by crucible rotation alone. The low value of Re used is for computational simplicity. One can see from Figure 30 that there are sharp radial and axial gradients in the azimuthal velocity near the stationary crystal. The magnitude of these gradients increases as Re is increased, so that considerable refinement of the finite element mesh is required to obtain an accurate result. Implementation of this refinement would cause significant increases in the amount of computational time required. A supercomputer program effort may be needed. Time is available on supercomputer and this will be put to use.

The flow pattern here is a single counter-clockwise vortex. This would tend to favor oxygen evaporation but would be detrimental to the radial dopant distribution. Crochet et. al. (1983) have found that for higher Reynolds numbers, which are more in line with those observed in practice, a second vortex forms. This vortex is of low intensity, rotating clockwise along the crucible wall. This will block the transport of oxygen to the melt surface. For these reasons the crucible is generally only rotated when the crystal is rotated at a higher rate.

4. Thermocapillary Flow

Thermocapillary flow can be isolated from other flow mechanisms only in conditions of microgravity. In fact, Langlois (1980) has found it to be the dominant mode of momentum transport in microgravity. The result of the simulation is shown in Figure 31. The flow is similar to that of natural convection, but is restricted to the area directly below the free surface. The remainder of the melt is essentially stagnant.
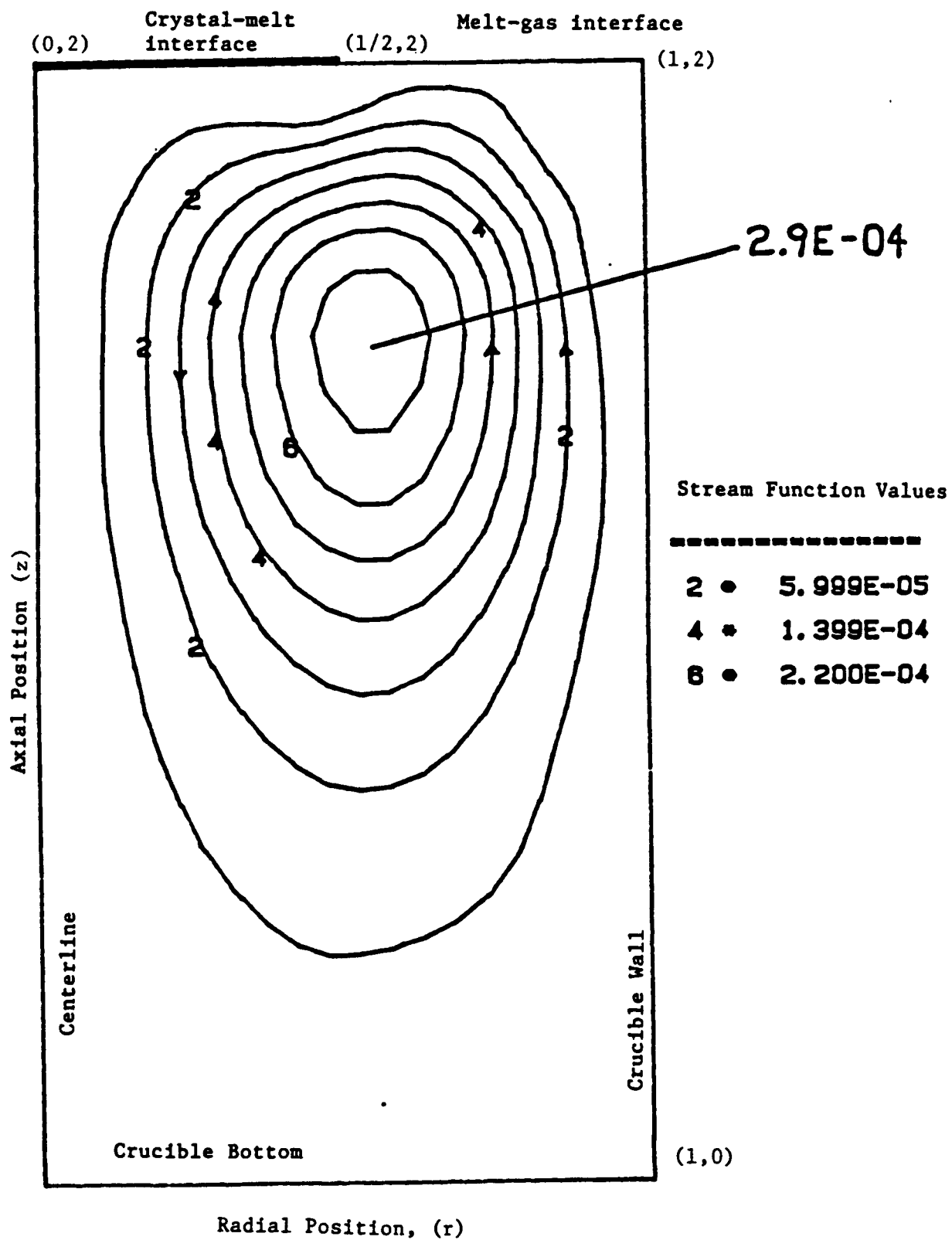
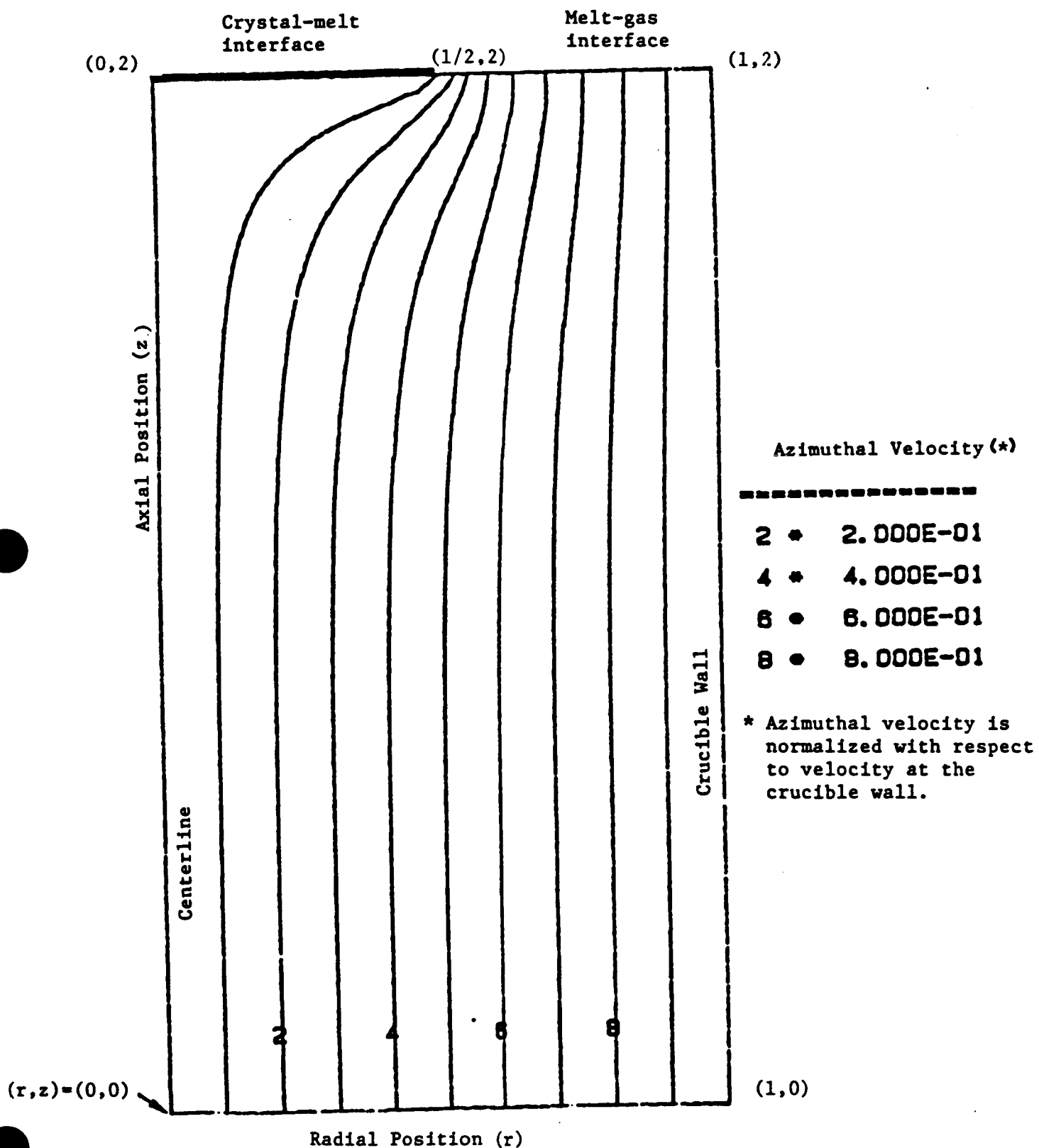Figure 29. Effect of Crucible Rotation on the Melt Flow Field, Re = 1.

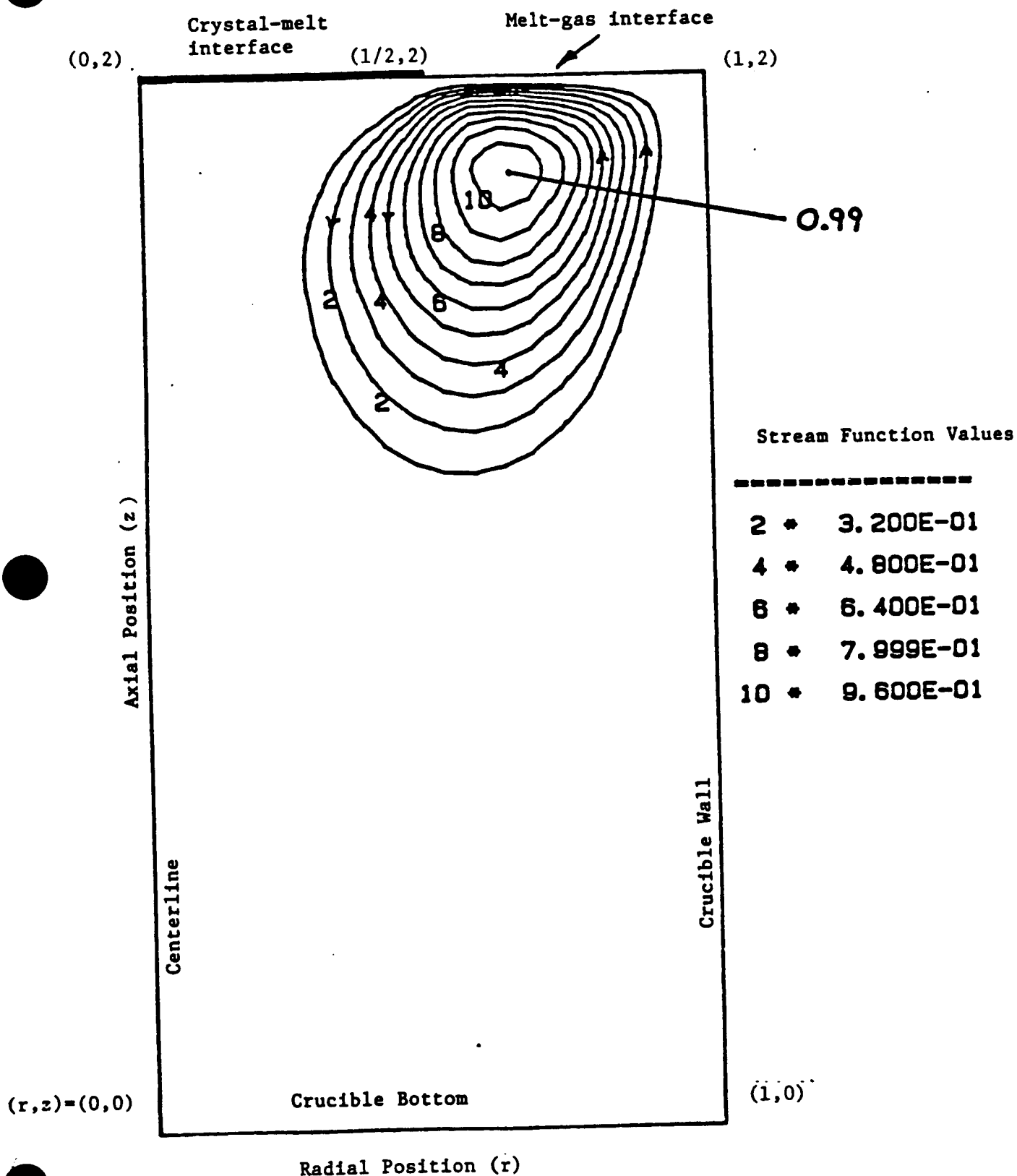Figure 30. Azimuthal Velocity Field in the Melt due to
Crucible Rotation, Re = 1.

Figure 31. Effect of Thermocapillary Flow on the Melt
Flow Field.

Stream Function Values

2	*	3.200E-01
4	*	4.800E-01
6	*	6.400E-01
8	*	7.999E-01
10	*	9.600E-01

Due to the limited extent of the vortex, this flow pattern will not enhance oxygen evaporation as much as in the case of natural convection. Radial segregation of dopant will be poor for this case as well.

5. Heat Transfer

Figures 32 and 33 show the transition from the conduction dominated case to the case where convection is significant. In Figure 33 there is a dramatic change in the isotherms from the previous cases (no flow situation), indicating that the convective terms have become significant. (Note that the Grashof number used here is very low compared to those actually observed in practice). The above results tend to cast some doubts on conduction dominated models (those that neglect the hydro-dynamics in the melt).

The above results are not conclusive, however, as radiation from the melt surface is not considered. Also there is some question as to the appropriate boundary condition along the crucible bottom. In the present work it is considered to be thermally insulated. Crochet et. al. (1983) specified that it had the same temperature as the crucible wall. Lee et. al. (1984) chose a linear temperature profile decreasing towards the center of the crucible. The effect of these factors need to be examined in detail. These studies and development of a transient hydrodynamics code are not within the scope and time frame of the current study.
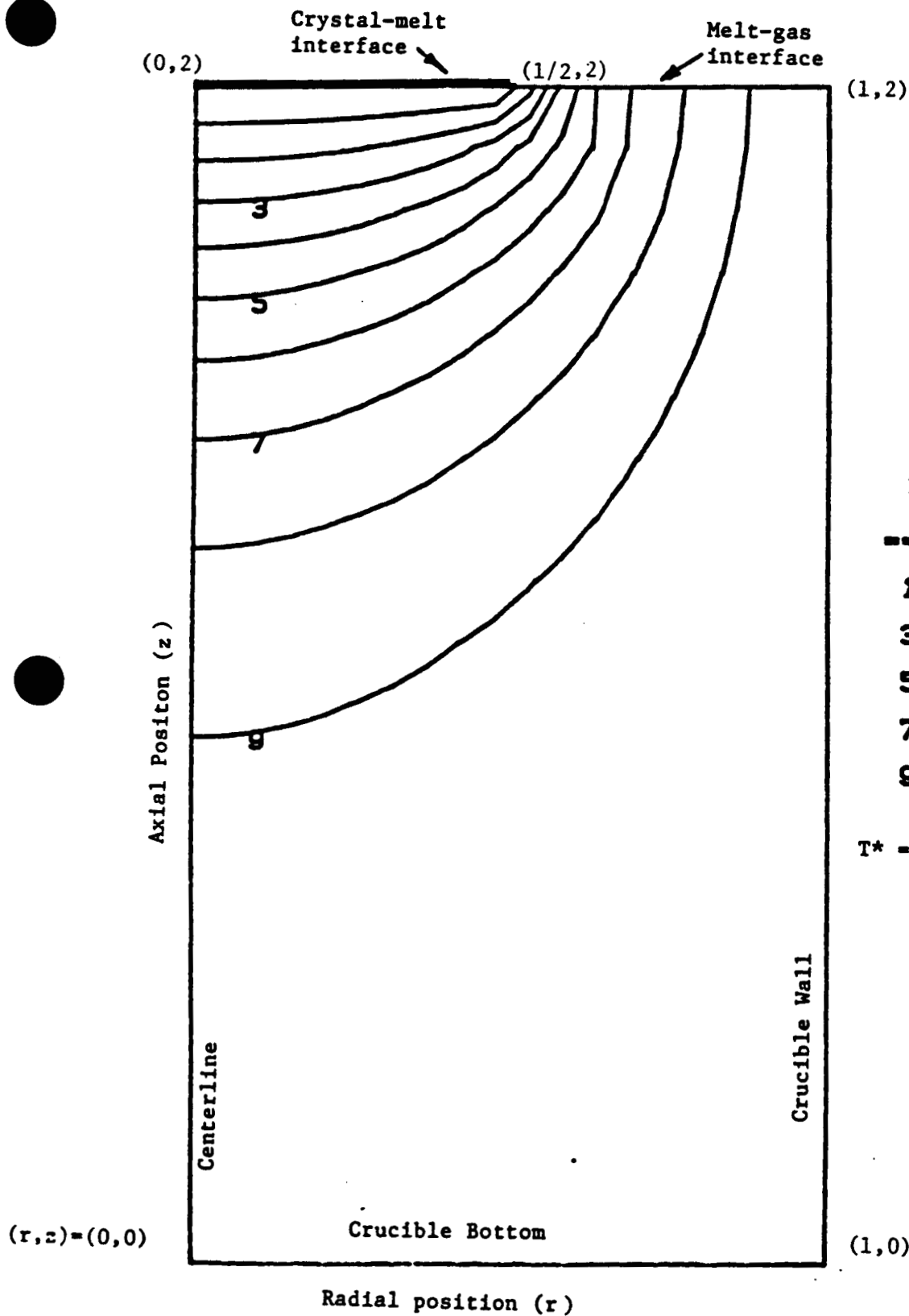
Figure 32. Temperature Field in the Melt for the Case of Conduction alone (NO FLOW).
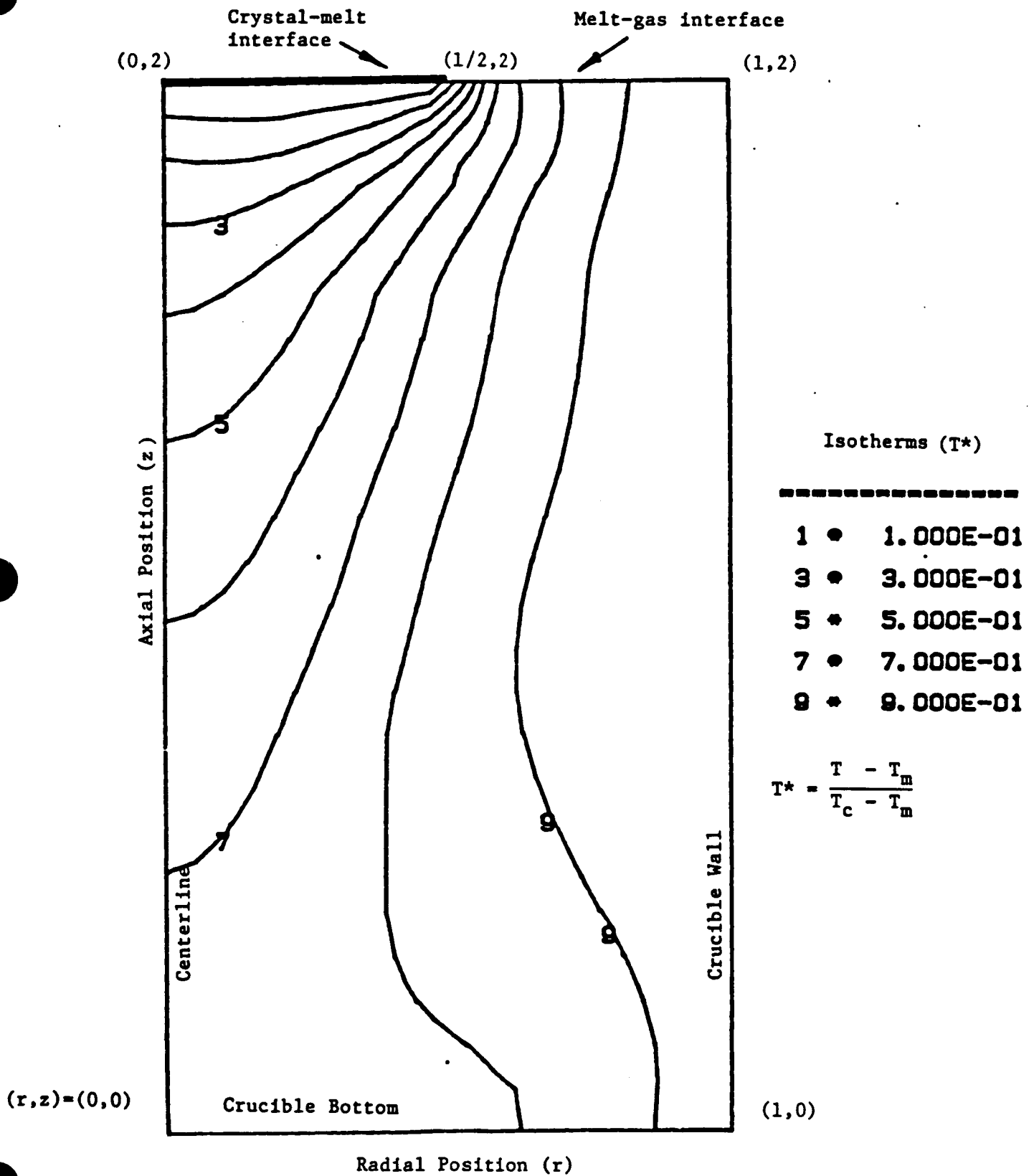
Figure 33. Effect of Natural Convection (Gr = 2 x 10^5) on the Melt Temperature Field.

- 103 -

VIII.   STRESS ANALYSIS

Preliminary stress calculations were done to estimate the generation
of dislocations in the crystal. The temperature field maintained in the
crystal during its growth by the Czochralski process plays an important
role in determining the crystal quality. It has been well established
that the thermal stresses induced during the growth process are one of the
major causes of the generation of dislocations in the crystal. The nature
and the magnitude of the induced thermal stresses are directly related to
the temperature profiles in the crystal. The dislocations are generated
if the stress field in the crystal exceeds a certain threshold value.

The motivation for this study was to investigate the induced
thermal stresses in silicon crystals grown by the Czochralski process.
The accurate estimation of the stress field in the crystal is closely
linked with the knowledge of the realistic temperature field in the crystal.
Therefore, the temperature field was predicted using the rigorous heat
transfer model of the CZ apparatus, as described in Section III. The shape
of the curved crystal-melt interface, predicted by the heat transfer
model, is included in the stress calculations. The stress field is cal-
culated numerically using a finite element formulation and also with the
plane strain approximation. The concept of von Mises stress is used to
examine the dislocation distribution in the crystal.

The calculation of the stress field is based on the theory of
thermoelasticity. In this theory it is assumed that elastic and thermal
strains can be superimposed in Hooke's law. The finite element for-
mulation is based on the principle of minimum potential energy. In
this approach the displacement field is derived from the known temperature
field. The strain and stress field is then calculated from the displace-
ment field. The crystal is assumed to be an axisymmetric solid and

therefore the displacement is confined to only radial, u, and axial, w, directions. The displacement along the θ-direction, v, is zero on account of symmetry. Axisymmetric ring elements with a triangular cross-section are used for the finite element formulation. The results of this study are briefly discussed next.

Figure 34 shows the axial variation of the von Mises stress in the crystal at the outer edge. The radial temperature variation ΔT $(T_{r=0} - T_{r=R})$ is also plotted. The results based on the plane strain approximation are shown together with the rigorous finite element predictions. The stress profiles basically follow the axial variation of the radial temperature variation. The plane strain approximation is able to predict the stress profile in a qualitative sense but it predicts much lower values of the stress. The von Mises stress profile has several maxima, the location of each coincides with the maximum in $|\Delta T|$. The possibility of the dislocations generation is the highest around these maxima. However, one should keep in mind that the yield stress increases with decreased temperature so that a smaller ΔT at higher temperature is more likely to cause dislocations. The key to reducing the level of induced stresses (and hence dislocation density) is to restrict the level of the radial temperature gradient in the crystal, especially in the region close to the interface. The extent of the radial temperature difference is mainly determined by the value of the Biot number and therefore lowering the Biot number will result in smaller stresses. This can be done by lowering the heat transfer coefficient and/or increasing the ambient temperature and by suitable design of the furnace configuration. Of course, these changes in the parameters will lower the growth rate of the crystal and therefore an optimum needs to be found between increasing the growth
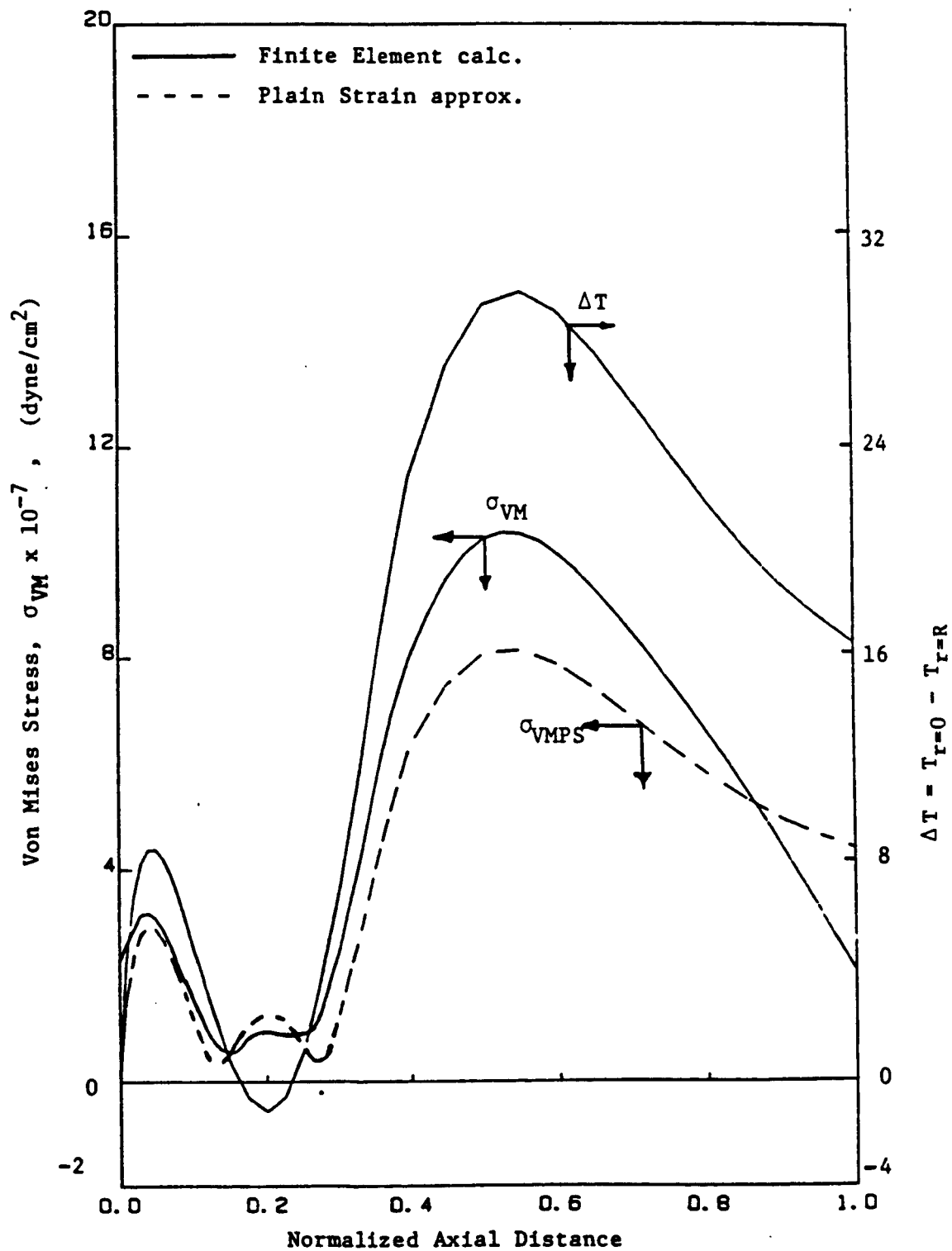
Figure 34. Axial Variation of Von Mises Stress at the
            Outer Edge of the Crystal.

rate and restricting the extent of thermally induced stresses in the growing crystal.

The detailed distribution of the von Mises stress field in the crystal is plotted in Figure 35 in the form of iso-stress contours. The pattern of the stress field matches well with the results of Duseaux (1983) and of Schvezov et. al. (1986). The region of maximum stress is about 10 cm above the crystal-melt interface. It should be remembered that the maximum radial temperature gradient occurs in this region. The iso-stress lines with large stress values are concentrated at this axial location, particularly near the outer periphery and around the center axis of the crystal. Thus maximum dislocation density is expected in this region. The minimum dislocation density at the wafer surface is found to be in the region which is between the center and the periphery. This has also been observed experimentally from the dislocation distribution revealed by x-ray topography of a cross section of the wafer (Chen and Holmes, 1983). The stresses in the vicinity of the crystal-melt interface have low values. This is due to the effects of the hot crucible wall which restricts the radial temperature variation in the crystal in this region.

The detailed stress field needs to be analyzed in terms of resolved shear stress distribution on the wafer surface. This distribution can then be correlated with the expected defect density (wafer quality) on the wafer surface. This work is in progress but was not part of the original objective of this study.
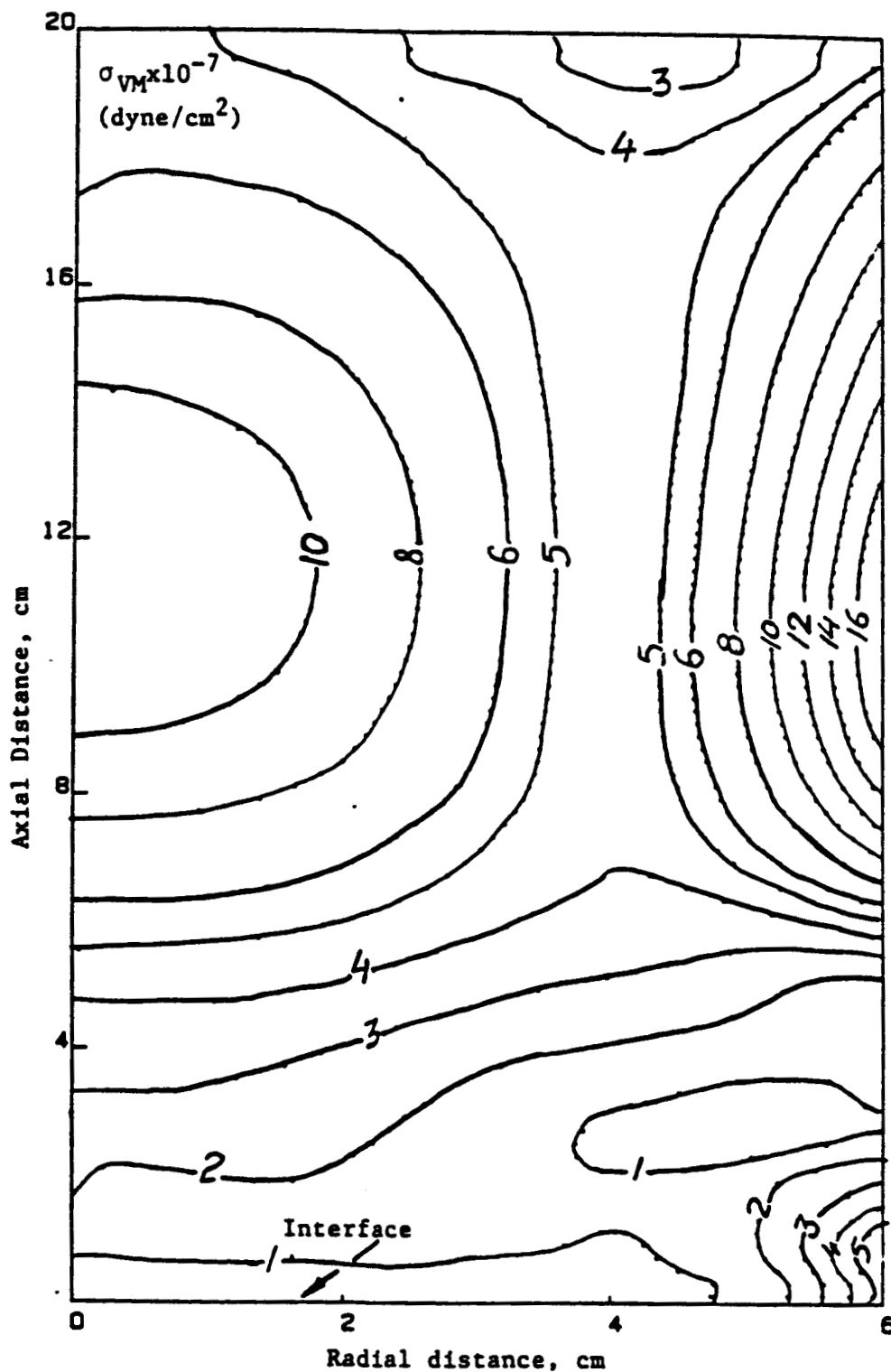
Figure 35. Von Mises Stress Field ($\sigma_{VM} \times 10^{-7}$, dyne/cm^2) in a Crystal With a Planar Interface.

IX. CONCLUSIONS

A detailed heat transfer model for the simulation of the Czochralski (CZ) process has been developed. The model considers the combined crystal + melt system and accounts for both direct and reflected radiation interactions among the various surfaces in the enclosure. The heat transport in the melt is assumed to be by conduction only. The shape of the crystal-melt interface is not assumed "a-priori", but is predicted, along with the pull rates, as a part of the solutions. A sequential modular approach is used for the computer implementation. The algorithm is flexible and can be readily extended without significant reprogramming to accommodate a more sophisticated model for the melt which includes the melt hydrodynamics and subsequently the effect of an applied magnetic field.

The effects of the melt-gas meniscus and of various process parameters on the interface shape (crystal quality) and the pulling rate (process productivity) have been investigated in detail and explained. It appears that the shape of the melt-gas meniscus has a significant effect on both the pulling rate and the interface shape and must be included for accurate modeling of the crystal growth process, especially when the three phase contact angle is very small (as in the case of silicon).

Radiation from the exposed crucible wall plays an important role in the growth process and it seems to control the extent of the radiation heat losses from both the lower portion of the crystal and from the melt. This indicated the need for properly accounting for both direct and reflected radiation among the various 'surfaces' present in the crystal growing apparatus. This study confirms that Stefan's model is inadequate to model the radiation heat exchange behavior (which is the dominant mode

here) in the enclosure and that detailed radiation calculations, as pre-
sented here, are essential.

Additionally, simple models have also been proposed which describe
the relationship between the important process variables affecting the
growth process. The parameters of the model can be determined either
from the results of the rigorous models or from actual operating data.
The use of these models in implementing various operating policies has
been demonstrated.

A novel technique to improve the controllability of the crystal
diameter has been introduced. The concept relies on regulating the con-
vecting cooling component of the crystal by using gas jets. This scheme
also facilitates a simultaneous control of crystal diameter and interface
shape.

A preliminary computer code was developed for a steady-state model
of the hydrodynamics of the melt. The model is useful for a quantitative
study of the effects of various phenomena, such as natural convection,
forced convection, and thermocapillary flow, on the melt flow field.
However, it appears that in the real operating region, the melt flow field
is of oscillatory nature and thus a transient code may be needed. Also,
the melt hydrodynamics need to be coupled with the model of the crystal
to develop a complete model of the CZ system.

The distribution of dislocations in the crystal is qualitatively
related to the thermally induced stress field. The stress field is
calculated from the known temperature distribution and the finite element
solutions of the thermoelastic equations. The magnitude of the induced
stresses is mainly governed by the radial temperature gradients in the
crystal.

X. FUTURE EFFORT

Future effort should concentrate on complete model validation by comparison to experimental data. Extension of the model in the following specific areas, related to the CZ process is recommended:

1. Transient code needs to be developed to describe the hydrodynamics of the melt in the operating region of interest.

2. Heat transfer model of the crystal + melt should be coupled with the melt hydrodynamics to develop a complete model of the CZ process.

3. Effects of an applied magnetic field (both axial and transverse) to suppress the convective currents should be modeled.

4. A model describing the solute transport in the crystal + melt is needed. The model should be able to predict both the axial and the radial dopant profiles.

XI. NEW TECHNOLOGY

The work described within this report is related to two new technological developments. It provides the elements for a future on-line digital control of the CZ process. It introduces the concepts of improved growth rates via jet-cooling and simultaneous interface shape-crystal diameter control via jet cooling.

A,B   empirical constants in equation (22a)

A'   empirical constant in equation (26)

a   constant for convective heat transfer

A_k area of surface 'k'

A_s cross-sectional area of the crystal

B_1, B_2 empirical constants in equations (24b) and (25)

B_1', B_2' empirical constants in equation (26)

C_{ps} specific heat of the crystal

C_{tc} thermocapillary constant

d   distance between the jet nozzle and the crystal surface

D   nozzle diameter (inner)

dc_i node spacing at radial position i in the z-direction in the crystal at the interface

dm_i node spacing at radial position i in the z-direction in the melt at the interface

f_i fractional deformation of the interface at node i for updating the interface

F_{ij} view factor from i to j

G_{ik} radiation factor representing the fraction of the radiation emitting from surface 'i' which is absorbed by surface 'k'

Gr   Grashof number, $Gr = \beta g \Delta T R_c^3 / \nu^2$

h   convective heat transfer coefficient

h_c height of the exposed portion of the crucible wall

k_a thermal conductivity of the gas phase in the puller

k_s thermal conductivity of the crystal

k_ℓ thermal conductivity of the melt

L   crystal length

m_i slope of the interface at location i

Ma	Marangoni number, $Ma = C_{tc}\Delta T R_c/\alpha$
n	direction of outward normal from the melt at the melt-crystal interface or melt-gas interface
N	total number of surfaces
NC	number of surfaces for the crystal side
NM	number of surfaces for the melt surface
NT	number of surfaces for the crystal top
Nu_o	Nusselt numbers for jet cooling, hD/k_a
P	pressure
Pr	Prandtl number, $Pr = \nu/\alpha$
q_R	heat loss by radiation per unit area
Q_s	heat flux at the interface in the crystal
Q_ℓ	heat flux at the interface in the melt
Q_f	heat flux due to solidification at the interface
r	radial coordinate
R	crystal radius
R_c	crucible radius
R_1, R_2	principal radii of curvature of the melt surface
Re	Reynolds number, $Re = V_{\theta max} R_c/\nu$
Re_o	Reynolds number for jet cooling
Re_c	crucible Reynolds number $Re_c = \dfrac{\omega_c^2 R_c}{\nu}$
Re_s	crystal Reynolds number $Re_s = \dfrac{\omega_s^2 R_c}{\nu}$
t	time
T	temperature at position (r,z)

T_a	average argon temperature
T_c	crucible temperature
T_e	effective temperature for radiation
T_{eff}	effective temperature for radiation in the Stefan's model
T_k	temperature of surface k
T_m	melting point of silicon
v_r	radial velocity
v_z	axial velocity
v_θ	azimuthal velocity
v	crystal pulling rate
v_{max}	maximum pulling rate
V_c	volume of the crucible
V_m	melt volume
z	axial co-ordinate
z	also represents distance from impingement point in equation (41)
$z_1(r)$	equation of the interface shape
$z_2(r)$	equation of the melt free surface

Greek Symbols

α	thermal diffusivity
$\alpha_1, \alpha_2, \alpha_3$	empirical constants in equation (30)
$\alpha_1', \alpha_2', \alpha_3', \alpha_4'$	empirical constants in equation (31)
β	volume expansivity of the melt
$\beta_1', \beta_2', \beta_3', \beta_4'$	empirical constants in equation (37)

ΔH	heat of fusion
Δr	deviation of the interface from the planarity
ΔT	difference between crucible temperature and melting point
ρ_m	density of melt
ρ_s	density of crystal
ε_i	emissivity of surface indicated in the subscript
σ	Stefan-Boltzman constant
ν	kinematic viscosity of the melt
$\partial \sigma_{ST}$	surface tension of the melt
μ	viscosity of the melt
ψ	dimensionless group defined by Equation (18)
θ	azimuthal co-ordinate
ω_c	crucible rotation rate
ω_s	crystal rotation rate

Subscript

a	ambient
i	radial position at the interface
k	denotes k^{th} surface emitting or receiving radiation
m	melt
s	crystal
r	radiation

XIII. BIBLIOGRAPHY

1. Billig, K., Proc. Roy, Soc. Lond. A235, 37, (1955).

2. Bird, R. B., W. E. Stewart and E. N. Lightfoot, Transport Phenomena, John Wiley and Sons, (1960).

3. Brice, J. C., Acta Electronica, 16, 291, (1973).

4. Brice, J. C., O. F. Hill, P. A. C. Whiffin and J. A. Wilkinson, J. Crystal Growth, 10, 133, (1971).

5. Brice, J. C., O. F. Hill and P. A. C. Whiffin, J. Crystal Growth, 6, 297, (1970).

6. Brown, R. A. and H. M. Ettouney, J. Crystal Growth, 62, 230, (1983).

7. Chen, R. T. and D. E. Holmes, J. Crystal Growth, 61, 111, (1983).

8. Crochet, M. J., P. J. Wouters, F. T. Geyling and A. S. Jordan, J. Crystal Growth 65, 153, (1983).

9. Derby, J. J. and R. A. Brown, J. Crystal Growth, 73, 227-240 (1986).

10. Derby, J. J., R. A. Brown, F. T. Geyling, A. S. Jordan and G. A. Nikolakopoulou, J. Electrochem Soc., 132, 470, (1985).

11. Dorsey, D., P. A. Ramachandran and M. P. Duduković, presented at AIChE Symposium '85, St. Louis Chapter, 1985.

12. Duseaux, M., J. Crystal Growth, 61, 576 (1983).

13. Finlayson, B. A., Nonlinear Analysis in Chemical Engineering, McGraw-Hill, (1980).

14. Gardon, R. and J. G. Akfriat, J. Heat Transfer, 2, 101, (1966).

15. Gebhart, B., "Heat Transfer", McGraw-Hill, p. 117-122, (1961).

16. Gresho, P. M., B. L. Lee and R. L. Sani, "On the Time-Dependent Solution of the Incompressible Navier-Stokes Equations in Two and Three Dimensions", in Chapter 2 of Recent Advances in Numerical Methods in Fluids, Volume I, Taylor, C. and Morgan, K. editors, Pineridge Press Limited (1980).

17. Howell, J. R., "A Catalog of Radiation Configuration Factors", McGraw-Hill, (1982).

18. Hurle, D. T. J., J. Crystal Growth, 63, 12, (1983).

19. Inoue, T., Trans. JIM, 17, 227, (1976).

20. Kim, K.M., A. Kran, P. Smetana and G. M. Schwuttke, J. Electrochem. Soc., 130, 1156, (1983).

21. Kobayashi, N. and T. Arizumi, Japanese J. Appl. Physics, 9, 361, (1970).

22. Kobayashi, N. and T. Arizumi, J. Crystal Growth, 13/14, 515, (1972).

23. Kobayashi, N. and T. Arizumi, J. Crystal Growth, 30, 177, (1975).

24. Kobayashi, N., "Heat Transfer in CZ Crystal Growth", Marcel Dekker, Inc.

25. Langlois, W. E. and C. C. Shir, Comp. Meth. in Appl. Mech. & Eng., 12, 145, (1977).

26. Langlois, W. E., J. Crystal Growth, 42, 386, (1977).

27. Langlois, W. E., J. Crystal Growth, 48, 25, (1980).

28. Langlois, W. E., J. Crystal Growth, 70, 73, (1984).

29. Lee, K., W. E. Langlois & K. M. Kim, PhysicoChemical Hydrodynamics, 5, 135, (1984).

30. McAdams, W. H., "Heat Transmission", McGraw-Hill, New York, 1954, Chapter 7.

31. Mihelcic, M., C. Schroek-Pauli, K. Wingerath, H. Wenzl, W. Uelhoff and A. Van Der Hart, J. Crystal Growth, 53, 337, (1981).

32. Mihelcic, M., C. Schroek-Pauli, K. Wingerath, H. Wenzl, W. Uelhoff and A. Van Der Hart, J. Crystal Growth, 57, 300, (1982).

33. Mihelcic, M., K. Wingerath and Chr. Pirron, J. Crystal Growth, 69, 473, (1984).

34. Mihelcic, M. and K. Wingerath, J. Crystal Growth, 71, 163 (1985).

35. Mil'vidskii, M. G., and B. I. Golovin, Sov. Phys.-Solid State, 3, 737, (1961).

36. Minning, C. P., AIAAJ, 17, 1406, (1979).

37. Ramachandran, P. A. and M. P. Dudukovic, J. Crystal Growth, 71, 399-408 (1985).

38. Rao, S. S.,"The Finite Element Method in Engineering", Pergamon Press, (1983).

39. Rea, S. N., AIAAJ, 13, 1122, (1975).

40. Rea, S. N., J. Crystal Growth, <u>54</u>, 267, (1981).

41. Schvezov, C., I. V. Samarasekera and F. Weinberg, J. Crystal Growth, In Press (1986).

42. Siegal, R. and J. R. Howell, "Thermal Radiation Heat Transfer", McGraw-Hill, p. 798, (1972).

43. Srivastava, R. K., P. A. Ramachandran and M. P. Duduković, J. Crystal Growth, <u>73</u>, 487-504, (1985a).

44. Srivastava, R. K., P. A. Ramachandran and M. P. Duduković, J. Electrochem. Soc., Solid State Sci. Techn., <u>133</u>, 1007-1015, (1985b).

45. Srivastava, R. K., P. A. Ramachandran and M. P. Duduković, J. Crystal Growth, <u>74</u>, 281-291, (1986a).

46. Srivastava, R. K., P. A. Ramachandran and M. P. Duduković, "Effects of Jet Cooling in CZ Growth", J. Crystal Growth. In Press. (1986b).

47. Taylor, C. and T. G. Hughes,"Finite Element Programming of the Navier-Stokes Equations", Pineridge Press Limited, (1983).

48. Vlachopoulos, J. and J. F. Tomich, Can. J. Chem. Eng., <u>49</u>, 462, (1971).

49. Westerberg, A. W. and R. L. Motard, "Process Flowsheeting", Cambridge University Press, (1979).

50. Wilcox, W. R. and R. L. Duty, J. Heat Transfer, <u>45</u>, 88, (1966).

XIV. LIST OF FIGURES AND CAPTIONS

Figure 1.   Schematic of Czochralski Single Crystal Puller --- Indicates Radiation Interaction Between Various Surfaces.

Figure 2.   Overall Schematic of CZ Modeling.

Figure 3.   A Typical Finite Element Mesh with Triangular Basic Cells for Crystal + Melt.

Figure 4.   Temperature Field in the Crystal and Melt. (Flat Melt - Gas Interface).

Figure 5.   Temperature Field in the Crystal and Melt. (Curved Melt-Gas Interface).

Figure 6.   Effect of Crucible Temperature on Interface Shape. (Flat Melt - Gas Interface).

Figure 7.   Effect of Crucible Temperature on Interface Shape. (Curved Melt - Gas Interface).

Figure 8.   Effect of Crystal Radius on Interface Shape.

Figure 9.   Efficiency of Radiation of the Crystal Side Surface.

Figure 10. Temperature Profile on Crystal Surfaces: Effect of Radiation Interactions.

Figure 11. Variation of Growth Rate with Respect to Crucible Temperature. ——: Detailed Model: **: Linear Model.

Figure 12. Variation of V_{max} and B with Crystal Radius. ——:   Simple Model: ● ,*: Detailed Model Numerical Solution.

Figure 13. Variation of Growth Rate with h and h_c and Variation of Interface Shape with h_c.

Figure 14. Effect of Increasing the Height of Exposed Crucible Wall on the Pull rate; * Denotes the Simple Model while the Full Lines Denote Numerical Solution.

Figure 15. Variation of Interface Shape with Crystal Radius. ——: Detailed Model; **: Simple Model.

Figure 16. Variation of Interface Shape with Crucible Temperature. ——: Simple Model; **: Detailed Model.

Figure 17. Effect of Increasing Height of Crucible Wall on Interface Shape.

XV. LIST OF TABLES

XVI. APPENDICES

1. Procedure For Updating The Interface Shape And The Pulling Rate

The procedure for updating the interface shape and the pulling rate is as follows: Let z_i $(i=1, 2,..., nr)$, where nr is the number of nodes in the radial direction, define the z-coordinate of the interface. z_1 is the center point $(r=0)$ and z_{nr} refers to the edge of the crystal $(r=R)$. Equation (10) at $i=nr$ is used to update the pulling rate as follows:

$$v = \left[\frac{Q_{s,nr} - Q_{\ell,nr}}{\rho \Delta H}\right] \sqrt{m^2_{nr} + 1} \qquad \text{(A1)}$$

The melt volume balance (Equation 12) along with the shape of the melt meniscus is used to update z_{nr}. To update the other points, z_i, [$i=1$ to $(nr-1)$] the following procedure is used. Consider a fixed radial position corresponding to node i. Let dc_i = element size in the z direction into the crystal at the interface at node i. Assume that the interface needs to be moved a distance $f_i dc_i$ in the positive z direction in order to satisfy the heat flux requirement (Equation 10)). We then have the axial flux in the crystal (which is also assumed to be proportional to the overall flux as an approximation) at node i at the current interface location as:

$$Q_{si} \propto - k_s \left(\frac{\partial T}{\partial z}\right)_{s,i} \approx \frac{- k_s (T_2 - T_m)}{dc_i} \qquad \text{(A2)}$$

where T_2 is the temperature at $z_i + dc_i$.

Similarly the axial heat flux from the melt at node i at the current interface location is:

$$Q_{\ell 1} \propto - k_\ell \left(\frac{\partial T}{\partial z}\right)_{\ell,1} = \frac{- k_\ell (T_m - T_1)}{dm_1} \tag{A3}$$

where dm_1 = element size in the z direction into the melt at the interface at node i and T_1 is the temperature in the melt at location $z_1 - dm_1$.

The axial heat flux in the crystal at node i after relocation of the interface becomes:

$$- k_s \left(\frac{\partial T}{\partial z}\right)_{s,1}^{new} = \frac{- k_s (T_2 - T_m)}{(z_1 + dc_1) - (z_1 + f_1 dc_1)} = \frac{- k_s (T_2 - T_m)/dc_1}{1 - f_1} =$$

$$\frac{- k_s \left(\frac{\partial T}{\partial z}\right)_{s,1}}{1 - f_1} \tag{A4}$$

$$Q_{s1}^{new} = \frac{Q_{s1}}{1 - f_1} \tag{A5}$$

Similarly the axial heat flux from the melt at node i after relocation of the interface becomes:

$$- k_\ell \left(\frac{\partial T}{\partial z}\right)_{\ell,1}^{new} = \frac{- k_\ell (T_m - T_1)}{(z_1 + f_1 dc_1) - (z_1 - dm_1)} = \frac{- k_\ell (T_m - T_1)/dm_1}{1 + f_1 d_1} =$$

$$\frac{- k_\ell \left(\frac{\partial T}{\partial z}\right)_{\ell,1}}{1 + f_1 d_1}$$

or

$$Q_{\ell 1}^{new} = \frac{Q_{\ell 1}}{1 + f_1 d_1} \quad ; \quad \text{where } d_1 = \frac{dc_1}{dm_1} \tag{A6}$$

Since the heat fluxes after interface relocation must satisfy Equation (10) we obtain:

$$\frac{Q_{s1}}{1 - f_1} = \frac{Q_{\ell 1}}{1 + f_1 d_1} + Q_{f1} \tag{A7}$$

- 124 -

The values of f_i can be calculated from the above equation. A semi-implicit rearranged form of this equation is

$$f_i = \frac{Q_{fi} - (Q_{si} - Q_{\ell i})}{f_i^{old} \, d_i \, Q_{fi} + Q_{si} \, d_i + Q_{\ell i} - Q_{fi} \, (d_i - 1)} \qquad (A8)$$

Therefore the location of the new interface shape is given by

$$z_i^{new} = z_i + f_i \, dc_i \qquad (A9)$$

$$i = 1,2,\ldots,nr - 1$$

This procedure is an adaptation of the method used by Kobayashi (1981) to the finite element solution case. Kobayashi (1981) used a similar approach in the context of finite difference solution method.

A quadratic interpolation of the predicted temperature profile is used for calculation of Q_{si} and $Q_{\ell i}$ in Equation (A7) and also for calculation of the slope of the interface.